

Electronic Powered Prosthetic Device for Transradial Amputees using Pattern Classification

by

Landolf Theron



*Thesis presented in partial fulfilment of the requirements for
the degree of Master of Engineering (Mechatronic) in the
Faculty of Engineering at Stellenbosch University*

Supervisors: Mr. J. van der Merwe
Dr. JH. Müller

December 2016

The financial assistance of the National Research Foundation (NRF) towards this research is hereby acknowledged. Opinions expressed and conclusions arrived at, are those of the author and are not necessarily to be attributed to the NRF.

Declaration

By submitting this thesis electronically, I declare that the entirety of the work contained therein is my own, original work, that I am the sole author thereof (save to the extent explicitly otherwise stated), that reproduction and publication thereof by Stellenbosch University will not infringe any third party rights and that I have not previously in its entirety or in part submitted it for obtaining any qualification.

Date: December 2016

Copyright © 2016 Stellenbosch University
All rights reserved.

Abstract

Electronic Powered Prosthetic Device for Transradial Amputees using Pattern Classification

L. Theron

*Department of Mechanical and Mechatronic Engineering,
University of Stellenbosch,
Private Bag X1, Matieland 7602, South Africa.*

MEng Research

December 2016

This document presents a Masters dissertation on the development of an affordable electronic prosthetic device for transradial amputees. A mechanical prosthetic hand was converted to an electronic actuated prosthetic device. EMG signals on the forearm were classified to grant amputees natural control over the prosthetic device.

Three pattern classification techniques and several feature sets were validated using an existing database (NinaPro, 2014) of amputated subjects and non-amputated subjects. This verification established the classification technique and feature sets to be implemented in the rest of the project. It was established that a self-organizing map will be used with three different feature sets. A t-test suggested that there was no statistical difference between the classification rate of amputated subjects and non-amputated subjects.

The prosthetic hand and all its components were designed, manufactured and assembled. A current sensor was designed and tested. The current sensor measured the current of each motor individually to relate the torque of the motor to the grasp strength of this prototype. The reaction time of the prosthetic device was tested and could reach the same position as a non-amputated hand in 2.48 seconds. The force measured at the tip of the finger was 15.56 N which compared well with commercial devices.

An Android application was developed to process the EMG signals measured by a Myo Armband. The classifier was implemented on the Android application and the user interface provided the training and live classification platform. A prosthesis guided training method was used for amputated subjects.

The classification technique and three feature sets were tested on both amputated and non-amputated subjects. Different window sizes were used for the EMG data and the best feature set and window size was determined. The average training classification rate using a sample size of 15 non-amputated subjects was calculated as 96.2 % with a live classification rate of 87.2 %. The average training classification rate using a sample size of two amputated subjects was calculated as 94.3 % with a live classification rate of 85.3 %. There was no statistical difference between the different feature sets, window sizes and window shift sizes.

An offline muscle verification test was done to establish which sensors were dominant for each grasp. The sensors were related to the muscles they were placed on. This verification confirmed the muscles used for each grasp type and was consistent with literature.

It was concluded that a mean live classification rate of 85.3 % was achievable when amputated subjects ($n = 2$) used this prosthetic device. This prosthetic device prototype was developed for R7 265.54. The prototype cost are promising for developing countries like South Africa. This means that this device could be funded by medical aids or the WCF.

Uittreksel

Elektroniese Prostetesis vir Trans-Radiale Geamputeerdes deur die gebruik van Patroon Klassifikasie

(“Electronic Powered Prosthetic Device for Transradial Amputees using Pattern Classification”)

L. Theron

*Departement Meganiese en Megatroniese Ingenieurswese,
Universiteit van Stellenbosch,
Privaatsak X1, Matieland 7602, Suid Afrika.*

MEng Navorsing

Desember 2016

Hierdie dokument bied ‘n Meestersgraad verhandeling oor die ontwikkeling van ‘n bekostigbare elektroniese prostetiese hand vir transradiale geamputeerdes. ‘n Meganiese prostetiese hand was omgeskakel na ‘n elektroniese prostetiese hand. EMG seine op die voorarm was geklassifiseer om geamputeerdes ‘n natuurlike beheer oor die prostetiese hand te gee.

Drie patroon klassifiseringstegnieke en verskeie EMG kenmerk stelle was getoets met behulp van ‘n bestaande databasis (NinaPro, 2014) wat geamputeerde en ongeskonde vrywilligers se EMG data bevat. Hierdie verifikasie het die klassifikasie tegniek en kenmerk stelle vasgestel. Dit was vasgestel dat ‘n self-organiserende kaart gebruik sal word met drie verskillende kenmerk stelle. ‘n T-toets het bevestig dat daar geen statistiese verskil tussen die klassifikasie koers van geamputeerde vrywilligers en ongeskonde vrywilligers was nie.

Die prostetiese hand en al sy komponente was ontwerp, vervaardig en aanmekaar gesit. ‘n Stroom sensor was ontwerp en getoets. Die stroom sensor meet die stroom van elke motor afsonderlik om die wringkrag van die motor met die greep krag van hierdie prototipe te vergelyk. Die reaksietyd van hierdie prototipe was bereken as 2.48 sekondes. Die maksimum krag wat by die punt van die middel vinger gemeet was is 15.56 N wat goed vergelyk met kommersiële produkte.

‘n Android toepassing was ontwikkel om die EMG seine te verwerk wat deur ‘n Myo Armband opgetel was. Die klassifiseerder was geïmplementeer

op die Android toepassing en die gebruikerskoppelvlak het die opleiding en aanlyn klassifikasie platform gebied. 'n Prostetiese geleide opleiding metode was gebruik vir geamputeerde vrywilligers.

Die klassifikasie tegniek en drie EMG kenmerk stelle was getoets op beide geamputeerde vrywilligers en ongeskonde vrywilligers. Verskillende venster groottes is gebruik vir die EMG data en die beste kenmerk stel en venster grootte was vasgestel. Die gemiddelde opleiding klassifikasie koers onder 15 ongeskonde vrywilligers was bereken as 96,2 % met 'n aanlyn klassifikasie koers van 87,2 %. Die gemiddelde opleiding klassifikasie koers onder twee geamputeerde vrywilligers was bereken as 94.3 % met 'n aanlyn klassifikasie koers van 85.3 %. Dit was vasgestel dat daar geen statistiese verskil tussen die verskillende EMG kenmerk stelle en venster groottes was nie.

'n Aflyn spier verifikasie toets was gedoen om vas te stel watter sensore dominant was vir elke greep. Die sensore hou verband met die spiere waarop hulle geplaas was. Hierdie verifikasie bevestig die spiere wat gebruik word vir elke tipe greep en was in ooreenstemming met literatuur.

Die gevolgtrekking was gemaak dat 'n aanlyn klassifikasie koers van 85.3 % bereik kan word op geamputeerde vrywilligers ($n = 2$). Die prostetiese hand was ontwikkel vir R7 265,54. Dit het beteken dat hierdie toestel befonds kan word deur mediese fondse of die WVF.

Acknowledgements

I would like to express my sincere gratitude and thank the following people for their contribution to this project:

- Mr Eugene Rossouw for his assistance and contribution to this project. Eugene Rossouw's knowledge regarding amputees and prosthetic devices were invaluable to this project.
- My fellow BERG colleagues for participating in the study and sharing their knowledge.
- Mr van der Merwe and Dr Müller for their expertise and guidance throughout this project.
- The amputees for offering their time to test the prototype.

Lastly, I would like to thank my family and friends for their support and advice.

Contents

Declaration	i
Abstract	ii
Uittreksel	iv
Acknowledgements	vi
Contents	vii
List of Figures	x
List of Tables	xii
Nomenclature	xiii
1 Introduction	1
1.1 Background	1
1.2 Objectives	2
1.3 Motivation	3
2 Literature Review	4
2.1 Anatomy and Physiology	4
2.1.1 Arm Anatomy	4
2.1.2 Amputee Anatomy	6
2.2 Grasp Requirements	7
2.3 Biosignals	9
2.3.1 History of EMG signals	9
2.3.2 Types of EMG	10
2.3.3 EMG Considerations	10
2.3.4 Electrode Considerations	11
2.3.5 EMG Signal Features	12
2.4 Biosignal Processing	12
2.4.1 Pattern Classification	12
2.4.2 Pattern Classification Success	14

CONTENTS

2.4.3	Control Considerations	15
2.4.4	Amputee Training Techniques	15
2.5	Prosthetic Feedback Interfaces	16
2.5.1	Feedback Information	17
2.5.2	Types of Feedback	17
2.6	Existing Technologies	18
2.6.1	i-limb™ - Touch-bionics	19
2.6.2	bebionic™ - Steeper	20
3	Pattern Classification Model	22
3.1	Theory	22
3.1.1	Feature Extraction	22
3.1.2	Pattern Classification Techniques	24
3.2	Pattern Classification Verification	25
3.2.1	Methodology	25
3.2.2	Results	26
3.2.3	Discussion	30
3.3	Pattern Classification Model Implemented	32
4	Design Methodology	35
4.1	Hardware Design	35
4.1.1	Determine Motor Torque to Close Unloaded Hand	36
4.1.2	Calculate Total Grasp Force as a Function of Motor Torque	39
4.1.3	Motor Selection	40
4.2	Electronic Design	41
4.2.1	Motor Drivers	43
4.2.2	Current Sensors	43
4.2.3	Power Supply	44
4.2.4	Rotary Encoders	44
4.2.5	Electromyography	45
4.2.6	Microprocessor	46
4.3	Microprocessor Software Design	46
4.4	Mobile Application Software Design	48
4.4.1	Java	48
4.4.2	User Interface	49
4.5	Affordability	53
5	Prototype Testing	55
5.1	Introduction	55
5.2	Phase I - Non-Amputated Arm Grasp Classification	56
5.2.1	Phase I Methodology	56
5.2.2	Phase I Results	58
5.2.3	Phase I Discussion	61
5.3	Phase II - Grasp Force	63

CONTENTS

5.3.1	Phase II Methodology	63
5.3.2	Phase II Results	65
5.3.3	Phase II Discussion	67
5.4	Phase III - Amputee Grasp Classification	67
5.4.1	Phase III Methodology	67
5.4.2	Phase III Results	69
5.4.3	Phase III Discussion	73
5.5	Offline Muscle Verification	74
5.5.1	Methodology	74
5.5.2	Results	75
5.5.3	Discussion	76
6	Conclusion	78
6.1	Outcomes	78
6.2	Limitations	80
6.3	Future Recommendations	81
	List of References	82
	Appendices	86
A	Classification Verification	87
A.1	Classification Techniques	87
A.2	Preliminary Results	88
B	Design	91
B.1	Analytical Model	91
B.2	PCB Design	93
B.3	Android Development	96
B.4	Assembly	96
B.5	Affordability	98
C	Results	100
C.1	Phase I	103
C.2	Phase II	104
C.3	Phase III	105
C.4	Offline Muscle Verification	111

List of Figures

2.1	Description of Finger Joints (Adapted from: Eorthopod (2015)) . . .	5
2.2	Physiology and Anatomy of the Human Forearm (Adapted from: NoExcuseHealth (2013))	6
2.3	Taxonomy Tree of Various Grasps (Adapted from: Cutkosky (1989))	8
2.4	Grasp Recognition from raw EMG signal (Adapted from: Ferguson and Dunlop (2002))	9
2.5	The Use of Situational Awareness to Supplement Myoelectric Control (Adapted from: Castellini <i>et al.</i> (2014))	14
2.6	Semi-Autonomous Control of a Myoelectric Prosthesis (Adapted from: Castellini <i>et al.</i> (2014))	17
2.7	The i-limb™ Prosthetic Hand (Touchbionics, 2015))	19
2.8	The bebionic™ Prosthetic Hand ((Steeper, 2015))	21
3.1	Comparison of Different Classification Techniques for Non-Amputated Subjects. a) SOM; b) LDA; c) kNN	27
3.2	Comparison of Different Classification Techniques for Amputated Subjects. a) SOM; b) LDA; c) kNN	29
3.3	Comparison of Non-Amputated Subjects and Amputated Subjects for SOM and Selected Feature Sets	31
3.4	Kohonen Self-Organizing Map (Illustration: LC Theron)	32
3.5	Flow Diagram for SOM (Illustration: LC Theron)	33
4.1	Electromechanical Components Layout (Illustration: LC Theron)	35
4.2	Force Diagram Indicating Grasp Forces as a Function of Flexion Angle θ (Adapted from: Tenim (2014))	37
4.3	5th Digit Tension Moments vs. Internal Moments as a function of Flexion Angle	38
4.4	Total Grasp Force vs Motor Torque vs Flexion Angle	40
4.5	Specifications of Micro Metal Gearmotor	41
4.6	Electronic Components Diagram (Illustration: LC Theron)	42
4.7	Battery Specifications (Illustration: LC Theron)	44
4.8	Myo Armband Specifications (Illustration: LC Theron)	45
4.9	Flow Diagram for Microprocessor (Illustration: LC Theron)	47

LIST OF FIGURES

4.11	User Interface of MyoProsthesis (Illustration: LC Theron)	49
4.10	Flow Diagram for Android Application (Illustration: LC Theron)	50
4.12	Orientation Calibration of MyoProsthesis (Illustration: LC Theron)	51
4.13	User Interface of MyoProsthesis (Illustration: LC Theron)	52
5.1	Protocol Flowchart (Illustration: LC Theron)	56
5.2	Test Setup for Phase I (Illustration: LC Theron)	57
5.3	Live Confusion Matrix for the Best Parameters - Phase I	58
5.4	Comparison of Different Feature Sets - Phase I	60
5.5	Live Confusion Plot with Overall Best Parameters - Phase I	61
5.6	Test Setup for Phase II Stage 1 (Illustration: LC Theron)	63
5.7	Test Setup for Phase II Stage 2 (Illustration: LC Theron)	64
5.8	Example of Phase II, Stage 1 Results	65
5.9	Example for Phase II Stage 2	66
5.10	Results for Phase II, Stage 2	66
5.11	Test Setup for Phase III	68
5.12	Live Confusion Matrix for the Best Parameters - Phase III	70
5.13	Comparison of Different Feature Sets - Phase II	71
5.14	Live Confusion Plot with Overall Best Parameters - Phase III	72
5.15	Average RMS values Non-Amputated Subjects for 8 sensors	75
A.1	Flow Diagram for LDA (Illustration: LC Theron)	87
A.2	Flow Diagram for kNN (Illustration: LC Theron)	87
A.3	Comparison of Different Classification Techniques and Feature Sets for Non-Amputated Subjects	89
A.4	Comparison of Different Classification Techniques and Feature Sets for Amputated Subjects	90
B.1	Free Body Diagram (Adapted from: (Tenim, 2014))	91
B.2	Current Sensor Schematic	94
B.3	Current Sensor Calibration Curve	94
B.4	Power Supply Schematic	95
B.5	Assembly of Prosthesis	97
C.1	Classification Results for all Non-Amputated Subjects per Feature	102
C.2	Calibration Curve for Pressure Gauges	104
C.3	Calibration Curve for FSR	105
C.4	Classification Results for Two Amputated Subjects per Feature	106
C.5	Average MAV values Non-Amputated Subjects for 8 Sensors	111
C.6	Average WL values Non-Amputated Subjects for 8 Sensors	112
C.7	Average WAMP values Non-Amputated Subjects for 8 Sensors	113

List of Tables

2.1	Forearm Muscles and their Functions (Taylor, 1999)	5
3.1	Best Features for Different Classifiers for Non-Amputated Subjects	28
3.2	Best Features for Different Classifiers for Amputated Subjects . . .	29
3.3	Calculation Time for Features in Seconds	30
4.1	Electromechanical Components Used	36
4.2	Input motor torque for flexion of unloaded joints [N.mm]	38
4.3	Electrical Specifications of Custom Current Sensor	43
4.4	Total Cost Breakdown	54
5.1	Summary of best Parameters - Phase I	59
5.2	Summary of Subject Information	69
5.3	Summary of best Parameters - Phase III	71
5.4	Muscle-Sensor Relationship	74
5.5	Summary of Dominant Sensors for each Grasp Type and Feature .	76
A.1	Description of Feature Set Numbers	88
B.1	Functions Written in Java	96
B.2	Cost Breakdown A	98
B.3	Cost Breakdown B	99
C.1	Classification Results per Non-Amputated Subject	103
C.2	ANOVA Probability with Window Size as Groups for Non-Amputated Subjects	103
C.3	ANOVA Probability with Shift Size as Groups for Non-Amputated Subjects	104
C.4	Classification Results per Amputated Subject	105
C.5	ANOVA Probability with Window Size as Groups for Two Ampu- tated Subjects	105
C.6	ANOVA Probability with Shift Size as Groups for Two Amputated Subjects	107
C.7	PEQ Results from Amputated Subjects	107

Nomenclature

Abbreviations

ANN	Artificial Neural Networks
AR	Auto Regressive Model
BLE	Bluetooth 4.0 Low Energy
BMU	Best Matching Unit
DIP	Distal interphalangeal
DOF	Degrees of Freedom
DWT	Discrete Wavelet Transform
EMG	Electromyography
EPP	Extended Physiological Proprioception
EWC	Energy of Wavelet Coefficients
FSR	Force Sensitive Resistor
GPR	Gaussian Process Regression
HREC	Health Research Ethics Committee
IC	Integrated Circuit
IDE	Integrated Development Environment
IMU	Inertial Measurement Unit
ISR	Interrupt Service Routine
kNN	k-Nearest Neighbours
LDA	Linear Discriminant Analysis
LIFE's	Longitudinal intrafascicular electrodes

NOMENCLATURE

LLGMN Log-linearized Gaussian Mixture Network

MAV Mean Absolute Value

MCP Metacarpophalangeal

MCU Microcontroller Unit

MUAP Motor Unit Action Potential

MVF Mirror Visual Feedback

MYOP Myopulse Percentage Rate

PCB Printed Circuit Board

PEQ Prosthetic Evaluation Questionnaire

PGT Prosthesis Guided Training

PIP Proximal interphalangeal

PNS Peripheral Nervous System

RMS Root Mean Square

SDK Software Development Kit

sEMG surface-Electromyography

SOM Self-Organizing Map

SSC Slope Sign Changes

STFT Short-Time Fourier Transform

TMR Targeted Muscle Reinnervation

UCT University of Cape Town

VAR Variance

WAMP Willison Amplitude

WCF Workmanship Compensation Fund

WL Waveform Length

NOMENCLATURE

Symbols

α	Angle of deviation of actuating wire	[°]
α_{LR}	Learning rate	[-]
β	Angle of interphalangeal phalanx face	[°]
β_{decay}	Decay rate	[-]
μ_c	Coefficient of channel friction (static)	[-]
μ_r	Estimated coefficient of hinge friction (static)	[-]
θ	Flexion angle of each phalange	[°]
i	Identifier for fingers	[-]
a_j	Estimate of the AR coefficients	[-]
B_w	Between-class matrix	[-]
C	Capacitor	[F]
CR	Classification rate	[%]
D	Mean coil diameter	[m]
d	Spring wire diameter	[m]
d_v	Distance between each vector	[-]
E	Young's Modulus of spring material	[GPa]
e_k	Residual white noise of AR model	[-]
f	Number of features	[%]
F_G	Applied grasp force	[F]
F_i	Input force	[F]
g	Gravitational acceleration	[m/s ²]
h	Distance of tendon friction force from hinge/pivot	[m]
I_s	Shunt Resistor Current	[A]
L	Length of phalanx	[m]
L_F	Distance from pivot to applied grip force and/or normal force	[m]
L_G	Distance from pivot to centre of gravity	[m]

NOMENCLATURE

m	Mass of phalanx	[kg]
M_O	Hinge reaction moment	[N.m]
M_{Grasp}	Grasp moment	[N.m]
M_{Hinge}	Hinge moment	[N.m]
M_{Mass}	Mass moment	[N.m]
M_{Spring}	Spring moment	[N.m]
$M_{Tension}$	Tension moment	[N.m]
N	Normal reaction force of cable/tendon on the phalanx	[N]
n	Number of EMG samples	[—]
N_{AR}	Order of AR model	[—]
Na	Number of active turns of spring	[—]
r	Radial channel distance from pivot	[m]
R_L	Load Resistor	[Ω]
r_p	Hinge pin radius	[m]
R_S	Shunt Resistor	[Ω]
R_X/Y	Hinge reaction forces in x and y directions	[F]
S_w	Within-class matrix	[—]
T	Cable (tendon) tension	[F]
V	Input Vector	[—]
V_o	Output Voltage	[V]
W	Eigenvector matrix	[—]
W_{BMU}	Weight of BMU	[—]
X	Feature samples	[—]
x_i	EMG signal measured	[—]
Y	Transformed samples	[—]

Chapter 1

Introduction

1.1 Background

Since the late 1960's electromyography has been used to control prosthetic devices to improve amputees' quality of life. The level of complexity has not yet reached the same abilities as the human hand. This is mainly due to two reasons: the prosthesis usually only offers 2-3 degrees of freedom and the movement of the hand is not 'natural' (Atzori *et al.*, 2013).

This project entailed the development of an affordable prosthetic hand. Every year 50 000 people in the United States of America (USA) receive an amputation. Currently 105 000 people have an amputated upper limb in the USA. According to Kulley (2003) 60 % of arm amputations occur during the ages of 21 and 64 while 10 % of arm amputations are below 21 years old. The main cause leading to amputation is traumatic accidents with 77 % followed by congenital upper limb deficiency with 8.9 % of live births.

According to the Arms Within Reach Foundation (2015) a person who has lost an upper limb has six prosthetic options: electrically powered prosthesis, cosmetic restoration, body powered prosthesis, activity specific prosthesis, hybrid prosthesis or no prosthesis. Many amputees choose not to wear prosthetic devices. It is estimated that only half of all upper limb amputees receive prosthetic services. Of the amputees who receive services, half will stop using the prosthetic device after a year. This could be because of the level of function which is not accomplished by the prosthetic device or because of the inadequate funding to obtain the correct prosthetic device.

The maximum amount medical aids in South Africa usually give a trans-radial amputee is around R58 000 (Rossouw, 2015). The functionality and complexity of the prosthetic devices increase with the price of the device. A body-powered prosthesis often causes fatigue and difficulties for the amputee. In a study done by Millstein *et al.* (1986) the electrical prosthesis had the highest acceptance rate among amputees. Next was the cable-operated hook, the cosmetic prosthesis and then the cable operated hand. In Millstein *et al.*

1. INTRODUCTION

(1986) the low acceptance level of the body operated hand was due to the difficulty to operate the hand and the weak grip. Part of the aim of this project was to develop an affordable myoelectric device which was simple to use and minimizes effort of use. The prosthetic device was developed for transradial amputees. Transradial prosthetic devices are designed for people who have an amputation through their forearm.

This project was suggested by Dr. G. Vicatos from the University of Cape Town (UCT) and Prof. C. Scheffer from Stellenbosch University. Tenim (2014) developed a body-powered mechanical prosthetic hand. This project was done in cooperation with UCT to develop an electrically powered prosthetic device for transradial amputees. The mechanical prototype developed by Tenim and Vicatos was used to develop an electrical actuation system for the same mechanical prototype. The mechanical prototype was actuated using a cable system attached to the amputee's shoulder. The cable was attached to a single differential mechanism to control all five fingers. The user was able to adjust the thumb position by using his healthy hand. Each finger was connected to the differential mechanism via cables. Tests regarding the mechanical structure was conducted by Tenim (2014) and were therefore not considered in this project. The literature study, design and testing phase therefore only included information regarding the electrical actuation system and interface with the mechanical prototype. The mechanical design and calculations are described in Tenim (2014).

An experienced prosthetist, Rossouw (2015), was consulted to provide deeper insight into the practical use and training for amputees. The prosthetist was also responsible for recruiting amputees. Mr. Russouw does approximately 6-7 arm prosthetic fitments each year.

The available facilities included various laboratories, rapid-prototyping facilities and the Mechanical Workshop. This document serves as the final thesis document and will discuss the objectives, motivation, literature review, design methodology, prototype testing and conclusion.

1.2 Objectives

The aim of the project was to develop an affordable electrical prosthetic device for transradial amputees. An electronic control system and electrical actuator was designed which could be integrated into the mechanical prototype developed by Tenim (2014). The following objectives were defined in this project:

- Determine the needs and requirements of transradial amputees.
- Develop an electrical actuation system for the mechanical prototype developed by Tenim (2014).
- Design and implement an electrical sensing and feedback system to grant the user control over the mechanical prosthetic hand.

1. INTRODUCTION

- Test the electrical prosthetic device on non-amputated subjects as well as transradial amputees.

The above mentioned objectives outline the scope of this project.

1.3 Motivation

The motivation of this project was to develop an electronic prosthetic device that was able to reduce the limitations on commercially available prosthetics while still being affordable. Upper limb amputees often have to choose a prosthetic device which provides almost no functionality because of the cost. Artificial limbs evolved to a point where it is possible to develop a functional and affordable prosthetic hand. According to UCSF Medical Centre (2006) a standard upper body prosthesis costs \$30 000 where the equivalent electric prosthesis costs \$100 000. According to Rossouw (2015) the price of myoelectric prosthetic hands in South Africa can range between R100 000 and R500 000. 3-D printing has become an essential aspect in prosthetics. It is possible to 3D-print an open-source mechanical prosthetic hand with a material cost of \$20.

In South-Africa an amputee normally has five options to fund a prosthetic device. About 10 % of Russouw's patients use their private funds. Two other funds which are used are the Road Accident Fund and the Workmanship Compensation Fund (WCF). The WCF only provides enough funding for a mechanical prosthetic device. It was suggested by Rossouw (2015) that a myoelectric prosthetic device which is cheap enough to be funded by the WCF would be able to succeed on the market. Third party claims and medical aids serve as the remaining two options. Medical aids provide an average of R15 000 and a maximum of R58 000 to amputees.

During the initial phases of this project it was established that there is a need for an affordable prosthetic device which could provide more functionalities for transradial amputees. The aim of this project was to determine if such a device could be developed.

Chapter 2

Literature Review

This section reports on the literature available on the development of electrical prosthetic devices for transradial amputees. This section includes a study done on the anatomy of transradial amputees compared to the anatomy of a non-amputated subject, an analysis on the required grasps of an electrical prosthetic device, methods for obtaining myoelectric information and the existing technology associated with prosthetic devices.

2.1 Anatomy and Physiology

This section describes the anatomy of the human arm. It was necessary to study the anatomy of the human arm in order to develop the electronic and mechanical characteristics of the system. This section includes the arm anatomy of a person without amputation as well as the anatomy of an amputated arm. As this system was developed for transradial amputees only the forearm and hand was investigated. The study was based on the muscles required to assure movement in the hand and wrist areas.

2.1.1 Arm Anatomy

A description of the different joints of the hand is given in Figure 2.1. Fingers two to five has three joints each called the Distal interphalangeal (DIP), the Proximal interphalangeal (PIP) and the Metacarpophalangeal (MCP).

In order to develop an electrical system for transradial amputees it was required to know the muscles used for hand and finger movements. According to Taylor (1999) most of the muscles required for wrist, hand and finger movement are located in the forearm. These muscles are extended from the ulna, radius and humerus and inserted in the phalanges, carpals and metacarpals.

The muscles on the anterior side of the forearm form the flexor group of the hand. The muscles on the posterior side of the forearm are the antagonists to the flexor group and are responsible for extending the fingers and wrist

2. LITERATURE REVIEW

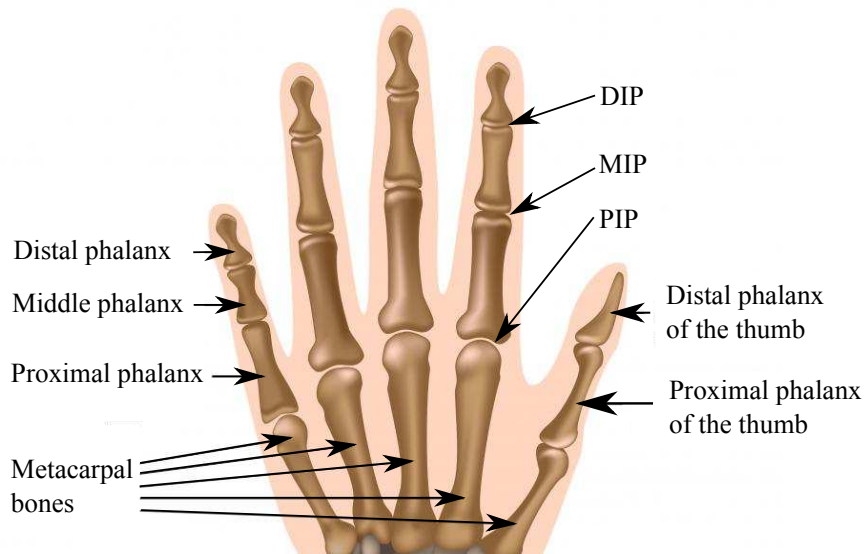


Figure 2.1: Description of Finger Joints (Adapted from: Eorthopod (2015))

(Taylor, 1999). The muscles required for hand and forearm movement were summarised in Table 2.1 while Figure 2.2 illustrates all forearm muscles.

Table 2.1: Forearm Muscles and their Functions (Taylor, 1999)

	Muscle	Function
1	Brachioradialis muscle	Flexing the elbow
2	Pronator teres	Rotate the arm toward the inside - pronation
3	Flexor carpi radialis	Flex the wrist, fingers
4	Flexor carpi ulnaris	Flexion of wrist and movement of the thumb across the palm
5	Flexor digitorum superficialis	2-5th finger PIP flexion
6	Flexor digitorum profundus	2-5th finger DIP flexion
7	Pronator quadratus	Assists the pronator teres in rotating the arm toward the inside
8	Extensor carpi radialis brevis	Functions to extend the wrist
9	Extensor carpi radialis longus	Abducting the hand
10	Extensor digitorum profundus	2-5th finger extension
11	Extensor carpi ulnaris	Extend the wrist
12	Palmaris longus	Flex the hand and wrist

2. LITERATURE REVIEW

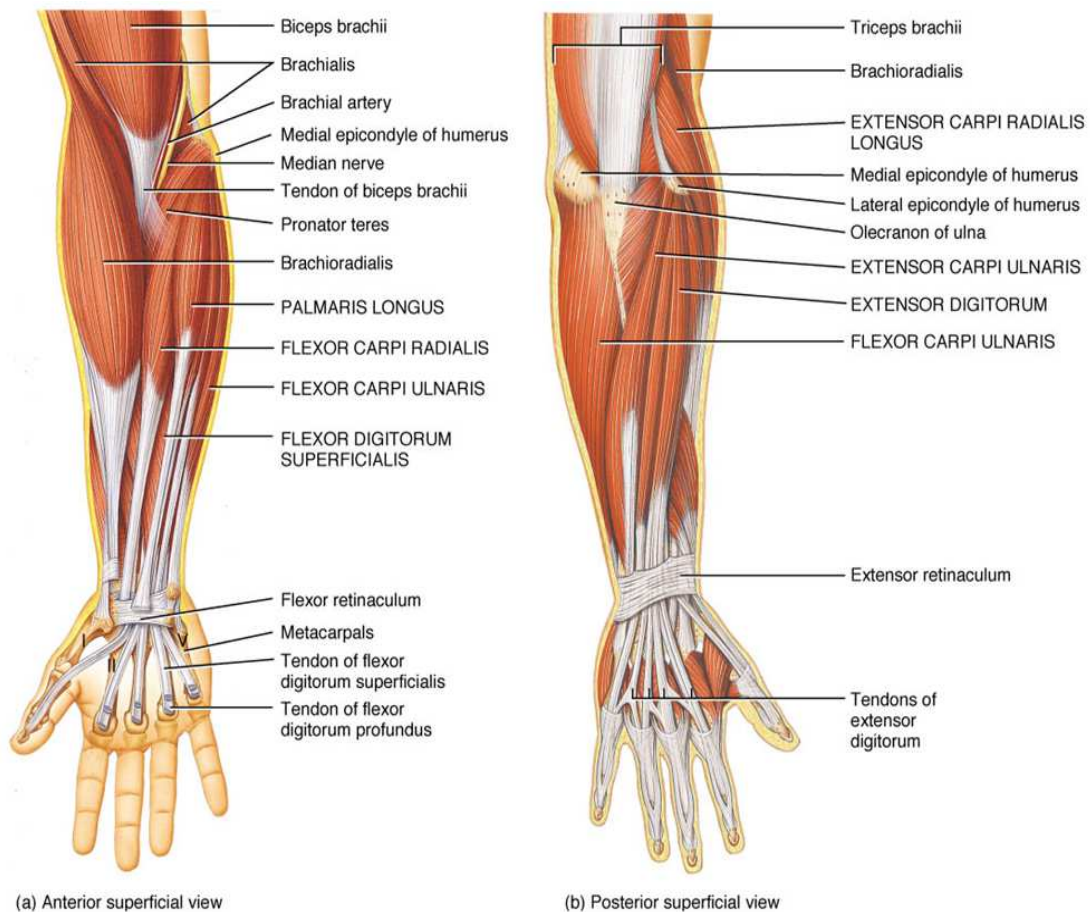


Figure 2.2: Physiology and Anatomy of the Human Forearm (Adapted from: NoExcuseHealth (2013))

Gazzoni *et al.* (2014) states that complete independent movements of the fingers are not possible because of the mechanical coupling across adjacent fingers. Antagonist muscles are required to limit the movement of other fingers.

2.1.2 Amputee Anatomy

The anatomy of a transradial amputee vary from patient to patient. The anatomy and physiology remains intact to a certain degree after amputation. The remaining muscles can still contract and relax where the nerves are connected to the muscles. When a muscle is disconnected from a tendon during an amputation the muscles are either connected to another muscle which is still intact or to an intact tendon. This is done to ensure that the muscle can still be used (Rossouw, 2015).

2. LITERATURE REVIEW

2.2 Grasp Requirements

Feix *et al.* (2009) defines a grasp as ‘every static hand posture with which an object can be held securely with one hand’. Their study has found 33 different grasp types which fit this definition. It was essential to understand the possible movements of a healthy hand and to study the required movements of an amputee. Two factors should be kept in mind when selecting the possible grasps for a prosthetic device: the first is the complexity to operate the device and the second the affordability of a device which could do all possible movements.

The human hand has 38 muscles, 21 Degrees of Freedom (DOF) and thousands of sensory organs. An extensive description of the possible human hand grasps were given in MacKenzie and Iberall (1994). Two general types of grasps were described by Cutkosky (1989). The first type of grasp was the power grasp. This grasp is used when stability and power are of importance and the area between the object and the surface of the finger and the palm is large. The second type of grasp was the precision grasp. This grasp is used when sensitivity is of importance and the object is supported between the tip of the fingers and the thumb.

According to Napier (1956) the movements of the hand can be divided into prehensile and non-prehensile movements. Prehensile movement is when an object is firmly held within the compass of the hand and the non-prehensile is when no grasping is involved but pushing or moving aspects of the hand is involved either with a single finger or the whole hand. Cutkosky (1989) has identified several common grasps which humans use on a day-to-day basis. These grasps are outlined in Figure 2.3.

The taxonomy tree in Figure 2.3 is divided by power and precision grasps from left to right and by shape and function from the top to the bottom. Even though the shape and size of certain objects may differ from those depicted in Figure 2.3, the orientation and position of the fingers and hand only differs slightly. This model provided a good description of the human hand capabilities. Napier (1956) summarised the prehensile grip of the human hand as follows:

- The human hand moves in two basic patterns namely the precision grip and the power grip
- With precision grip the object is pinched between the flexor aspects of the fingers and the thumb
- With power grip the object is held between the flexed fingers and the palm with pressure being applied with the thumb
- These two patterns cover the prehensile movement of the hand.

A study was done by Zheng *et al.* (2011) to determine the frequency of grasps used in daily household tasks and machine shop tasks. According to Zheng *et al.* (2011) it is not possible to implement the full spectrum of hand

2. LITERATURE REVIEW

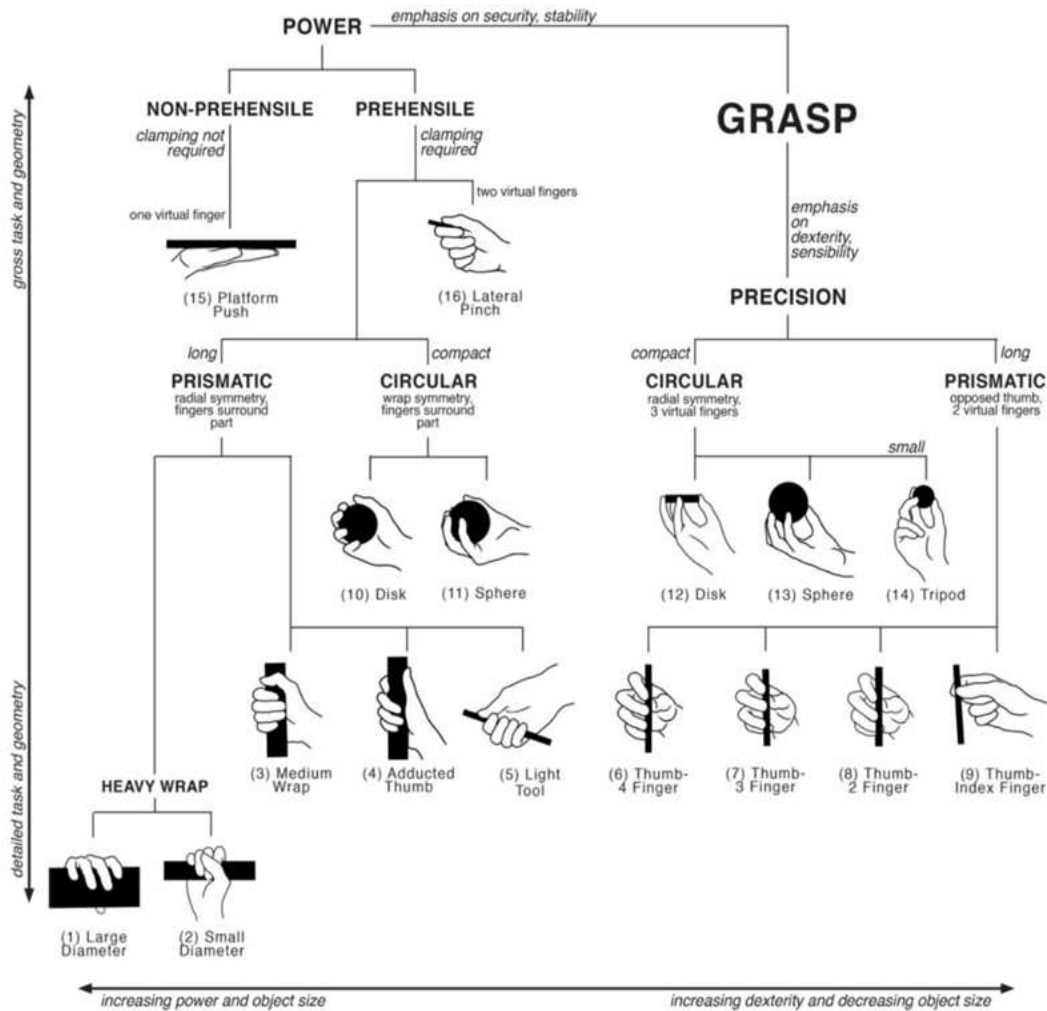


Figure 2.3: Taxonomy Tree of Various Grasps (Adapted from: Cutkosky (1989))

capabilities and therefore a smaller subset of grasps should be chosen when designing a prosthetic hand. In their study the most frequent grasps used with household tasks were Medium Wrap, Index Finger extension, Power Sphere and Lateral Pinch. The most frequent grasps used by a Machinist were Lateral Pinch, Light Tool, Tripod and Medium Wrap.

According to Rossouw (2015) the four most important grasps for amputees are the Tripod Grip, Power Grip, Index Point and also a Clothes Donning Grip. The last grip is used when the hand needs to be pushed through a long sleeve.

2. LITERATURE REVIEW

2.3 Biosignals

The human brain communicates with the rest of the body through a neural network. The neural network conducts electrical charges which is caused by chemical reactions in the body (Bronzino, 2006). The body consists of materials which are electrically conductive. The three types of biosignals are electroencephalogram (brain neural activity), electrocardiogram (heart muscle activity) and Electromyography (EMG) (skeletal muscle activity) signals. EMG signals are widely used in electrical prosthetic devices. Figure 2.4 illustrates the flow of information used in Ferguson and Dunlop (2002) for grasp recognition. Figure 2.4 served as starting point for the discussion to follow. The pattern recognition phase is discussed in Section 2.4.

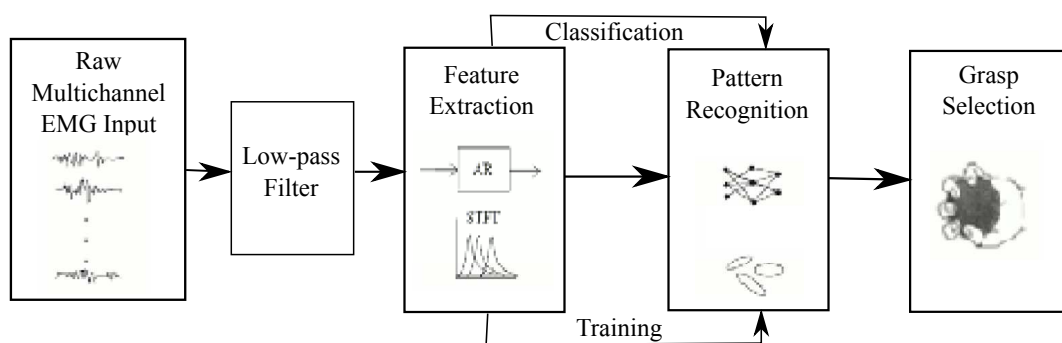


Figure 2.4: Grasp Recognition from raw EMG signal (Adapted from: Ferguson and Dunlop (2002))

2.3.1 History of EMG signals

The first basic principles of the EMG concept were discovered in 1666 by Francesco Redi when he conducted tests on the muscles of an Electric Ray Fish. Luigi Galvani published an article in 1792 named ‘De Viribus Electricitatis in Motu Musculari Commentarius’, which explained that the muscle initiates a contraction when electricity is applied to the muscle. In 1890 Marey recorded the first actual muscle contractions and introduced the term EMG which was ‘a method for evaluating and recording the activation signal of muscle’ (Cahan, 1993). EMG signals were used in a clinical environment in 1990 by Cram and Steger for the first time (Daley *et al.*, 1990). A group of impulse signals called the motor unit is generated when the brain decides to move a group of muscles. Muscle fibres exchanges ions and this results in an electrical current known as the Motor Unit Action Potential (MUAP) (Day, 2002). This electrical signal is called an electromyogram. An electromyogram can be captured using electronic circuitry.

2. LITERATURE REVIEW

2.3.2 Types of EMG

The residual motor branches of the arm nerves of an amputee can be transferred to alternative muscles. Targeted Muscle Reinnervation (TMR) is a surgical procedure where sensory nerves are surgically reconstructed and attached to other muscle groups. If the surgery was successful the muscles of the hand can be projected to the chest for shoulder disarticulated patients (Castellini *et al.*, 2014). TMR surgeries however are only intended for a small population of amputees (Christiansen *et al.*, 2013).

A surface-Electromyography (sEMG) signal is captured on the surface of the skin. The sEMG is the temporal and spatial sum of MUAP's within multiple muscles around the electrode. This stochastic signal has a typical amplitude of 0-6 mV with the most energy concentrated in the 50-150 Hz bandwidth (Ferguson and Dunlop, 2002). Ambient electrical noise is a problem regarding sEMG applications particularly in the 50 Hz range.

2.3.3 EMG Considerations

Ngeo *et al.* (2014) suggested that the discrete classification of hand gestures has been successful and consistent in the past 30 years. Decoding accuracies above 95% have been reached while classifying more than six gestures. Ngeo *et al.* (2014) notes that the wrist and arm position have an influence on the EMG patterns captured. Studies suggested that arm position and orientation during the use of myoelectric prosthesis could impair the sEMG pattern recognition algorithms (Gazzoni *et al.*, 2014). It was stated that this impairment is a little stronger in subjects with a non-amputated arm than in subjects with an amputated arm.

Some factors which influence prosthetic control via sEMG are muscular fatigue, a dispositioned socket, sweating causing signal degradation, cognitive effort and residual limb volume fluctuation (Castellini *et al.*, 2014). Data from shifted electrodes should be pooled during training to minimize the performance deterioration due to electrode shift. Rossouw (2015) stated that he has never had a problem with shifted electrodes. The inner socket is not supposed to move and therefore the electrodes will also not shift.

User dependency is one of the challenges that need to be managed when biofeedback is recorded with sEMG (Castellini *et al.*, 2014). The cause of this is the difference in skin impedance, muscle synergies and the quantity of sub-cutaneous fat. Therefore information gathered from one subject does not make it naively reusable.

A study done by Sebelius *et al.* (2005) suggested that subjects with old amputations did not perform with less motion capabilities than subjects with recent amputations. The time of amputation to testing varied from 1-20 years and this implied that the adult brain can relearn and undergo plastic changes.

2. LITERATURE REVIEW

2.3.4 Electrode Considerations

A study done by Gazzoni *et al.* (2014) implied that it was possible to identify areas on the forearm relating to different finger movements. The study suggested that targeted positioning of the electrodes could improve the performance of sEMG based prosthesis. Gazzoni *et al.* (2014) suggested that by carefully placing the electrodes finer motor tasks can be recognized to control a prosthesis.

The most common sensor configuration in literature was researched by Hermens *et al.* (2000). This configuration was a Ag/AgCl sensor with a diameter of 10 mm, an inter-electrode distance of 20 mm with the skin shaved, rubbed and cleaned before sensor placement. The sensor placement influences the signal-to-noise ratio, signal quality, amplitude and frequency (Hermens *et al.*, 2000).

A procedure for preparing subjects for a myoelectric device is described by Zecca *et al.* (2002). This preparation is normally done by a qualified prosthetist. During the patient evaluation phase the skin condition, skeletal anatomy, muscle strength, EMG signal and tissue condition is observed. After this observation the prosthetist obtain a plaster impression of the amputee's residual limb and conduct a static and dynamic diagnosis of the proposed design for the prosthesis. The site identification for electrode placement is dependent on the skin condition, EMG separation and EMG signal level. If the prosthetist is satisfied with the design the socket is manufactured and conducts a postdelivery evaluation on the patient's function, cosmesis and comfort.

In a study done by Ngeo *et al.* (2014) four electrodes were placed on the flexor muscles and four on the extensor muscles. An average inner-electrode placement of 20 mm was used. The ground electrode was placed on the olecranon (elbow). Electrode placement on amputees differ from non-amputated subjects as amputees have varying degrees of muscle removal which depends on the level of amputation. In these cases amputees would require more extensive training (Ferguson and Dunlop, 2002).

Active electrodes were suggested by Ferguson and Dunlop (2002) as opposed to the disposable silver/silver chloride disc electrodes for several reasons. The latter needs to be applied in pairs on specific locations on the skin while a small difference in placement may result in large changes in the sEMG signals. The problem with passive electrodes is that amplification is performed a distance away from the electrode which results in extra unwanted electrical noise. The signal-to-noise ratio can be improved by amplifying the signal as close as possible to the electrode. An active electrode can be used to aid in the application phase. An active electrode was developed by Ferguson and Dunlop (2002) where each surface was connected to an instrumentation amplifier and the common mode voltage was fed back to a point on the arm with minimal underlying muscle.

2. LITERATURE REVIEW

2.3.5 EMG Signal Features

According to Ngeo *et al.* (2014) the conventional time domain features are Mean Absolute Value (MAV), Waveform Length (WL), Willison Amplitude (WAMP) and Variance (VAR). The information provided by these features are the signal amplitude, frequency, extent of muscle contraction and extent of the firing of MUAP's.

Ferguson and Dunlop (2002) suggested that a Short-Time Fourier Transform (STFT) should be used to indicate at which point in time different frequencies occur. A Discrete Wavelet Transform (DWT) is a fast, linear operation which transforms the time domain to a different domain. This decomposition is more complicated and many different families of wavelets exists.

According to Ajiboye and Weir (2005) the RMS is an accepted maximum likelihood estimator for EMG amplitude as it provides the average power of the muscle. Zecca *et al.* (2002) gives an extensive explanation of the available time domain features. Zecca *et al.* (2002) suggested that time-frequency representation gives a more accurate description of the physical phenomenon.

By reducing the dimensionality of the problem, the classification performance could be increased. Two strategies to achieve this is feature projection or feature selection. With feature projection the best combination of the original features is used to form a smaller new feature set. Principal component analysis provides a linear map from the original set of variables to a reduced dimension set of uncorrelated variables. With feature selection a new feature set is chosen based on some criteria chosen by the designer. The different features used in this project is described in Section 3.1.1.

2.4 Biosignal Processing

This section describes the signal processing methods used in prosthetic devices. The available signal features described in Section 2.3.5 are used to decrease the signal information and to be able to classify a certain signal.

2.4.1 Pattern Classification

Conventional pattern classification techniques work on a basis where distinguishing characteristics of EMG patterns are used to identify an intended movement (Li *et al.*, 2010). The conventional pattern classification techniques includes: Artificial Neural Networks (ANN), Gaussian Process Regression (GPR), Linear Discriminant Analysis (LDA), k-Nearest Neighbours (kNN), fuzzy logic and a Self-Organizing Map (SOM). According to Ngeo *et al.* (2014) ANN provides a very fast computational time. In a study done by Ajiboye and Weir (2005) a heuristic fuzzy logic approach was used to classify EMG patterns. This system had an update rate of 45.7 ms. Ngeo *et al.* (2014) stated that the pattern classification approach to EMG signals was inadequate for

2. LITERATURE REVIEW

robotic devices because of the sequential strategy where only one movement is active at a time. Natural hand movements have simultaneous control over multiple degrees of freedom and are continuous in movement. Proportional and simultaneous control strategies are preferred over discrete classification (Ngeo *et al.*, 2014).

To decrease functional prosthesis abandonment a device needs to be developed with an adaptive system which is informed of the possible hand movements and can refine this knowledge with a few signals collected from the specific amputee (Castellini *et al.*, 2014).

Ngeo *et al.* (2014) presented a method for the continuous extraction of control information for 15 DOF's. The simultaneous estimation of finger kinematics was done using both ANN and nonparametric GPR. The MCP, PIP and DIP joint positions of all 5 fingers were continuously mapped from EMG signals using machine learning regression techniques.

Ngeo *et al.* (2014) introduced an EMG-to-Muscle activation model. This model transforms EMG signals to a suitable force and muscle activation representation. Neural activation depended on both the current EMG and the recent history of the EMG. A multi-layer feedforward ANN was used in their study to map the EMG signals to the corresponding hand/finger kinematics. The network contained an input layer, tan-sigmoidal activation, a hidden layer and a single linear output layer. A GPR was also implemented in their study and created for each DOF. The ANN provided one network to produce all 15 joint angles. A fixed interval sampling was used to reduce the hyperparameter learning and training time. Ngeo *et al.* (2014) proved that GPR can give a better estimation of the 15 joint angles while requiring less training samples. This is a great advantage as EMG signals are highly variable from day to day. It is noted that the computation time increased with the size of the training data with GPR. Ngeo *et al.* (2014) stated that using a GPR technique could solve the issue when dealing with the effects of different positions of the arm and wrist.

Castellini *et al.* (2014) suggested using real-time machine learning of predictions and contextual information to provide situation-appropriate modulation for sEMG controllers. Using computational predictions the future position, motion and contact forces can be estimated. Figure 2.5 illustrates how real-time machine learning could be implemented in conventional machine interfaces.

2. LITERATURE REVIEW

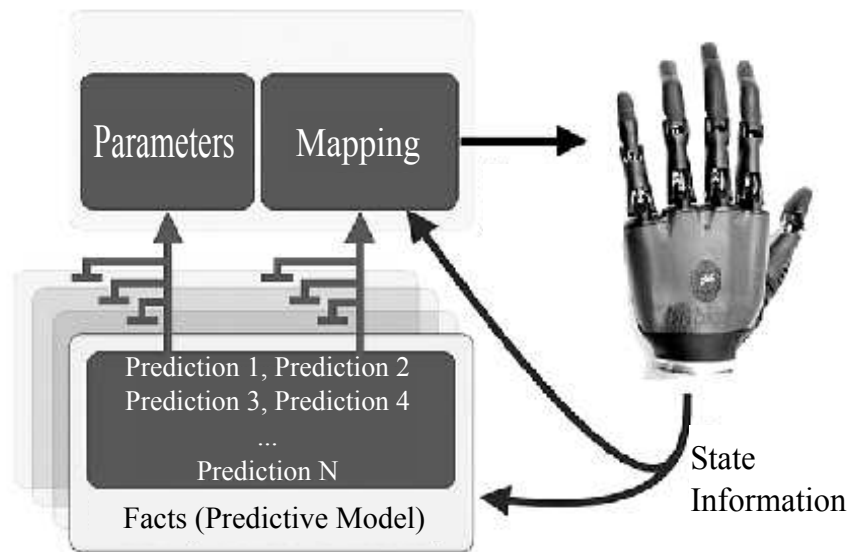


Figure 2.5: The Use of Situational Awareness to Supplement Myoelectric Control (Adapted from: Castellini *et al.* (2014))

This approach could use user-specific predictions to optimize the control of the device. Once the device has learned the facts (predictions) about past activities the machine interface could rank the control options to be available in real-time. The ranked predictions can serve as supplementary state information or could be mapped directly to control functions. The predictions can also be used to reorder control options, change gains or change thresholds and filters.

2.4.2 Pattern Classification Success

The success of the pattern recognition algorithm is based on the classification accuracy which is the ability to recognise the desired movement of the amputee. It was stated in Li *et al.* (2010) that this accuracy is mostly calculated in post-processing and some studies have revealed a low-correlation between classification accuracy and real-time performance.

Li *et al.* (2010) has quantified three real-time control performance metrics. The first was the motion-selection time which was the time to correctly select a target movement. This is the time taken for myoelectric commands to be translated to motion predictions. Ferguson and Dunlop (2002) states that a maximum of 200 ms is suitable for the identification process. The motion completion time was the second metric identified and this was the time taken to complete a movement. The time was taken from the onset of movement till

2. LITERATURE REVIEW

the end of the intended movement. The last metric was the motion-completion rate (Li *et al.*, 2010). According to Ferguson and Dunlop (2002) in order for an amputee to have confidence in the prosthesis a successful classification rate of above 90 % is required. Ferguson and Dunlop (2002) also states that when a user has had more experience with a system the muscle movements will become more constant which leads to higher classification rates.

2.4.3 Control Considerations

Most of the commercially available myoelectric devices which have two DOF's rely on the control algorithm to reliably switch between the two DOF's. The standard algorithms compare EMG signals to a pre-set threshold while recognizing a rapid co-contraction to switch between the DOF's. Some algorithms implement the 'first on' strategy which controls the DOF of the first signal to cross a pre-set 'ON' threshold and releases control when the pre-set 'OFF' threshold is reached, all other signals are therefore locked out (Ajiboye and Weir, 2005).

Fukuda *et al.* (2003) proposed to use a novel statistical neural network called Log-linearized Gaussian Mixture Network (LLGMN). This technique mapped the input EMG patterns to discriminating classes for a small sample size. The beginning and ending of the operator's motions were recognised by calculating the RMS of the EMG signal and compared to a pre-specified motion-appearance threshold. The EMG pattern was extracted by normalizing each channel and then used as the input vector for LLGMN. The LLGMN algorithm is described in Fukuda *et al.* (2003).

The algorithm indicated a probability of the corresponding motions after which the entropy was calculated. When the entropy exceeds the specified discrimination threshold the motor control was suspended because the network output was ambiguous. LLGMN is trained offline to adapt to the differences among amputees and the different locations of the electrodes. Online learning is of great importance because the EMG properties may change during use. Fukuda *et al.* (2003) suggested that task models should be introduced rather than grasp models. In these models the subject will be required to perform a certain task, e.g. picking up a spoon, and these EMG patterns could be mapped to the task.

2.4.4 Amputee Training Techniques

Ngeo *et al.* (2014) used a mirror training scheme, this is known as Mirror Visual Feedback (MVF). Ferguson and Dunlop (2002) applied the electrodes to a subject and the subject had to repeatedly perform six different grasp types. After the data was recorded an offline feature extraction techniques were performed on the dataset and used as training set for a neural network model.

2. LITERATURE REVIEW

In a study done by Sebelius *et al.* (2005) eight pairs of electrodes were attached to the residual limb and a data glove with 18 DOF's equipped to the healthy arm. The subjects were asked to perform 10 movements with their healthy hand and to imagine the same movements with the phantom hand. The subjects were asked to prepare for the training session six weeks earlier. The output from the data glove and the EMG signals were fed to an ANN for the training stage of the network.

Rossouw (2015) asks patients to try and imagine closing their amputated hand while simultaneously closing their healthy hand. With an electromyogram machine the prosthetist searches for a strong EMG signal on the flexor muscles. The prosthetist now searches for an antagonist muscle while the patient tries to imagine closing his amputated hand. The amputee then needs to learn to use these two muscles to control the myoelectric prosthetic device.

In a study done by Chicoine *et al.* (2012) a high classification accuracy was achieved using Prosthesis Guided Training (PGT). PGT is where the prosthetic device mimics the grasp which needs to be trained. The prosthesis aids in the visual feedback of the amputee. The advantage of this technique is that no other hardware is required for the training phase.

2.5 Prosthetic Feedback Interfaces

Amputees will often discard a prosthetic hand when the sensations of touch and effort experienced are not satisfactory (Christiansen *et al.*, 2013). According to Castellini *et al.* (2014) a major limitation of current prosthesis is the lack of feedback to the patient regarding force and position of device. A prosthesis feeding the mechanical response back to the muscle which activated the response can achieve Extended Physiological Proprioception (EPP). This is when the brain adopts the prosthetic device as an extension of the body (Christiansen *et al.*, 2013). The system is described by Castellini *et al.* (2014) in Figure 2.6.

The control system consists of a sensing interface which provides information for autonomous decision making e.g. cameras and inertial sensors; a feedback interface which can communicate the state of the device to the amputee e.g. vibrato- or electro tactile display; the upper limb prosthesis which has its own sensors e.g. force sensors; the user command interface which provides manual control e.g. myoelectric channels; a processing unit analyse and integrate the data from the sensing interface and the user command interface to pre-shape the hand to perform a required grasp. To close the loop to the user the processing unit communicates the current state of the prosthetic device to the user via the feedback interface. The control of the prosthetic device must be shared between the user and the artificial control to decrease the cognitive burden on the user. This is done by having the controller take care of the low level execution details (Castellini *et al.*, 2014).

2. LITERATURE REVIEW

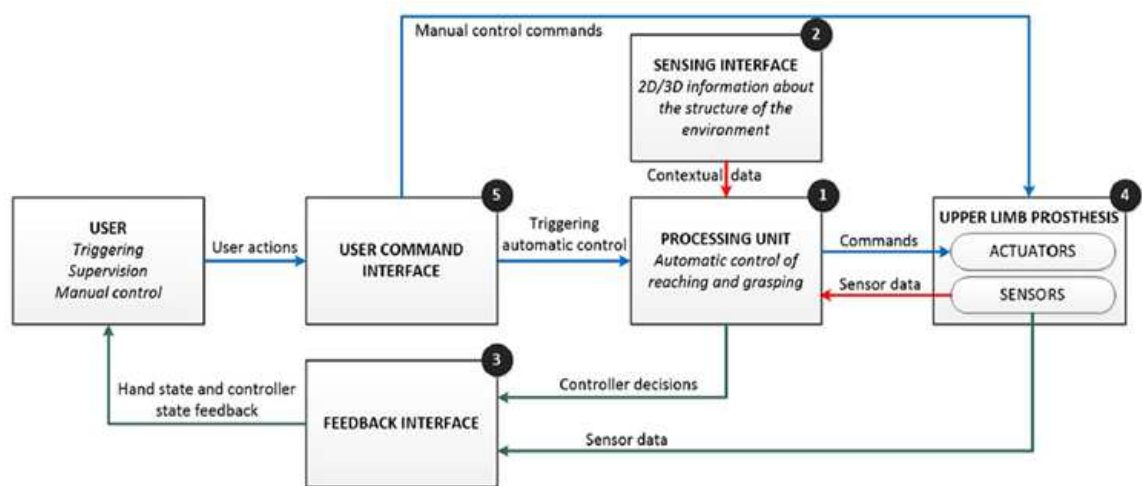


Figure 2.6: Semi-Autonomous Control of a Myoelectric Prosthesis (Adapted from: Castellini *et al.* (2014))

2.5.1 Feedback Information

Contact force with objects when conducting a task is the most significant sensation which needs to be felt (Rodriguez-Cheu and Casals, 2006). The grasping force is proportional to the current in the actuators and could therefore be measured in this way (Rodriguez-Cheu and Casals, 2006).

Slipping can be described as when an object is not grasped with enough force to keep the object steady. To measure the tactile pressure and slipping several sensors needs to be combined. These sensors include several Force Sensitive Resistor (FSR) cells, an accelerometer (detects vibrations in the structure) and a piezoelectric sensor to determine vibrations in the latex covering of a prosthesis. According to Rossouw (2015) the most important feedback to the patient is the grasp force. Rossouw (2015) also suggested to notify the amputee which grasp has been selected by the prosthetic device via a feedback mechanism.

2.5.2 Types of Feedback

The conventional command interfaces of myoelectric devices is a master (user) - slave (device) control setup. A different approach was advocated by Castellini *et al.* (2014) where the system was able to make autonomous and independent decisions while giving feedback to the user via a range of interfaces.

Castellini *et al.* (2014) suggested that a pair of special reading glasses could be fitted with a camera to recognise the shape of objects. The camera image is projected stereoscopically to the display and the user triggers the action via a two-channel myoelectric interface. When the user selects a certain object the system acknowledges the object by covering the object with an overlay. The

2. LITERATURE REVIEW

prosthetic hand is autonomously preshaped to the desired grasp form required for grasping the selected object.

The use of invasive neural interfaces are appealing due to the fact that a ‘physiological’ condition can theoretically be created where the prosthetic hand can communicate with the brain via the afferent and efferent fibres. The use of Longitudinal intrafascicular electrodes (LIFE’s) can be inserted into the fibres to provide sensory feedback from the prosthetic device. This technology indicated good results during short-term trails with human amputees (Micera *et al.*, 2011).

In the 1970’s at the University of Waseda research was done to develop a device which provided feedback in the form of an electrode matrix on the residual limb to communicate the shape of the object to the user (Rodriguez-Cheu and Casals, 2006). Rodriguez-Cheu and Casals (2006) proposed to use a single electro-stimulation signal applied to the residual member. Experiments implied that the feedback signal was perceived differently by the user depending on the frequency band. Between 100-120 Hz nervous fibres are stimulated and the subject perceived an object contact like sensation. Between 30-100 Hz the subjects perceived a sensation of force which increased with decreasing frequency. With lower frequencies the signal goes into some muscular fibres. Between 5-20 Hz the subjects perceived a sensation of sliding since a vibration effect is felt (Rodriguez-Cheu and Casals, 2006).

Christiansen *et al.* (2013) mentioned the use of vibrotactile feedback via an array of tactors which improved the control of a virtual object grasping task. A single tactor should rather be used than an array of tactors to prevent cognitive overloading. Psychophysical studies suggested the loss of skin sensitivity when the skin was exposed to prolonged intense vibration (Christiansen *et al.*, 2013). This phenomenon, adaptation, can be avoided by modifying the vibration amplitude. Assuming the amplitude of vibration to be a function of variable x , the skin sensitivity increases when the amplitude is changed as a function of the logarithm of x (Christiansen *et al.*, 2013).

Another method for feedback is by using the actuators which are already used in the prosthesis to exert a mechanical force on the residual limb. The tactile force exerted over objects can be transmitted to the user in this way (Rodriguez-Cheu and Casals, 2006). This type of feedback was preferred by Rossouw (2015) instead of electrical stimulation and vibrotactile feedback.

2.6 Existing Technologies

Castellini *et al.* (2014) stated that because of the high variability in the population of upper limb amputees, individual solutions are required for the control systems, training and mechatronic components. As discussed in Chapter 1 there are six prosthetic options an upper limb amputee can consider: no prosthesis, cosmetic prosthetics, electrically powered prosthesis, body-powered

2. LITERATURE REVIEW

prosthesis, activity-specific prosthesis and hybrid power prosthesis. The decision of which prosthetic device to use depends on the condition of the residual limb, the level of amputation, the individual goals of the amputee and the available funding. The existing technology in this section focused on electronic powered prosthetic devices for transradial amputees. Each existing device was analysed according to the degrees of freedom, feedback options, available grasps and miscellaneous features. Myoelectric prosthesis acceptance are influenced by the following factors: noise, weight, cosmetic appearance, battery duration, price and the expense of servicing (Castellini *et al.*, 2014). According to Carrozza *et al.* (2001) the main limitations of commercially available prostheses are the non-cosmetic appearance, reduced grasping capabilities, lack of feedback to the amputee and the need of a ‘natural’ command interface. Carrozza *et al.* (2001) suggested that to solve the first and second problems more active and passive degrees of freedom should be added to the hand. The third and fourth problems can be solved by developing a natural neural interface between the prosthetic device and the Peripheral Nervous System (PNS).

2.6.1 i-limb™ - Touch-bionics

The i-limb™ was created by touchbionics and comprises of a completely functional electrical prosthetic hand as seen in Figure 2.7.



Figure 2.7: The i-limb™ Prosthetic Hand (Touchbionics, 2015)

A range called the i-limb™ revolution is an externally powered, multi-articulating prosthetic hand which is able to produce 36 grip features. The thumb moves automatically to pinch or tripod positions. This hand moves

2. LITERATURE REVIEW

to a natural hand position after a certain time has elapsed. This hand is equipped with auto-grasp technology which tightens the grip if it senses slipping of the object. It is possible to assign certain grasps to a muscle activation pattern - for example a double pinch muscle contraction can be assigned to a tripod grip (Touchbionics, 2015). This prosthetic device uses two EMG-electrodes and implements a triggered control algorithm to select between different grasps.

An extra feature to this hand is the grip chips which can be used to perform daily tasks. A grip chip could be placed around your computer and will communicate to the i-limb via Bluetooth and the i-limb™ will form a grasp suitable for typing on the computer. The i-limb™ has an application installable on a mobile phone to activate 36 grip features or patterns (Touchbionics, 2015).

It is possible to rotate the wrist by either locking the wrist at certain angles or it could be free moving with a tension spring. The i-limb™ has five different actuators - one for each digit. A conductive tip is placed on the index finger to enable the amputee to type on touch-screens. The i-limb™ has natural skin coverings made from silicone which covers the device like a glove (Touchbionics, 2015). The device weighs between 0.5-0.6 kg dependable on the extra features added. The device is able to produce a power grasp force of 136 N and a lateral pinch force of 35 N. The static hand load limit is 90 kg (Touchbionics, 2015). The cost for this hand is from R509 618 upwards depending on the remaining limb length.

2.6.2 bebionic™ - Steeper

The bebionic™ prosthetic hand is a multi-articulating myoelectric hand. The bebionic™ has individual motors for each finger to provide natural movements when gripping an object and is seen in Figure 2.8. This hand has 14 selectable grip patterns with proportional speed control to allow precise movements of the fingers (Steeper, 2015).

2. LITERATURE REVIEW



Figure 2.8: The bebionic™ Prosthetic Hand (Steeper, 2015)

This prosthetic hand allows for passive wrist movement or locking the wrist in 30° flexion or 30° extension. The thumb position has to be moved manually. The auto-grip feature will adjust the grip when the system senses that an object is slipping. It is possible to fold away the fingers to provide a natural looking hand when walking (Steeper, 2015).

The bebionic™ has a mobile application which can be used to adjust the grip power, speed and to rank different gripping patterns. It is possible to wear a skin-matchable silicone glove with the bebionic™. This device uses a bio-compatible titanium skin contact which is situated within the socket to ensure better myoelectric signal readings. This prosthetic device uses two EMG-electrodes and implements a triggered control algorithm to select between different grasps.

The weight of the bebionic™ ranges between 0.56-0.6 kg. A maximum power grip of 140 N is possible and a maximum tripod grip of 36.6 N (Steeper, 2015). This hand is offered at R147 589.

Chapter 3

Pattern Classification Model

3.1 Theory

This section describes the theory of different features and pattern classification models. A pattern classification model can be described as a model which makes inferences from a dataset based on probability, computational geometry, signal processing and statistics. As mentioned in Section 2.4, a pattern classification model can be applied to a dataset of forearm EMG signals to distinguish between different grasp types.

3.1.1 Feature Extraction

A signal feature can be defined as a distinctive characteristic of a signal. Features can be combined to form a feature vector in a f -dimensional feature space, where f is the number of features. Features were selected based on computational time and complexity. Time-domain features have a low computational time and are easy to calculate. The most common EMG features used in literature were tested. The following features were used in this study.

Root Mean Square (RMS): The RMS is the square root of the arithmetic mean of in a segment with n values.

$$x_{RMS} = \sqrt{\frac{1}{n} \sum_{i=1}^n (x_i^2)} \quad (3.1)$$

Here x_i was the EMG signal measured, x_{RMS} the RMS value for a specific segment and n the number of EMG samples.

Mean Absolute Value (MAV): The MAV is the mean of the absolute value of the signal.

$$x_{MAV} = \frac{1}{n} \sum_{i=1}^n |x_i| \quad (3.2)$$

3. PATTERN CLASSIFICATION MODEL

Auto Regressive Model (AR): According to Zecca *et al.* (2002) an EMG signal can be regarded as a stationary Gaussian process for a short interval. The EMG signal can be modelled as:

$$x_i = \sum_{j=1}^{N_{AR}} a_j x_{i-j} + e_i \quad (3.3)$$

Here N_{AR} is the order of the AR model, a_j is an estimate of the AR coefficients and e_k is the residual white noise

Variance (VAR): The variance is a measure of the power of the EMG signal and is given by:

$$x_{VAR} = \sigma^2 = \frac{1}{n-1} \sum_{i=1}^n x_i^2 \quad (3.4)$$

Willison Amplitude (WAMP): The number of times the absolute value of the signal is above a specified threshold:

$$x_{WAMP} = \sum_{i=1}^n f(|x_i - x_{i+1}|) \quad (3.5)$$

$$\text{Where: } f(z) = \begin{cases} 1, & \text{if } z > \text{threshold} \\ 0, & \text{otherwise} \end{cases}$$

Myopulse Percentage Rate (MYOP): This feature calculates the percentage of EMG signals that are above a specified threshold in a segment.

$$x_{MYOP} = \frac{1}{n} \sum_{i=1}^n f(|x_i|) \quad (3.6)$$

$$\text{Where: } f(z) = \begin{cases} 1, & \text{if } z > \text{threshold} \\ 0, & \text{otherwise} \end{cases}$$

Slope Sign Changes (SSC): The SSC provides information regarding the frequency of the EMG signal. The SSC is determined using three consecutive samples in a segment.

$$x_{SSC} = \sum_{i=1}^n f((x_i - x_{i-1})(x_i - x_{i+1})) \quad (3.7)$$

$$\text{Where: } f(z) = \begin{cases} 1, & \text{if } z > 0 \\ 0, & \text{otherwise} \end{cases}$$

Waveform Length (WL): The WL is the sum of the length of the waveform over a segment.

3. PATTERN CLASSIFICATION MODEL

$$x_{WL} = \sum_{i=1}^n |x_i - x_{i-1}| \quad (3.8)$$

Energy of Wavelet Coefficients (EWC): The EWC calculates how much of the signal was kept after a Wavelet Transform. This feature was found to be one of the best features in Bach (2009). This function performed a wavelet decomposition and then calculated the wave energy using MATLAB functions.

3.1.2 Pattern Classification Techniques

Several pattern classification techniques were considered in this study. The three pattern classification techniques that were considered for this project were Linear Discriminant Analysis (LDA), k-Nearest Neighbours (kNN) and a Self-Organizing Map (SOM).

LDA was invented by Fisher (1936). LDA assumes that different classes generate data based on different Gaussian distributions. LDA is a supervised pattern classification technique which is used to reduce the dimensionality for pattern classification. Figure A.1 in Appendix A.1 illustrates a flow diagram for a LDA algorithm. In the first step the dimensionality is reduced by calculating the mean vectors of each class for each dimension to create a $1 \times f$ matrix where f is the number of features. Within-class scatter matrices for each class are calculated and added together to create a $f \times f$ matrix. Between-class scatter matrices are computed and the eigenvectors for $S_w^{-1}S_B$ are computed. Here S_w is the within-class matrix and S_B is the between-class matrix. The eigenvectors are sorted by decreasing eigenvalues and k eigenvectors with the largest eigenvalues chosen to form a $f \times k$ matrix. The transformed samples can be calculated by $Y = XW$ where W is the eigenvector matrix, X is the feature samples and Y the transformed samples.

Figure A.2 in Appendix A.1 illustrates a flow diagram for a kNN algorithm. kNN is a supervised learning method. With kNN the training phase consists of saving the feature vectors and class labels. When an unlabelled feature vector is submitted to the kNN algorithm the vector is classified by the label of the k-nearest training samples. The distance between vectors was calculated using the Euclidean distance.

The Kohonen SOM was invented by Teuvo Kohonen and is a vector quantisation technique to represent multidimensional data in much lower dimensions. The network consists of a lattice of nodes. These nodes are fully connected to the input vector. A SOM is a data clustering technique which was used as a data classification technique in this project. Each node contains a vector of weights. The weight vector has the same dimensions as the input layer. A SOM can classify data without supervision. It is not necessary to specify a target output when the lattice is optimized. The algorithm uses an initial dis-

3. PATTERN CLASSIFICATION MODEL

tribution of random weights for each node and iterates until the node weights match the input vector. After the zones in the map stabilizes each zone is effectively a class. Any new input vectors will stimulate the nodes with the same weights as the input vector.

To stabilize these nodes the training phase takes several iterations. Figure 3.5 in Section 3.3 illustrates a flow diagram for a SOM algorithm. A vector is chosen at random from the training set. This vector is compared to each node of the lattice and the Best Matching Unit (BMU) is calculated. The BMU is calculated using the Euclidean distance between the vectors. The radius of the neighbourhood of the BMU is calculated and this radius shrinks every iteration using a decay function. Each of the neighbouring nodes' weights is altered to be closer to the BMU's weights. The closer the node is to the BMU the more it gets adjusted. When the training is finished the neighbourhood will be the size of the BMU. The next step was to determine which one of these pattern classification techniques had the best performance with grasp classification.

3.2 Pattern Classification Verification

This section verified different classification techniques using an existing database. This section served as an introduction to the methods that was followed in Section 5. In this section the classifier and feature sets were established.

3.2.1 Methodology

An existing database was used to test the pattern classification techniques used in this project (NinaPro, 2014). The NinaPro project created a sEMG activity database to aid in the development of myoelectric prosthetic devices. The algorithms used in this project were tested with the NinaPro database using MATLAB[®] (2014). After the best technique was established it was implemented on an Android device in Section 5.

The NinaPro (2014) database included data acquired from 40 non-amputated subjects and 11 hand-amputated subjects. The subjects had to perform several tasks and grasps while the sEMG signals were recorded. The three pattern classification techniques mentioned in Section 3.1.2 were used for determining the classification performance. These pattern classification techniques were compared to each other based on classification accuracy.

The computational software required for this step was MATLAB[®] (2014). For this task the data sets from 20 non-amputated subjects and six hand-amputated subjects were used. The reason for using less subjects than the available data was because some of the subjects did not perform all of the grasps. The most important grasps for amputees were investigated in Section 2.2. The three grasp types were: large diameter grasp, tripod grasp and an

3. PATTERN CLASSIFICATION MODEL

index point gesture. Each movement was repeated six times. The training data varied from two to five repetitions while the sixth repetition was used as test data. Each repetition contributed to one training set.

Dataset two and three of NinaPro were used. This data was sampled at 2 kHz and was decimated in MATLAB by a factor of 10 to match the sampling rate of the EMG sensors used in this project. A fixed window size and window shift size was used to determine the best classification technique. Features were extracted on a 400 ms window with an increment of 100 ms which is equal to 80 EMG samples and 20 EMG samples respectively.

3.2.2 Results

A program was written to determine the features with the most accurate classification rate. Throughout this document the classification rate refers to the true positive rate. A true positive is an example correctly classified as a positive. The classification rate calculated here was the classification rate of the validation set. The classification rate (CR) was calculated as the number of correctly classified window segments divided by the total number of segments and is given in Equation 3.9.

$$CR = \frac{\text{Correct Windows}}{\text{Total Windows}} \times 100\% \quad (3.9)$$

It was determined that increasing the number of features extracted simultaneously increased the classification rate but decreased the computational time. It was decided to extract only three features simultaneously in a feature set. This decision was based on the computational time and classification accuracy which increased as more features were added to a feature set. The program iterated between the 84 feature set combinations, with three features per set, of the nine features mentioned in Section 3.1.1. Part of this study was to calculate the optimum size of the training sets required for accurate grasp classification. Figure 3.1 displays the 95 % confidence intervals and means using 20 non-amputated subjects. The best feature set for each classification technique was used to compare the three classification techniques at different training set sizes.

It can be seen that increasing the number of training sets had different effects on the classification techniques. The classification rate decreased after four training sets for SOM and kNN and increased for LDA over the five sets of training data. The 95 % confidence interval decreased for SOM up to four training sets while remaining almost the same for the other two techniques. It was decided to use three data sets for further calculations. The reason for this was to minimise muscle fatigue when training the classification technique using amputated subjects and to reduce computational time. It can also be seen that the classification rate did not increase substantially between three and four training sets.

3. PATTERN CLASSIFICATION MODEL

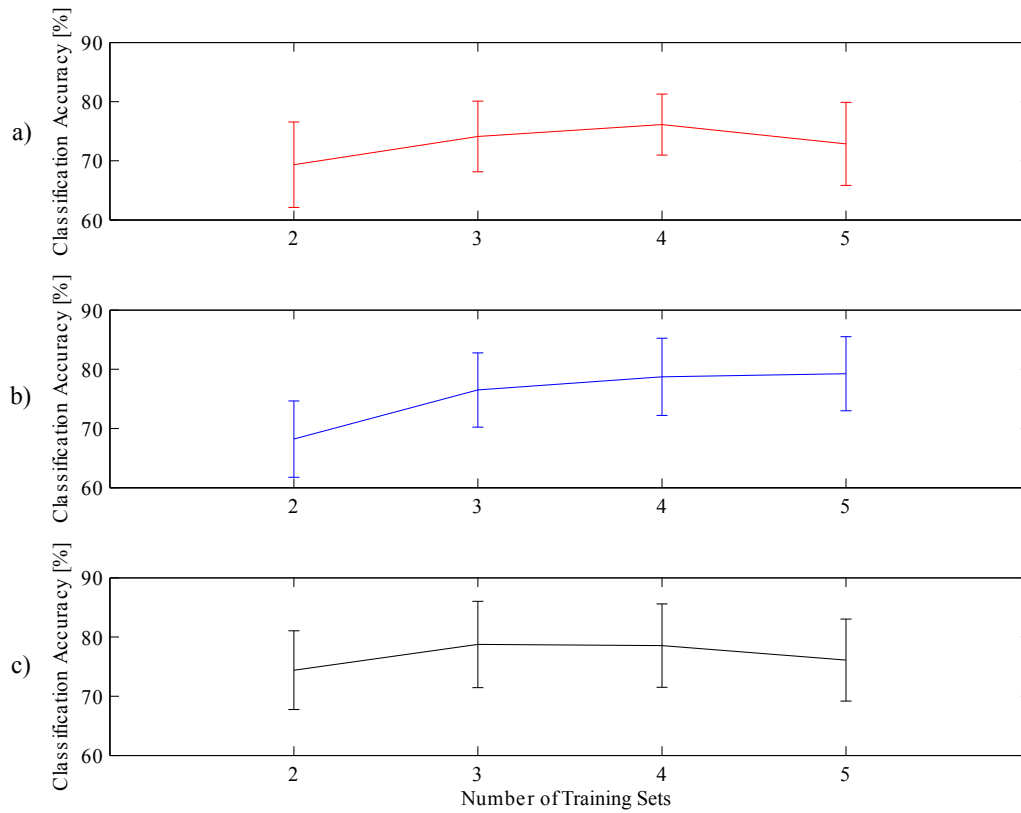


Figure 3.1: Comparison of Different Classification Techniques for Non-Amputated. a) SOM; b) LDA; c) kNN

The algorithm calculated a classification rate for each classifier and feature set combination for a specified window size and window increment size. The description of each feature set were categorised in Appendix A.2 in Table A.1. The overall 10 best features for each classification technique are given in Table 3.1.

3. PATTERN CLASSIFICATION MODEL

Table 3.1: Best Features for Different Classifiers for Non-Amputated Subjects

SOM		LDA		kNN	
Set Number	Classification Rate	Set Number	Classification Rate	Set Number	Classification Rate
43	74.11	3	76.50	24	78.75
25	69.63	23	76.49	45	78.75
19	68.36	5	75.90	69	78.75
4	68.19	44	75.23	79	78.75
15	68.05	7	74.47	83	78.75
7	68.00	47	73.94	6	78.57
22	67.45	26	73.72	17	78.57
6	67.43	4	73.11	21	78.57
21	67.43	21	73.09	28	78.57
24	67.43	81	73.08	38	78.57

The maximum standard deviation between different feature sets in the top 10 was 1.94 % for SOM. The feature sets which performed the best were MAV, MYOP, AR for SOM, RMS, MAV, MYOP for LDA and RMS, SSC, WL for kNN. Figure A.3 in Appendix A.2 displays an overall comparison of the different feature sets for each classification technique. It can be seen that the worst feature set for SOM and kNN was MAV, MYOP and EWC and MAV, VAR and WL for LDA. Except for nine feature sets the overall classification rate was above 60 % for each feature set. A t-test was done between the best feature set and worst feature set and indicated a statistical difference between the worst and the best feature set for all three classification techniques ($p < 0.001$).

The same procedure was followed using a database with data from amputated subjects. Figure 3.2 illustrates the different classification techniques for different training set sizes using six amputated subjects.

The SOM reached a maximum classification rate of 70.8 % at four data sets and LDA a maximum of 80.58 % at four sets. The classification rate decreased for kNN from two data sets onwards. The 95 % confidence interval reached a minimum for LDA using four data sets. The overall five best features for three data sets for the classification techniques are given in Table 3.2.

The feature sets which performed the best were RMS, SSC, EWC for SOM, RMS, EWC, WL for LDA and RMS, MAV, AR for kNN. Figure A.4 in Appendix A.2 illustrates an overall comparison of the different feature sets for each classification technique.

3. PATTERN CLASSIFICATION MODEL

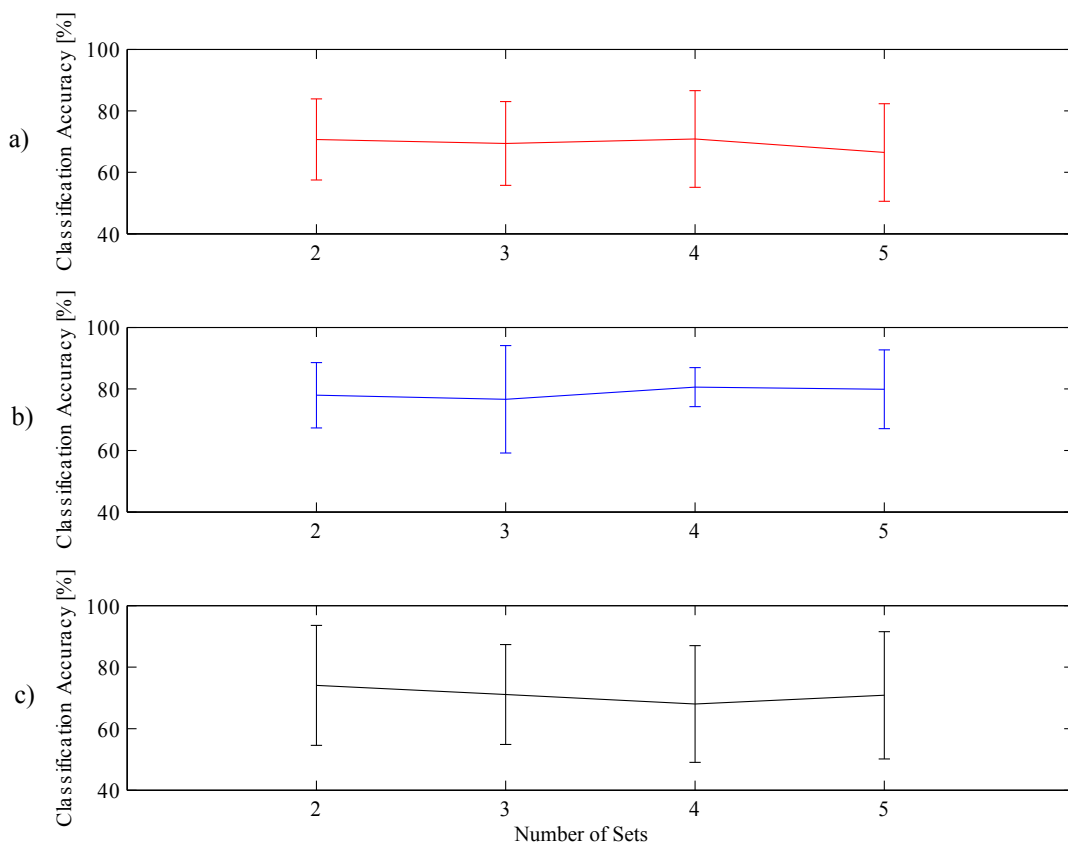


Figure 3.2: Comparison of Different Classification Techniques for Amputated Subjects. a) SOM; b) LDA; c) kNN

Table 3.2: Best Features for Different Classifiers for Amputated Subjects

SOM		LDA		kNN	
Set Number	Classification Rate	Set Number	Classification Rate	Set Number	Classification Rate
27	69.37	26	76.64	23	71.08
4	68.13	47	74.25	5	70.52
19	68.13	16	73.96	20	70.52
25	68.13	24	73.64	27	70.52
20	67.25	27	72.88	4	68.19

The feature calculation time can also be used to distinguish feature sets. Table 3.3 gives the time in seconds of each feature calculated in MATLAB.

3. PATTERN CLASSIFICATION MODEL

It should be noted that this time was dependent on the processing speed of the computer but this gave a relative idea of which features took longer to calculate.

Table 3.3: Calculation Time for Features in Seconds

Feature	Time [s]
RMS	0.0071
MAV	0.0083
VAR	0.0012
WAMP	0.0043
MYOP	0.0045
SSC	0.0059
EWC	0.3511
WL	0.0038
AR	0.0074

From this table it was clear that EWC took the longest to calculate while VAR took the shortest time to calculate.

3.2.3 Discussion

The preliminary results implied that a kNN classifier performed the best with 78.75 % using RMS, SSC and WL. It was, however, decided to implement a SOM classifier on an Android device for its simplicity. Previous experience within the research group also contributed to this decision. The reason for some of the less accurate feature sets using LDA was because the LDA classifier needed a non-singular and a good scaled matrix. The feature matrices from the amputated subjects were often singular and badly scaled.

The classification results for the top 10 feature sets for SOM were within 7 % from each other and it was decided to use the feature sets that could be calculated quickly in real time. The feature sets chosen for implementation on the Android device were also based on the fact that a different EMG acquisition device was used. It was decided not to use feature sets with the AR feature as this increased the size of the weights in the SOM which increased the classification time. It was concluded that EWC would not work in a live classification with window sizes as small as 0.4 seconds. The feature sets chosen, based on the above criteria, for implementation were RMS, MAV, SSC; RMS, WAMP, SSC and RMS, MAV, WL. These feature sets were ranked fourth, fifth and eighth respectively for SOM. These feature sets were compared in real time on the Android device in Section 5.

3. PATTERN CLASSIFICATION MODEL

A statistical analysis compared the data of the non-amputated subjects and the amputated subjects for a SOM, three data sets and the above selected features. The 95 % confidence intervals are shown in Figure 3.3. A two-sampled t-test was used for each feature set with the null hypothesis that the two data samples are from populations with equal means. RMS, MAV, SSC had the highest p-value of 0.99; RMS, MAV, WL was 0.59 and RMS, WAMP, SSC was 0.61. This indicated a greater similarity between amputated subjects and non-amputated subjects when using the RMS, MAV, SSC feature set. Using the p-values it was clear that there was no statistical difference between amputated subjects and non-amputated subjects for the different feature sets. The SOM classifier with the three feature sets mentioned above was tested in Section 5 using the acquisition system developed in this project.

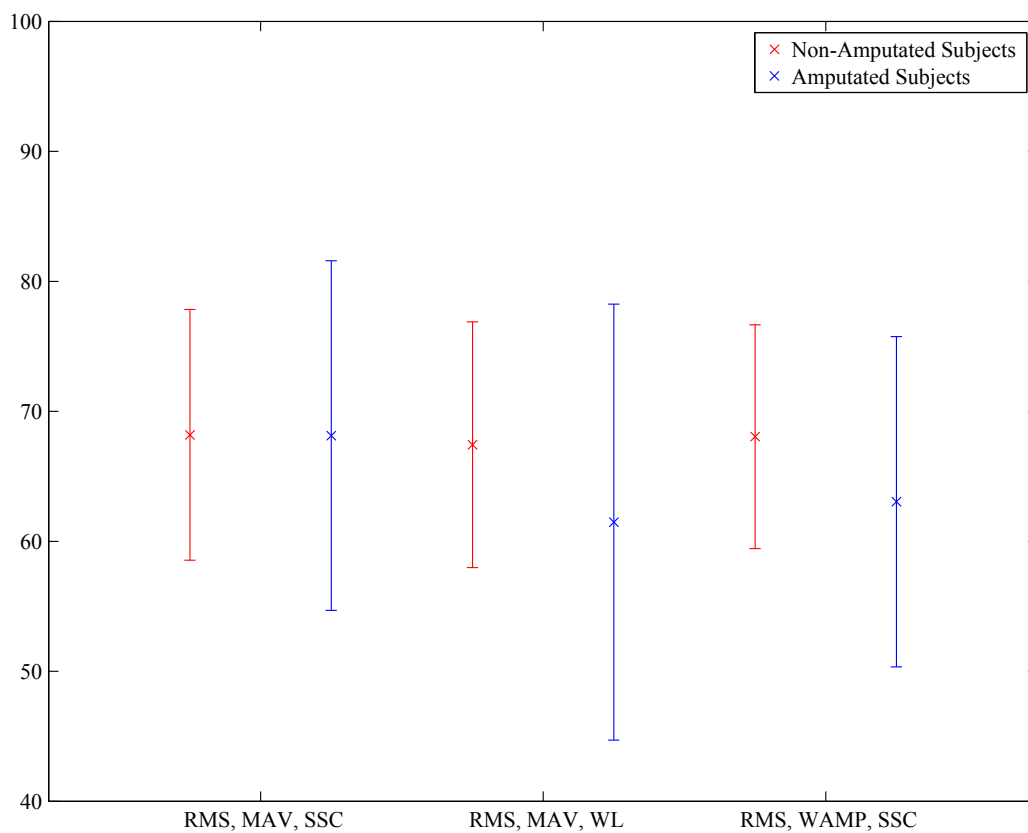


Figure 3.3: Comparison of Non-Amputated Subjects and Amputated Subjects for SOM and selected Feature Sets

3. PATTERN CLASSIFICATION MODEL

3.3 Pattern Classification Model Implemented

The SOM implemented on the Android device was a straightforward implementation of this pattern classification technique. This SOM can be improved by adding more nodes to create a bigger lattice and neighbourhoods or by implementing other decay functions. A bigger lattice will however have a longer calculation time. The preliminary results were satisfactory for this project and therefore this SOM was used.

The input vector consisted of 24 weights while the lattice had four rows for the four classes and one column. The four classes represented the four grasps to be classified. Each of these nodes consisted of 24 weights. This lattice is illustrated in Figure 3.4. The green circles represents the nodes while the blue circles represents the input vector. Figure 3.5 illustrates the flow diagram implemented for the SOM.

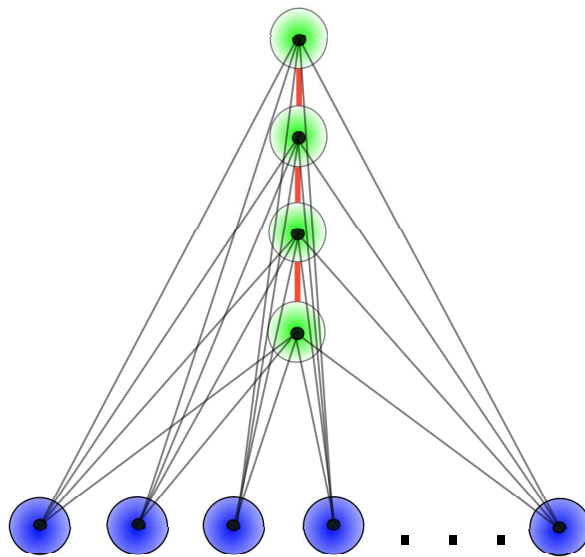


Figure 3.4: Kohonen Self-Organizing Map (Illustration: LC Theron)

3. PATTERN CLASSIFICATION MODEL

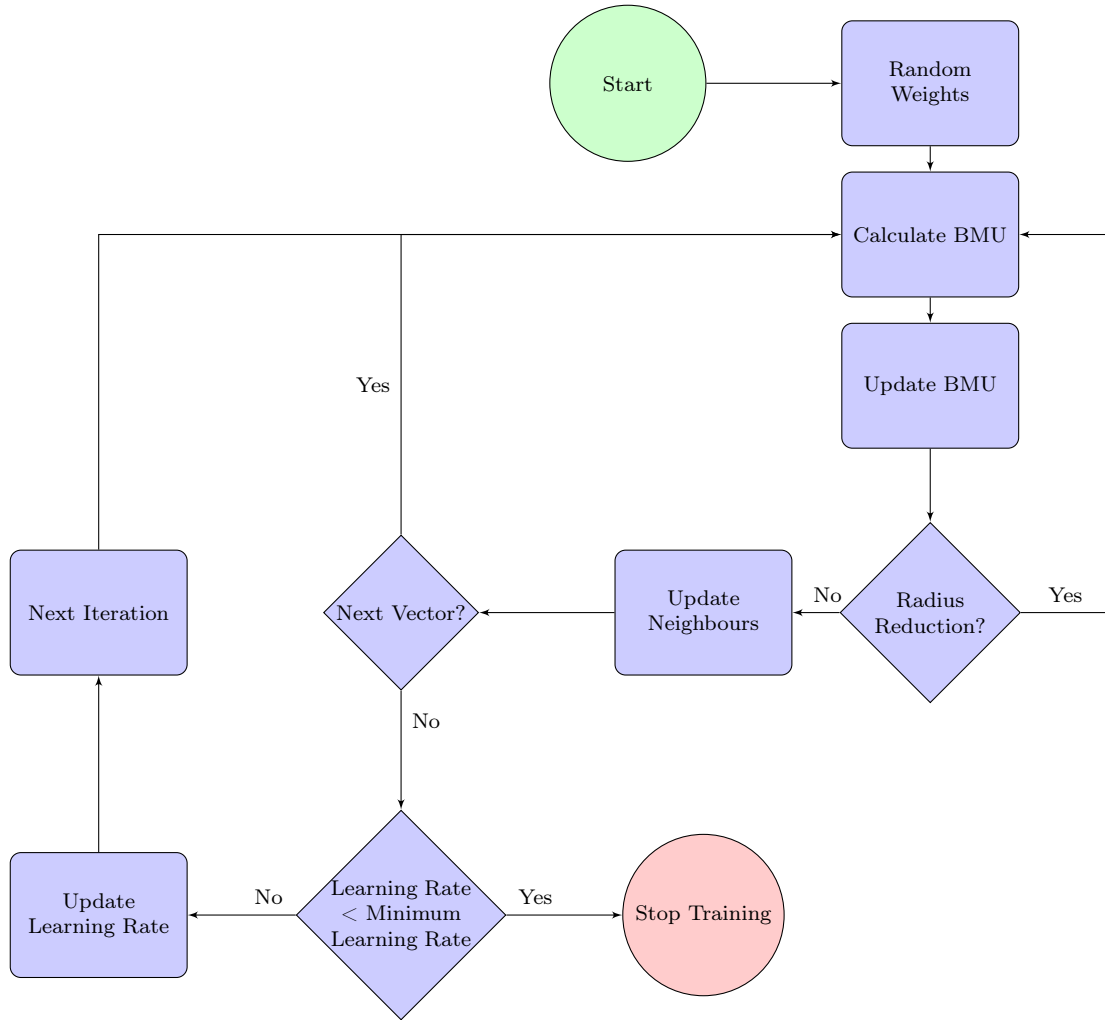


Figure 3.5: Flow Diagram for SOM (Illustration: LC Theron)

Random weights with 24 dimensions were assigned to each node in the lattice. After this a random vector was chosen from the training data as input to the lattice. The BMU was calculated using the Euclidean distance (without the square root) as given in Equation 3.10.

$$d_v = \sum_{i=1}^f (v_i - w_i)^2 \quad (3.10)$$

Here d_v was the distance between each vector, i indicated the vector index, f the number of features, v the input and w the weight. The node with the shortest distance was the BMU. The BMU was updated using Equation 3.11.

$$W_{BMU} = W_{BMU} + \alpha_{LR}(V - W_{BMU}) \quad (3.11)$$

3. PATTERN CLASSIFICATION MODEL

Here α_{LR} was the learning rate and W_{BMU} and V the weight and input vector respectively. After this the algorithm checked whether the SOM needed to update the neighbouring nodes. This was done by checking if the SOM had reached the radius reduction point which was set at the last 20 % of the iterations. If the SOM had passed the radius reduction point the algorithm will go to the next vector. If the SOM did not pass this point the neighbouring nodes were updated in the same way as in Equation 3.11 but substituting the W_{BMU} term with the weight of that particular node.

If the process had not reached the end of the training data set it looped back to calculating the BMU of the next vector. Otherwise the algorithm checked whether the learning rate was smaller than the minimum learning rate which was specified to achieve 110 iterations. If the learning rate was higher the learning rate would be updated with Equation 3.12

$$\alpha = \alpha \times \beta_{decay} \quad (3.12)$$

Here β_{decay} was the decay rate of the learning rate. After this the next iteration looped back to calculating the BMU of another vector from the training data. If the learning rate was smaller than the minimum learning rate the training was completed and the SOM was ready for use.

Chapter 4

Design Methodology

In this section the different design concepts developed for this project is discussed. The focus was on several concepts including the actuation system, electronic components and multi-platform software design. The design of the socket attaching the prosthetic hand to the amputated arm was not part of the objectives.

4.1 Hardware Design

A complete layout of the mechanical components used in this prosthesis is illustrated in Figure 4.1 and summarised in Table 4.1. The assembly is described in Appendix B.4.

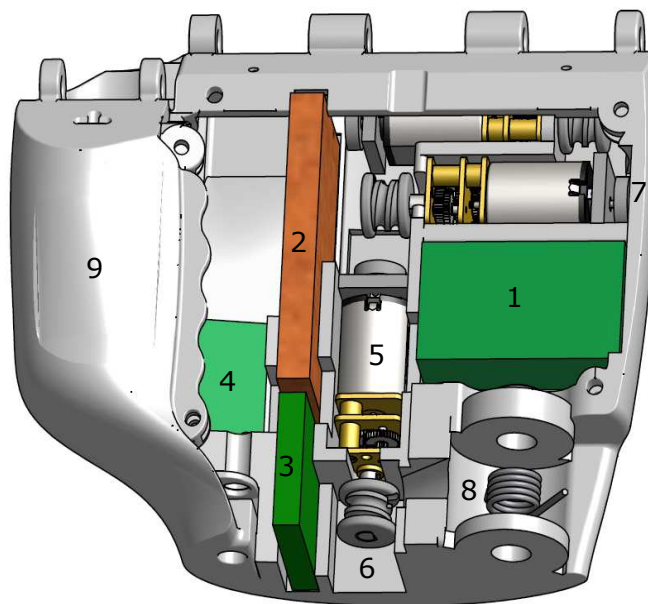


Figure 4.1: Electromechanical Components Layout (Illustration: LC Theron)

4. DESIGN METHODOLOGY

Table 4.1: Electromechanical Components Used

Number	Quantity	Component
1	2	Pololu Qik 2s9v1 Motor Driver
2	1	RedbearLab BlendMicro Controller
3	1	Custom Current Sensor PCB
4	1	Power Supply PCB
5	4	Micro Metal Gearmotor
6	4	Custom Spool
7	4	Pololu Magnetic Motor Encoder
8	1	Torsion Spring
9	1	Palm Enclosure

The mechanical prototype developed by Tenim (2014) implemented a mechanical differential mechanism which granted the amputee dexterous control over the prosthetic hand. This differential mechanism was actuated using one cable attached to a shoulder harness. The idea of converting the mechanical prosthetic hand to an electrical prosthetic hand was to keep some of the mechanical parts the same.

It was decided to remove the differential mechanisms inside the palm of the prosthetic hand to make room for actuators and electronic components. In order to grant control over all five fingers five actuators were required. As only four actuators could be fitted inside the palm it was decided to use one actuator for the fourth and fifth finger. With this concept all of the electronics could be fitted inside of the palm, except the battery which was situated inside of the socket.

The actuation system included the spools and cables required to move the fingers. The spool was connected to the motor shaft which had a cable wound around the spool. This spool was designed and 3D-printed and can be seen in Figure 4.1. All of the mechanical components that needed to be manufactured was printed using ABS material on an extrusion 3-D printer in the Biomedical Laboratory of the University of Stellenbosch (Zortrax, 2016).

4.1.1 Determine Motor Torque to Close Unloaded Hand

It was necessary to calculate the motor torque which could overcome the internal moments of the phalanges. These internal moments were a function of the flexion angle, θ , which is illustrated in Figure 4.2

4. DESIGN METHODOLOGY

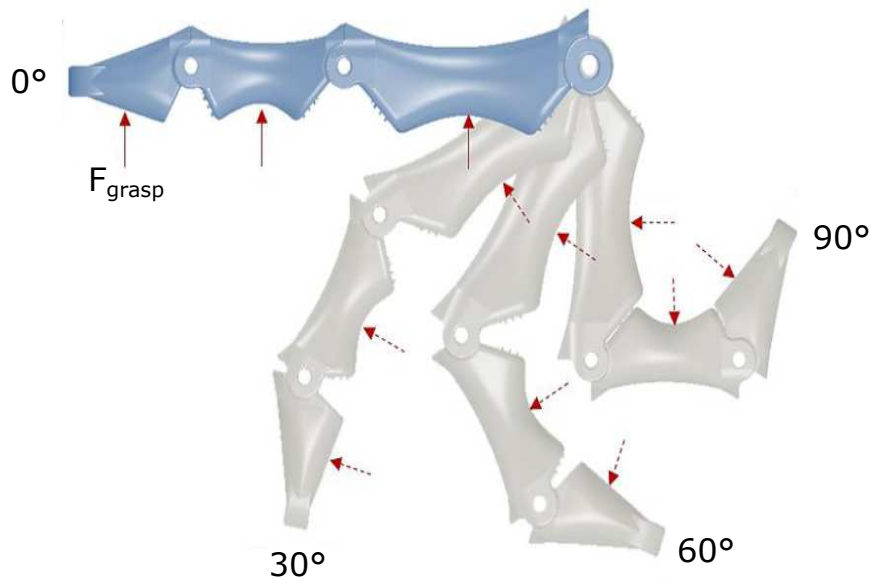


Figure 4.2: Force Diagram Indicating Grasp Forces as a Function of Flexion Angle θ (Adapted from: Tenim (2014))

An analytical finger model was adapted from Tenim (2014) to calculate the required motor torque. The flexion of the MCP and PIP of the 2nd to 5th digits had a maximum θ of 90° while the maximum θ of the DIP of the 2nd to 5th digits and the MCP of the thumb had a maximum of 60° . The IP of the thumb had a maximum of 80° .

The torque of each motor was increased to determine at which point the tension moments exceeded the internal moments for a full range of θ . Table 4.2 gives a summary of the minimum motor torque per finger required to close the unloaded hand. The motor torque was increased with 1 N.mm until the tension moments of the cable were greater than the internal moments. The internal moments were the spring moment, mass-moments and hinge friction moments. A description of these equations are given in Appendix B.1. It was assumed that the motor torque of the 4th and the 5th finger would be divided equally between the digits.

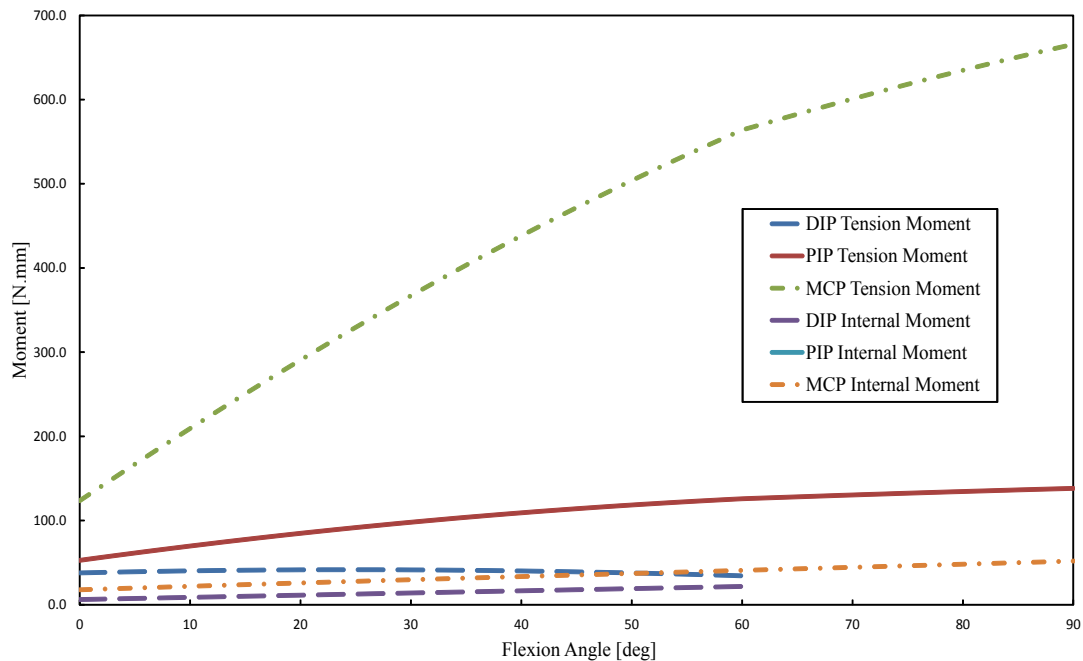
4. DESIGN METHODOLOGY

Table 4.2: Input motor torque for flexion of unloaded joints [N.mm]

Digit	DIP	PIP (IP Thumb)	MCP
1st	-	38	11
2nd	5	4	4
3rd	11	6	4
4th	15	8	7
5th	26	6	6

As the 4th and 5th digit were connected to the same motor it was clear that a motor which could supply at least 41 N.mm of torque will close the unloaded hand.

Figure 4.3 displays the tension moments of the 5th digit compared to the internal moments for a motor torque of 41 N.mm. The tension moment was the moment exerted on the phalanges as a result of the actuating cable.

**Figure 4.3: 5th Digit Tension Moments vs. Internal Moments as a function of Flexion Angle**

It can be seen that the tension moments were greater than the internal moments across all flexion angles which indicates that the finger will fully close at a motor torque of 41 N.mm.

4. DESIGN METHODOLOGY

4.1.2 Calculate Total Grasp Force as a Function of Motor Torque

Using the analytical model the grasp force could be calculated as a function of motor torque and flexion angle. The flexion angle θ was illustrated in Figure 4.2.

For this calculation it was assumed that all resultant moments were transferred to the object being grasped. This meant that each phalanx made contact with the grasped object. When an object was grasped a reaction force acts on each phalanx. It was assumed that these reaction forces were distributed equally between each phalanx. Equation 4.1 (Tenim, 2014) was used to calculate the grasp moment on each phalanx.

$$\sum M_{Grasp} = \sum M_{Tension} - \sum M_{Mass} - \sum M_{Spring} - \sum M_{Hinge} \quad (4.1)$$

Where M_{Grasp} was the grasp moment applied to an object, $M_{Tension}$ was the moments exerted on the phalanges as a result of the actuating cable, M_{Mass} was the mass moment of the finger, M_{Spring} was the spring moment and M_{Hinge} accounted for all friction losses.

Using the length of each phalanx at different angles the moment arm for each phalanx was used to calculate the grasp force of each phalanx. The grasp force on each phalanx was calculated as a function of motor torque and flexion angle and were summed together to get the grasp force per finger. To get the total grasp force the grasp force per finger were summed together.

Figure 4.4 illustrates a graph of the total grasp force as a function of flexion angle and motor torque. The motor torque in Figure 4.4 was the torque of individual motors. From Figure 4.4 it is clear that the grasp force increased as the motor torque and flexion angle increased. A maximum grasp force of 533 N was calculated at a flexion angle of 90° and 0.495 N.m motor torque. Objects are seldom grasped at a flexion angle of 90°, therefore the maximum grasp force was estimated at a 60° angle with 480 N. The motor torque had a linear relation to the total grasp force.

4. DESIGN METHODOLOGY

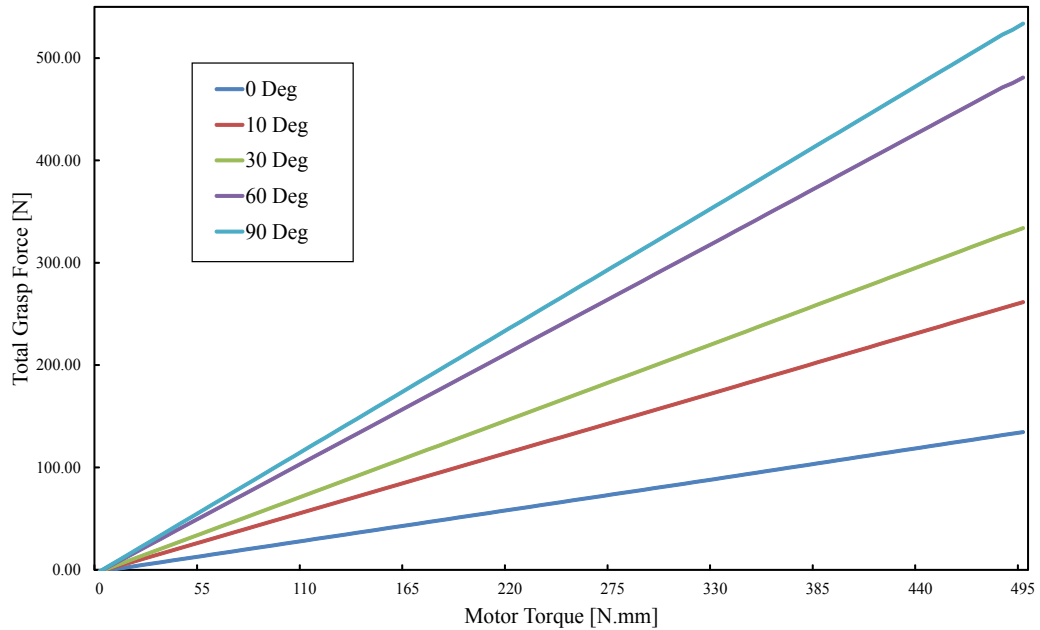


Figure 4.4: Total Grasp Force vs Motor Torque vs Flexion Angle

The torque of the motor can be related to the current drawn by the motor. Therefore using this model the grasp force can be controlled by controlling the current. As stated above this model was an estimation of the total grasp force if all phalanges were in contact with an object. This was applicable to cylindrical objects and not objects with an asymmetrical surface. Such objects would experience lower grasp forces.

4.1.3 Motor Selection

The four aspects that were considered for the actuators were speed, torque, dimensions and affordability. Four micro metal gearmotors with external shafts were used. These motors were manufactured by Pololu. These motors as well as the specifications can be seen in Figure 4.5.

4. DESIGN METHODOLOGY



Figure 4.5: Specifications of Micro Metal Gearmotor (Adapted from: Pololu (2016))

It was calculated that a motor supplying a torque of at least 0.041 N.mm will overcome the internal moments. The diameter of the pulley was based on the required speed, required force and available space inside of the palm. With a diameter of 6 mm a cable force of 82.3 N was achieved if the motors were running at 6 V. Using the datasheet from Pololu (2016) and the minimum torque required to close the fingers a maximum speed of 91.7 RPM could be achieved. The maximum revolutions to close the hand was two revolutions for the third finger. This gave a maximum of 1.3 seconds to close the unloaded hand. By using four of these motors this prosthetic hand could theoretically provide a grasp force of 480 N at a flexion angle of 60°. This was compared to the maximum grasp force of the Bebionic hand in Section 2.6 which was 140 N. It was expected that this grasp force was tested rather than calculated analytically. A grasp force test will confirm whether this hand could supply a grasp force of 480 N at 60° flexion and at maximum torque.

4.2 Electronic Design

The electronic components of this prosthetic hand consisted of the motor drivers, current sensors, power supply, microcontroller and motor encoders. The electronic devices used in this project was the Myo Armband and an Android device. The layout, data flow and electrical connections is illustrated in Figure 4.6. Each of these aspects will be discussed individually in this section.

4. DESIGN METHODOLOGY

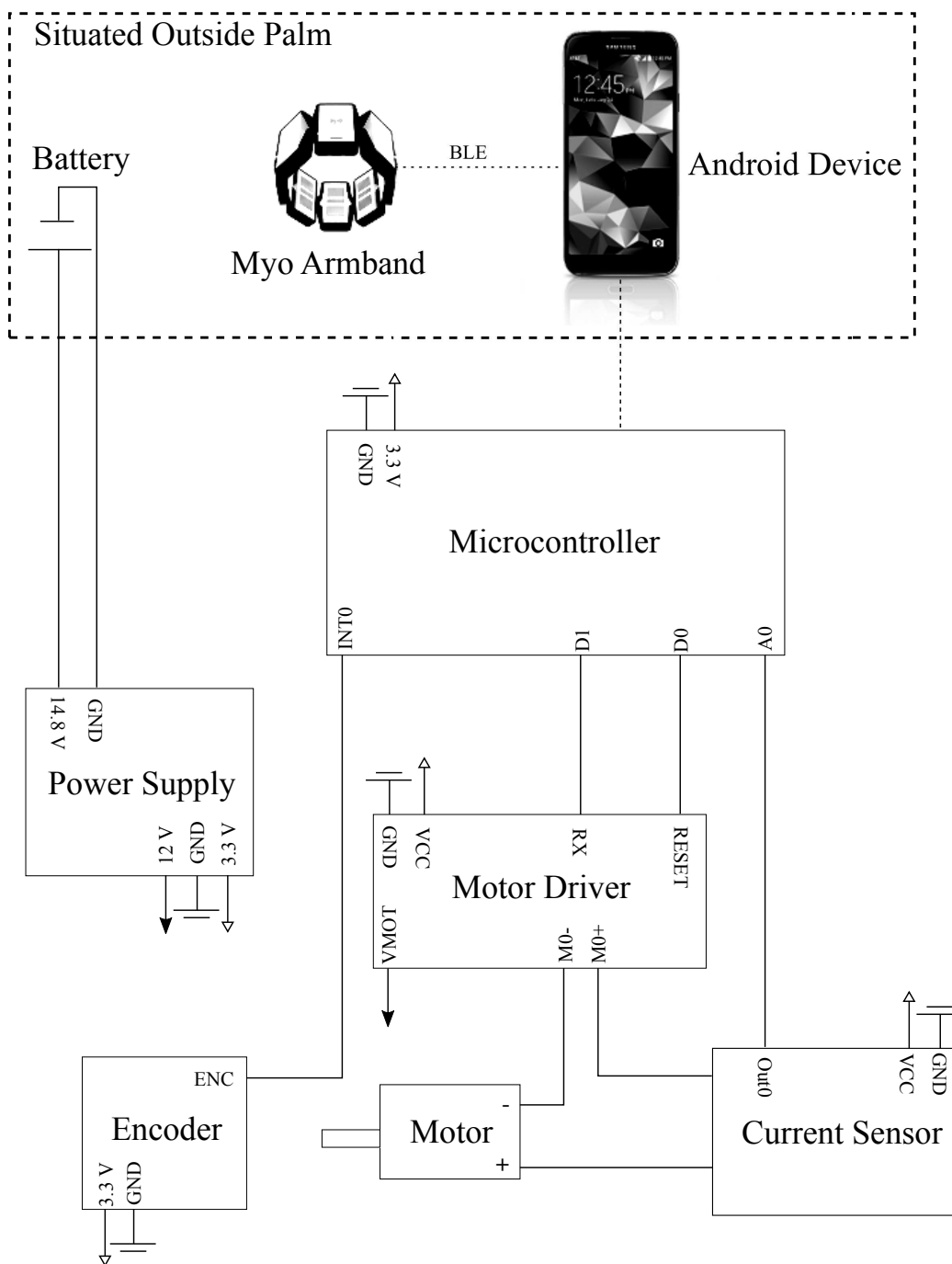


Figure 4.6: Electronic Components Diagram (Illustration: LC Theron)

All logic and analogue signals were transmitted and received at 3.3 V. All of these components except the battery, Myo Armband and Android device were situated inside the palm. Although the DC motors were rated at 6 V the motor driver was able to supply 0-12 V. This was limited on the microprocessor.

4. DESIGN METHODOLOGY

4.2.1 Motor Drivers

Four motors were used in this prosthetic device while each of these motors drew a maximum current of 1600 mA. Two Pololu - Qik 2s9v1 dual motor drivers were used to control the direction and speed of the DC gearmotors. These motor drivers were able to supply a continuous current of 1 A per channel and a peak current of 3 A per channel. The motor drivers could be controlled using serial commands issued from a microprocessor. A value between -128 to 128 was sent from the microprocessor over a TTL-serial connection to the motor drivers receive-pin to control the direction and speed of the motors. By programming each driver with a specific address and by placing the motor drivers in a daisy-chain, only one serial line was required for controlling all four motors.

4.2.2 Current Sensors

The current needed to be measured to calculate the torque of the motors and therefore calculating the grasp strength of the prosthesis. Each motor had a stall current of 1600 mA at 6 V. Therefore a current sensor which can measure between 0-1600 mA was required.

A custom current sensor Printed Circuit Board (PCB) was designed and manufactured to reduce the dimensions as well as increase the resolution of the measured current. The overall dimensions of the final PCB were 19 x 19 mm. The schematic and detailed discussion is given in Appendix B.2. The specifications of the board is listed in Table 4.3.

Table 4.3: Electrical Specifications of Custom Current Sensor

Characteristic	Rating	Unit
Supply Voltage	3.3	V
Measured Current Range	179 - 1602	mA
Sensitivity	1.43	V/A
Output Signal	0-2.28	V

The output of each current sensor was connected to an analogue input on the microprocessor. The microprocessor had a 10-bit ADC which gave a resolution of 3.22 mV/bit. With a sensitivity of 1.43 V/A and maximum output of 2.28 V when connected to the ADC the sensitivity when measured with this microprocessor was 2.25 mA/bit. The current sensor was calibrated and a linear equation was derived which is given in Equation 4.2. The methodology of the calibration is described in Section B.2.

4. DESIGN METHODOLOGY

$$V_o = 1.312I - 45.57 \quad (4.2)$$

Here V_o was the output voltage measured and I the current through the shunt resistor.

4.2.3 Power Supply

As a prosthetic device needs to be portable a lithium ion Ansmann battery was used to power the prosthesis. A battery with a large capacity was required and therefore the battery was not able to fit inside of the hand itself. After a consultation with Rossouw (2015) it was clarified that with most prosthetic hands the battery is situated inside of the socket. A mechanical switch was used to switch between charging the battery and providing power to the rest of the circuit. The specifications of the battery is given in Figure 4.7.

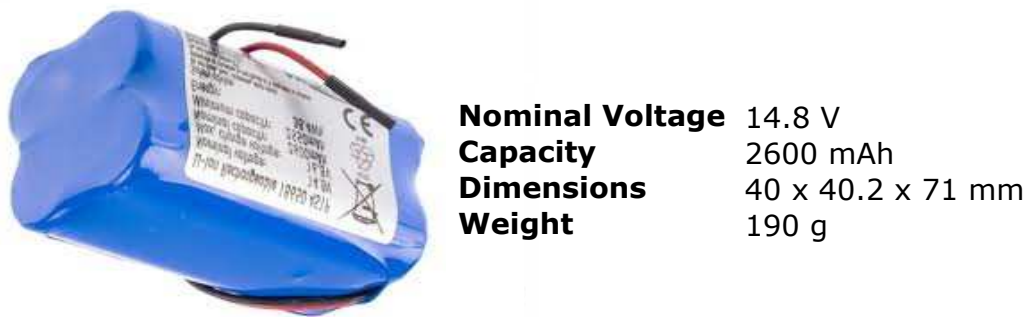


Figure 4.7: Battery Specifications (Illustration: LC Theron)

The motor drivers were rated at 12 V, while the rest of the circuit were powered on 3.3 V logic and power supply. A power supply PCB was designed and manufactured to distribute power inside of the palm to different modules and circuits. This PCB needed to be as compact as possible to be able to fit inside of the palm. The power supply schematic is given in Appendix B.2. The Myo Armband had its own power supply and charged using a mini-USB cable.

4.2.4 Rotary Encoders

The position of the motor shaft translated to the position of the distal phalanx on each finger. It was necessary to know the position of the distal phalanx to accurately control the fingers for all grasps. Four Pololu magnetic rotary encoders were used to determine the motor shaft position. These encoders were

4. DESIGN METHODOLOGY

chosen as opposed to the optical rotary encoders which could only support 5 V logic. The magnetic rotary encoders had a dual channel Hall Effect sensor with a 6-pole magnetic disc which provides a resolution of 12 counts per revolution.

With a 1:298 ratio gearbox a resolution of 3576 counts per revolution of the output shaft is calculated. It was decided to decrease the resolution to 1788 counts per revolution as the microprocessor could not keep up with the interrupts. When the motors run at a speed of 100 RPM the encoder counts were produced at 2.980 kHz. Each encoder output was connected to an external interrupt port on the microprocessor. These ports interrupted the microprocessor when a rising trigger was sensed on the port and increased the motor position variable.

4.2.5 Electromyography

It was decided to use active EMG sensors instead of passive EMG sensors as motivated in Section 2.3.4. This decision was based on the quality of the EMG signal and the available sensors on the market. The Myo Armband developed by Thalmic Labs consists of eight active medical grade stainless steel EMG sensors in a circular pattern. The Myo Armband also has haptic feedback in the form of vibration. This device is a portable device which provides accurate EMG signals.

The Myo armband streams raw EMG data via Bluetooth at a rate of 200 Hz. This baud rate was found to be within the range required for this application. Thalmic Labs provides the Software Development Kit (SDK) for both Windows and Android applications. At the time of this report no SDK providing raw EMG data was available for Arduino applications. The only way to access the raw EMG data through a microprocessor would be to hack the Bluetooth protocol. It was decided that this was not within the scope of this project. Figure 4.8 gives the specifications of the Myo Armband.


	Sensors	8 Stainless Steel EMG sensors Three-axis gyroscope Three-axis accelerometer Three-axis magnetometer
	Processor	ARM Cortex M4 Processor
	Arm Size	190 - 340 mm (Circumference)
	Weight	93 g
	Haptic Feedback	Short, Medium, Long Vibrations

Figure 4.8: Myo Armband Specifications (Illustration: LC Theron)

4. DESIGN METHODOLOGY

The Myo Armband has its own grasp classification built into the device. This classification algorithm was not used in this project as it did not provide an actual grasp classification but a gesture classification. These gestures included pronation and supination of the wrist and a ‘fist’ gesture. The EMG signals provided by the Myo Armband filters out the noise of the powerlines at 50/60 Hz with a Notch filter. The voltage difference measured on the skin is then amplified and scaled to a value between -128 and 128. The value for each sensor is normalised by the maximum of all sensors. These are the values that were used in the pattern recognition phase.

4.2.6 Microprocessor

The BlendMicro manufactured by RedBearLab had an Atmel Atmega32U4 Microcontroller Unit (MCU) and could be programmed using the Arduino Integrated Development Environment (IDE). This microprocessor unit also had an on-board Nordic nRF8001 Bluetooth 4.0 Low Energy (BLE) chip. This board suited this application with its compact design. The board had 17 I/O pins of which six were analogue inputs, five could be used as external interrupts and five had PWM capability. The BlendMicro had an available Flash Memory of 28 kB. The dimensions of the BlendMicro was $43.6 \times 18.4 \times 4.3$ mm.

4.3 Microprocessor Software Design

The microprocessor was responsible for controlling the motors, reading motor current, calculating motor position and communicating with the mobile telephone via BLE. Figure 4.9 illustrates a flow diagram of the software implemented on the microprocessor using the Arduino[®] (2016) platform.

When the microprocessor received power all variables were initialised and the microprocessor entered setup mode. In setup mode the microprocessor set up the Bluetooth in slave mode while waiting for interrupts from the master Bluetooth device. The setpoint, sample time and output limits of the PID control was set. Both PID routines were set to calculate on a 50 Hz cycle. The encoder interrupts were set up to enter the Interrupt Service Routine (ISR) when it received a rising edge on the external interrupt. The ISR incremented/decremented each motor’s position. The prosthetic hand was also calibrated in the setup.

After the setup the microprocessor enters an infinite loop. In this loop the shaft position of each motor was monitored and PID controlled to keep the fingers in a resting grasp. The microprocessor waited in this mode until a command was sent from the Android device. The command was either sent when a grasp was recognised or when the device needed to be calibrated. The command was processed to determine which grasp had been recognised by the

4. DESIGN METHODOLOGY

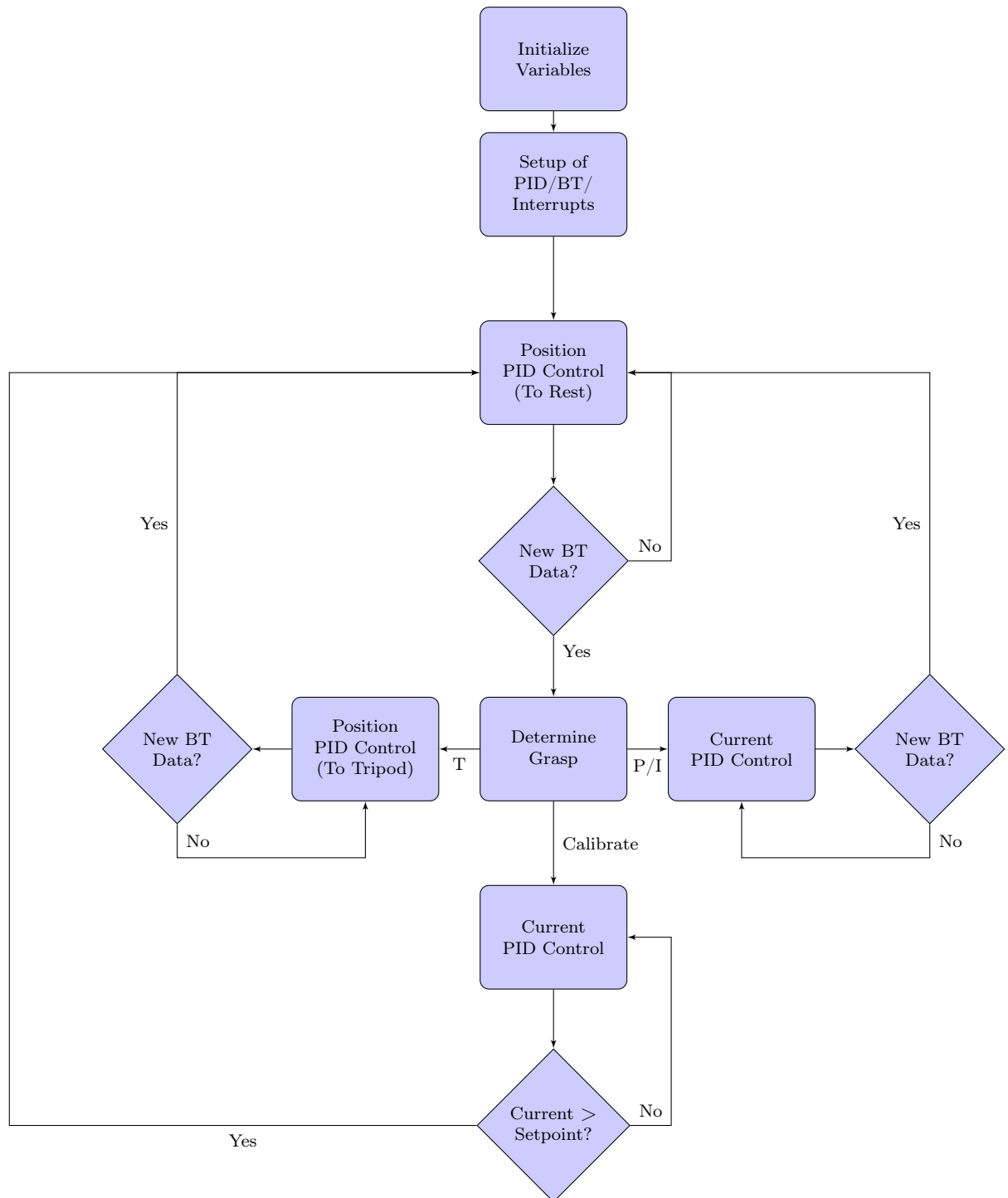


Figure 4.9: Flow Diagram for Microprocessor (Illustration: LC Theron)

4. DESIGN METHODOLOGY

Android device. While the fingers were closing the current and position of each motor were measured continuously.

The motor control depended on the grasp type received. When a ‘power grasp’ or ‘index’ command were received the fingers closed with PID control on the motor current which corresponded to the grasp strength of the prosthesis.

If new Bluetooth data was received the microprocessor returned the motors to the setpoints set for the resting grasp. Each finger had a different setpoint depending on the mechanics of each finger. When a ‘tripod’ grasp was received the fingers move to the tripod position using position PID control as this was a more precise grasp than the other grasps.

If a power failure occurred while the hand was busy with a certain grasp the position of the motors would be lost. For this reason a calibration command was implemented to calibrate the positions of the motors. For this command the fingers needed to fully contract until the current setpoints were reached. The position of the motors was set to zero and extended until the positional setpoint for a resting grasp was reached.

4.4 Mobile Application Software Design

4.4.1 Java

The mobile application was developed in AndroidStudio[®] (2015) using Java as programming language. At the time of this report Thalmic Labs had not written a full Android SDK which was able to provide the raw-EMG data from the MYO armband. An open source library developed by Kutafina *et al.* (2015) was used to be able to send and receive data from the Myo armband to an Android device. This library contained several classes to be able to communicate with the Myo Armband.

Several classes were developed to group appropriate functions and callbacks together. A class named GetFeatures.java was responsible to extract the different features from the EMG channels. This class also contained functions responsible for training the algorithm, calculating the success and confusion matrix.

Another class called Calculations.java was responsible to calculate the success rate and confusion matrix for three different feature sets, eight different window sizes and four different window shift sizes. This class trained the SOM as described in Section 3.3. The success rate was calculated using Equation 3.9. As this operation required a lot of CPU power and could freeze the main thread, this process was started in a new thread. A class called Files.java was responsible for saving the data stored in matrices to text files. The text files were saved to be used in reporting and post processing.

The main class called MyoInfoView.java was responsible for the user interface as well as combining the different classes. DebugFragment.java, RBL-

4. DESIGN METHODOLOGY

GattAttributes.java and RBLService.java were responsible for controlling the Bluetooth protocol of the Myo Armband and the microprocessor. Table B.1 in Appendix B.3 gives a brief summary of all the classes and functions written for this Android application.

4.4.2 User Interface

Figure 4.10 illustrates a flowdiagram of the software implemented on the Android Device. This software was an important aspect of the prototype testing phase described in Section 5.

To start the program the Bluetooth of the Android device should be turned on. When the application was opened it started searching for available Myo Armbands. When a Myo armband was found the Android device automatically connected to it and configured the Myo Armband to stream raw-EMG data. After this connection had been established and was stable the RMS values of the 8 EMG channels were mapped to color values and displayed in a circular pattern corresponding to the Myo Armband. The user was able to select different channels by clicking on the channel that needed to be inspected. The selected channel was then displayed on a graph displaying EMG amplitude over time. Only two channels could be selected at a time to make it easier for the user to distinguish between channels. The graph color corresponded to the selected channel color. This is illustrated in Figure 4.11.

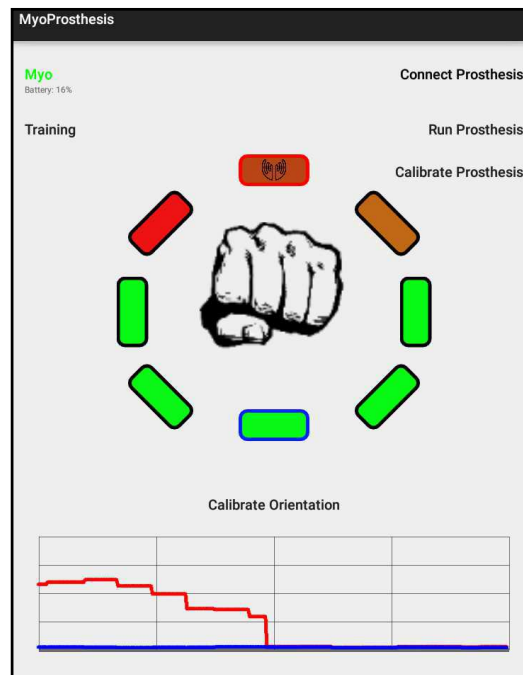


Figure 4.11: User Interface of MyoProsthesis (Illustration: LC Theron)

4. DESIGN METHODOLOGY

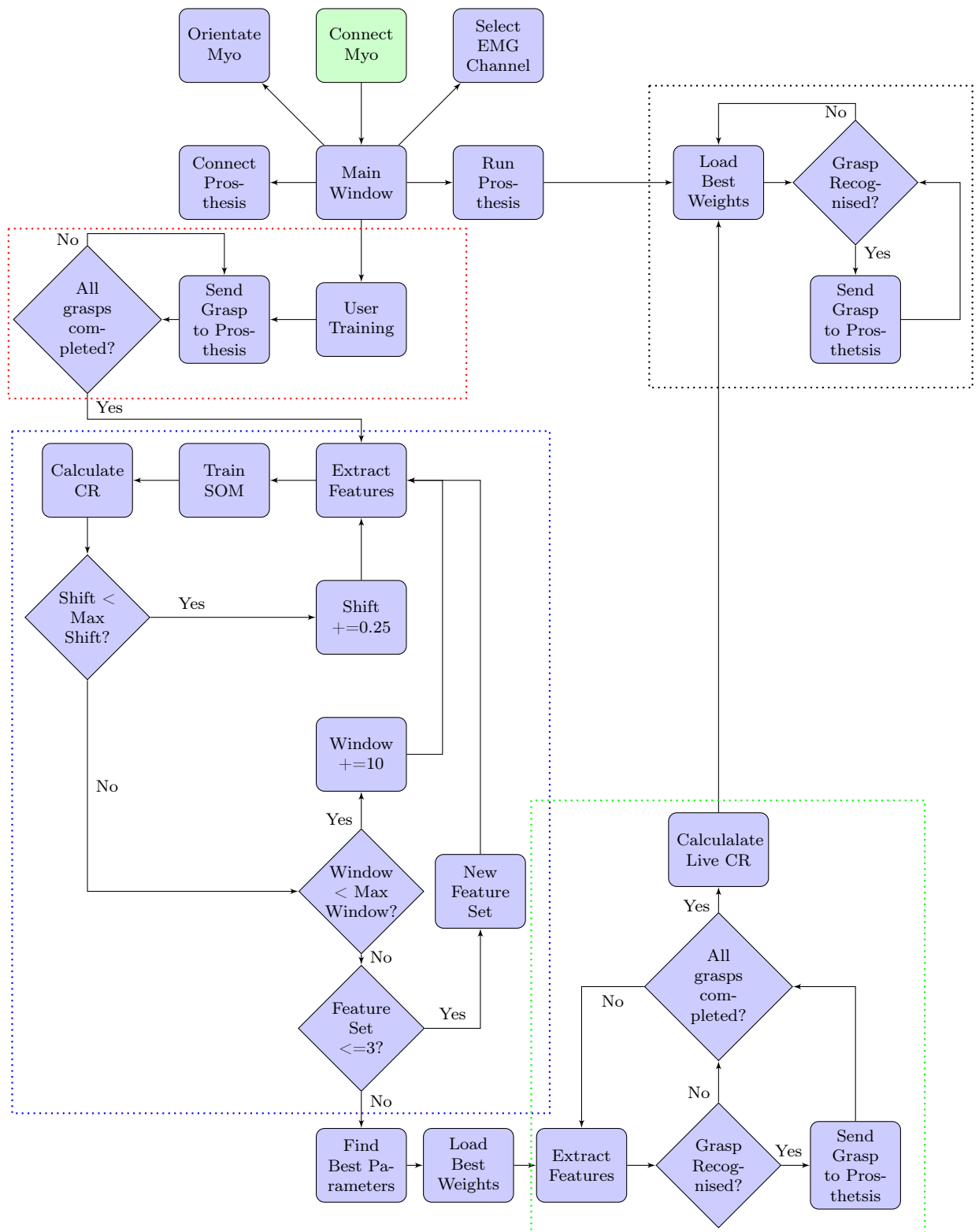


Figure 4.10: Flow Diagram for Android Application (Illustration: LC Theron)

4. DESIGN METHODOLOGY

This feature enabled the prosthetist to inspect the EMG signals captured by the Myo armband. The prosthetist can use this feature to establish better training data for the algorithm. This was also used as feedback during the training phase.

When the ‘Connect Prosthesis’ button was clicked the Android device established a BLE connection between the Android device and the BlendMicro. The BlendMicro waited for commands from the Android device. The ‘Calibrate Prosthesis’ button sent the calibration command as explained in Section 4.3.

When the ‘Calibrate Orientation’ button was clicked the Inertial Measurement Unit (IMU) of the Myo Armband was enabled and the user was able to orientate the Myo Armband to the correct orientation. A bar displayed the orientation of the Myo armband in relation to the arm. The Myo Armband was rotated until the orientation was at the desired orientation. Once this status bar was clicked the IMU data was turned off to eliminate interference with EMG data. This feature is illustrated in Figure 4.12.

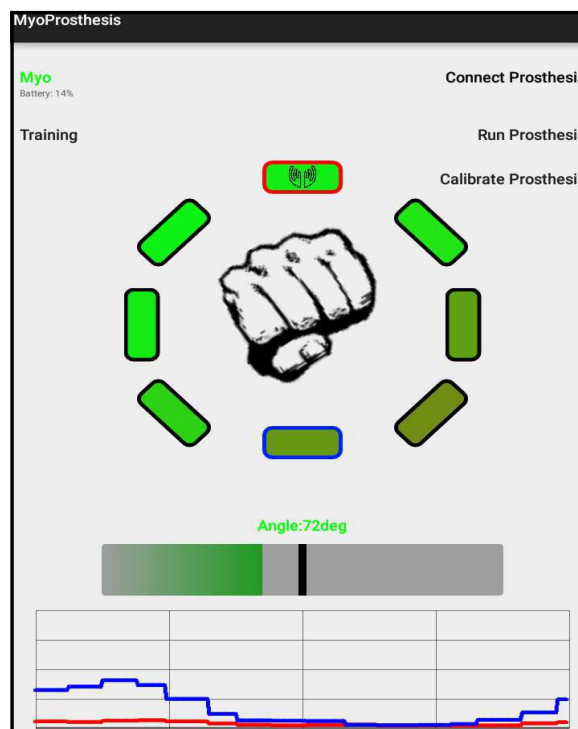


Figure 4.12: Orientation Calibration of MyoProsthesis (Illustration: LC Theron)

When the training phase was entered by clicking the ‘Training’ button, the instructions window told the user what to do next. The control algorithm of the training phase is illustrated in Figure 4.10 in the red block. While

4. DESIGN METHODOLOGY

training the algorithm the applicable grasps were displayed in the middle of the circular EMG sensors. These illustrations aided in the visual feedback for the amputee. When the ‘record’ button was clicked, the EMG data was saved for the specified time window (2 s). Each grasp was repeated three times. During this time the Android device also sent a command to the BlendMicro to perform the grasp that was recorded. This feature enabled the use of PGT which was motivated in Section 2.4.4. The training interface is illustrated in Figure 4.13.

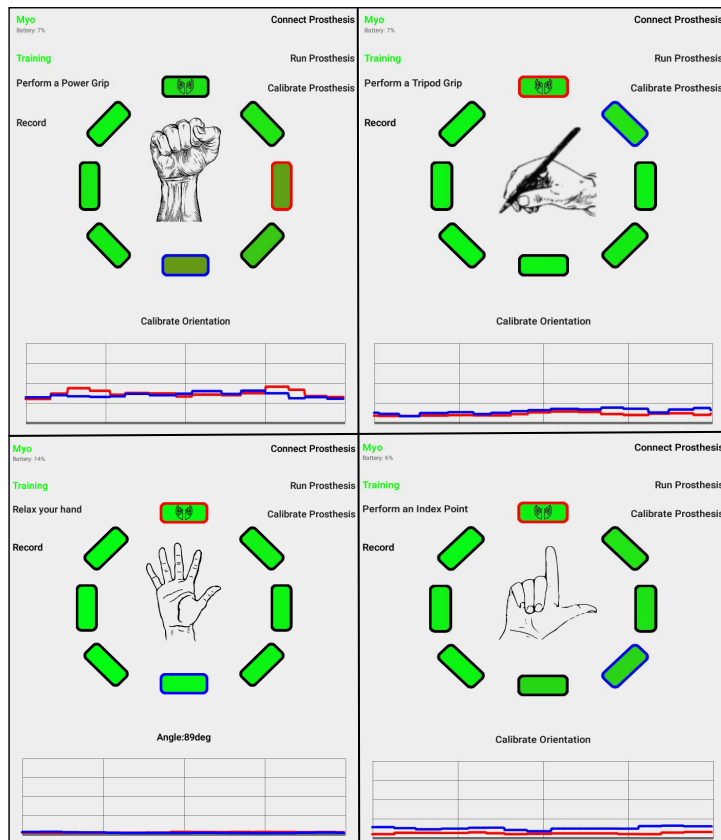


Figure 4.13: User Interface of MyoProsthesis (Illustration: LC Theron)

When the training phase was completed the information window asked the user whether he/she was satisfied with this success rate and if ‘Yes’ was clicked the Android device calculated the success rate for different feature sets, window sizes and window shift sizes. As seen in Figure 4.10 in the blue block the control algorithm extracted features for a certain set of parameters, train the SOM and calculates the classification rate. The algorithm looped through all the different shift sizes, window sizes and feature sets. The weights for

4. DESIGN METHODOLOGY

the best feature set at the best window and window shift size was selected to proceed to the live classification test which is illustrated in Figure 4.10 in the green block.

The user was now able to control the prosthetic device with the best parameters applicable to the user. By clicking on the different grasp types displayed on the screen the algorithm calculated whether that specific grasp was recognized by the algorithm. The control algorithm is illustrated in the green block in Figure 4.10. An online live classification success rate was calculated for the live test. If the user was not satisfied with this success rate the process needs to be started from the beginning and better training data needed to be captured. If the user was satisfied with the live classification rate, the user could now control the prosthetic device.

Each time a different grasp was recognised the command was sent to the BlendMicro and the appropriate grasp was also displayed in the graphics window. The Myo Armband also provided haptic feedback to the patient via the vibrotactile feedback mechanism of the Myo Armband. Each grasp had a different vibration length.

The user was also able to load previous calculated weights by clicking on 'Run Prosthesis'. The control algorithm is illustrated in the black block in Figure 4.10. This loaded the previous weights that was calculated and if the Myo armband was orientated correctly the user could control the prosthetic device with previous weights and therefore was not necessary to retrain the algorithm.

4.5 Affordability

One of the objectives of this project was to design an affordable prosthetic device for transradial amputees. This section gives a brief overview of the material costs involved in developing this prosthesis. A complete list of materials and components used in this project is given in Table B.2 and Table B.3 in Appendix B.5. Table 4.4 gives the costs divided into several categories.

4. DESIGN METHODOLOGY

Table 4.4: Total Cost Breakdown

Summary	Total Cost
Electronic Components	R6 416.30
Current Sensor	R72.27
Power Supply	R56.64
Manufactured Components	R107.51
Mechanical Components	R354.32
Fasteners	R42.50
Assembly	R216.00
	R7 265.54

Only the material cost was included for the 3D-Printing as this was done at BERG. The assembly costs were estimated based on the time it took to assemble the prosthetic hand at R60 per hour. It can be seen that the electronic components was the most expensive category with the Myo Armband comprising of R2 724.65 of this cost. If a cheaper EMG sensor could be designed the material cost of this prosthetic device could be less. The total weight of the prosthetic prototype without the battery and socket was 224 g.

Chapter 5

Prototype Testing

5.1 Introduction

The study performed was an experimental clinical trial. The research conducted intended to investigate the accuracy of the myoelectric prosthesis developed in this project. The methodology described in this section describes the testing phase of the project.

The overall study population consisted of both subjects with non-amputated upper limbs and subjects with transradial amputations. Transradial amputees were recruited by Rossouw and Theron while subjects with non-amputated upper limbs were recruited by Theron. The sample size for Phase III was dependent on the availability of transradial amputees. The aim was to recruit 15 healthy subjects as well as four transradial amputees. However, only two transradial amputees were found for this study. Subjects did not receive compensation for participating in this study. Figure 5.1 illustrates the phases completed in this protocol.

Before the study was conducted a pilot study was done using an existing database described in Section 3.2. The results from Phase 0 were used to develop the algorithms for Phase I and III. The study was further divided into three phases. In the first phase the grasp classification accuracy of the myoelectric prosthesis was determined while using non-amputated subjects. In Phase II grasp force tests were done with the myoelectric prosthesis using subjects with non-amputated upper limbs. In the third phase the grasp classification accuracy of the myoelectric prosthesis using transradial amputees was determined.

5. PROTOTYPE TESTING

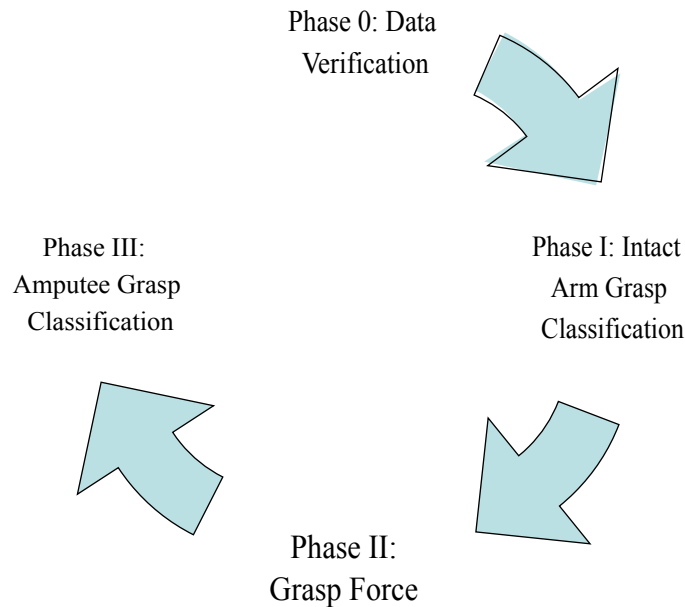


Figure 5.1: Protocol Flowchart (Illustration: LC Theron)

Each participant was given written and oral explanations of the procedure and associated risks before the tests were conducted. Before each test a written informed consent form was signed by the participant. Approval for the experimental clinical trials was required from the Health Research Ethics Committee (HREC) before the testing of this medical device could commence. Ethical approval was granted on 21 January 2016 with protocol number M15/09/031. The approval notice is given in Appendix C.

5.2 Phase I - Non-Amputated Arm Grasp Classification

5.2.1 Phase I Methodology

In this phase the grasp classification accuracy of the myoelectric prosthesis was tested using subjects with non-amputated upper limbs. This study served as a proof of concept before testing commenced using amputated subjects. Phase I was conducted in the Biomedical Engineering Research Group Laboratory in the Department of Mechanical and Mechatronic Engineering of Stellenbosch.

A minimum sample size of 15 subjects was calculated using power analysis. These subjects consisted of 12 male and 3 female subjects. Surface EMG signals were extracted from the subject's dominant arm. As discussed in Section 2.4.2 the classification accuracy needed to be calculated in real-time as there exists a low-correlation between post-processing classification and real-time performance.

5. PROTOTYPE TESTING

This phase implemented the classification technique developed in Phase 0. Phase I was divided into two stages. The first stage was the training stage. In this stage the classifier was trained for the specific subject. This gave the subject the chance to become familiar with the experimental setup. The Myo Armband was attached to the subject's forearm. The Myo Armband was orientated to the same orientation for each subject. The prosthesis was on a stand next to the subject. The EMG signals were processed by the Android device. The user interface for this setup was described in Section 4.4.2. Figure 5.2 illustrates the test setup that was used for Phase I. The Myo Armband [1] and the prosthetic device [2] is illustrated here.

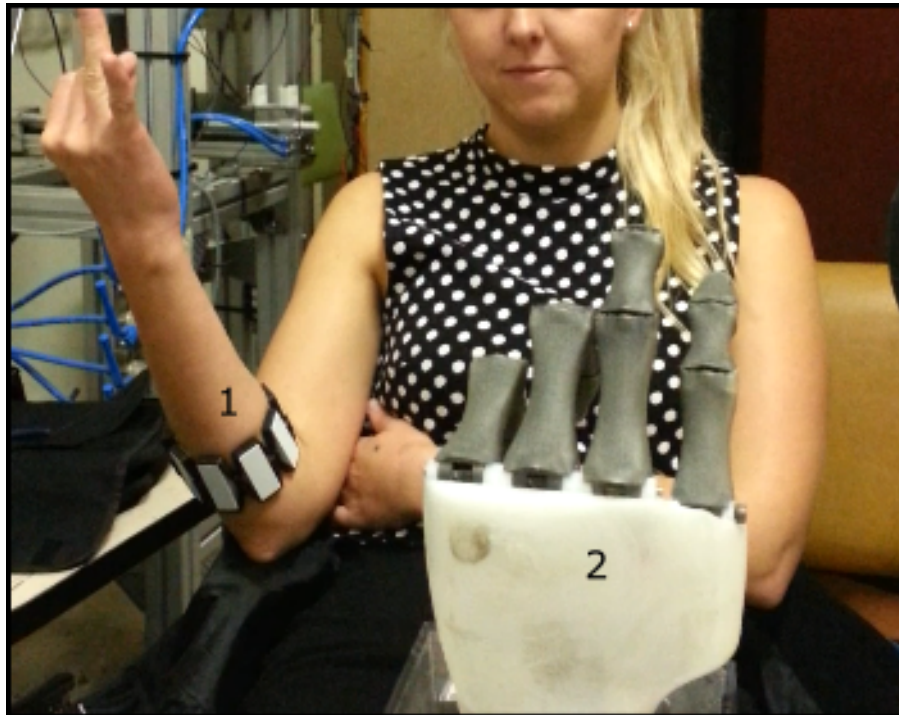


Figure 5.2: Test Setup for Phase I (Illustration: LC Theron)

Each subject was asked to perform each grasp three times to train the classifier. The grasp was held for two seconds. In between each repetition the subject rested for five seconds and in between each grasp type the subject rested for ten seconds.

In the second stage the same procedure was followed as in stage one except that a classification rate was calculated based on whether the SOM was able to classify a grasp correctly. Each subject was asked to perform the same grasp five times. The data was stored on the Android device to be processed in MATLAB. The data from stage two was used for the grasp classification rate. The grasp classification was calculated using Equation 3.9.

5. PROTOTYPE TESTING

5.2.2 Phase I Results

The feature sets were numbered 1 to 3 where feature 1 was RMS, MAV, WL; feature set 2 was RMS, MAV, SSC and feature set 3 was RMS, WAMP, SSC. The window sizes were given in number of EMG samples and the shift sizes were given as a percentage of the window size where 0.25 would be a quarter of the window size etc.

The results of each subject were summarised in Table C.1 in Appendix C.1. The first column gives the maximum training classification rate achieved for the best feature set, window size and shift size. The maximum average classification rate was 96.2 % with an average standard deviation between subjects of 3.57 %.

The live classification rate was based on the parameters which achieved the maximum training classification rate. The live classification rate was calculated online. The average live classification rate was 87.2 % with a standard deviation of 6.30 % between subjects. Figure 5.3 displays the confusion matrix of the best parameters selected for each subject.

Confusion Matrix

Output Class	1	612 15.9%	0 0.0%	19 0.5%	0 0.0%	97.0% 3.0%
	2	147 3.8%	735 19.1%	148 3.8%	27 0.7%	69.5% 30.5%
	3	86 2.2%	60 1.6%	691 18.0%	4 0.1%	82.2% 17.8%
	4	0 0.0%	0 0.0%	0 0.0%	1319 34.3%	100% 0.0%
		72.4% 27.6%	92.5% 7.5%	80.5% 19.5%	97.7% 2.3%	87.2% 12.8%
	1	2	3	4		
	Target Class					

Figure 5.3: Live Confusion Matrix for the Best Parameters - Phase I

5. PROTOTYPE TESTING

Each class in Figure 5.3 corresponded to a grasp type. Class 1 was the ‘Large Diameter Grasp’, class 2 the ‘Tripod Grasp’, class 3 the ‘Index Extend Gesture’ and class 4 the ‘Resting Grasp’. The green blocks display the percentage of classes correctly classified while the red blocks display the opposite. The grey blocks display the total for each class and the blue block displays the total average classification rate. For example 148 EMG windows were classified as class 2 but was supposed to be classified as class 3. This was equal to 3.8 % of the total number of EMG windows.

From Figure 5.3 it could be seen that class 4 had the highest classification rate with 100 % while class 1 was the second highest with 97.0 %. Class 2 had the highest misclassification rate of 30.5 % with most of the samples classified as class 3 and class 1.

Figure C.1 in Appendix C.1 displays the mean training classification rate across subjects compared to the window size and shift size for each feature set. This figure also displays the 95 % confidence interval for the different parameters. It can be seen that for feature set 1 and 2 the classification rate increased when the window size increased for a shift size of 0.25 and 0.5 and decreased as the window size increased for a window size of 0.75 and 1. The classification rate for feature 3 was the highest in the middle of the range of window sizes.

One-way ANOVA was used to determine whether this difference was statistically significant. The p-value for each group was calculated. For a significant difference between groups the p-value should be below 0.05. Table C.3 in Appendix C.1 gives the probability calculated when the data was arranged in shift size groups. Table C.2 in Appendix C.1 gives the probability calculated when the data was arranged in window size groups. It can be seen that there existed no statistical significance between the different groups as the p-values were not below 0.05. Feature set 3 with a shift size of 0.25 had the highest p-value while feature set 1 with a shift size of 1 had the lowest p-value of 0.106. The maximum mean training classification rate among subjects for each feature set was used to determine the best window and shift sizes. A summary of the best parameters per feature set is given in Table 5.1.

Table 5.1: Summary of best Parameters - Phase I

Feature Set	Mean	STD	Window Size	Shift Size
1	90.8	6.3	30	1.00
2	89.4	7.3	60	0.50
3	90.2	8.3	60	0.50

Using the parameters in Table 5.1 the three feature sets were compared and are illustrated in Figure 5.4.

5. PROTOTYPE TESTING

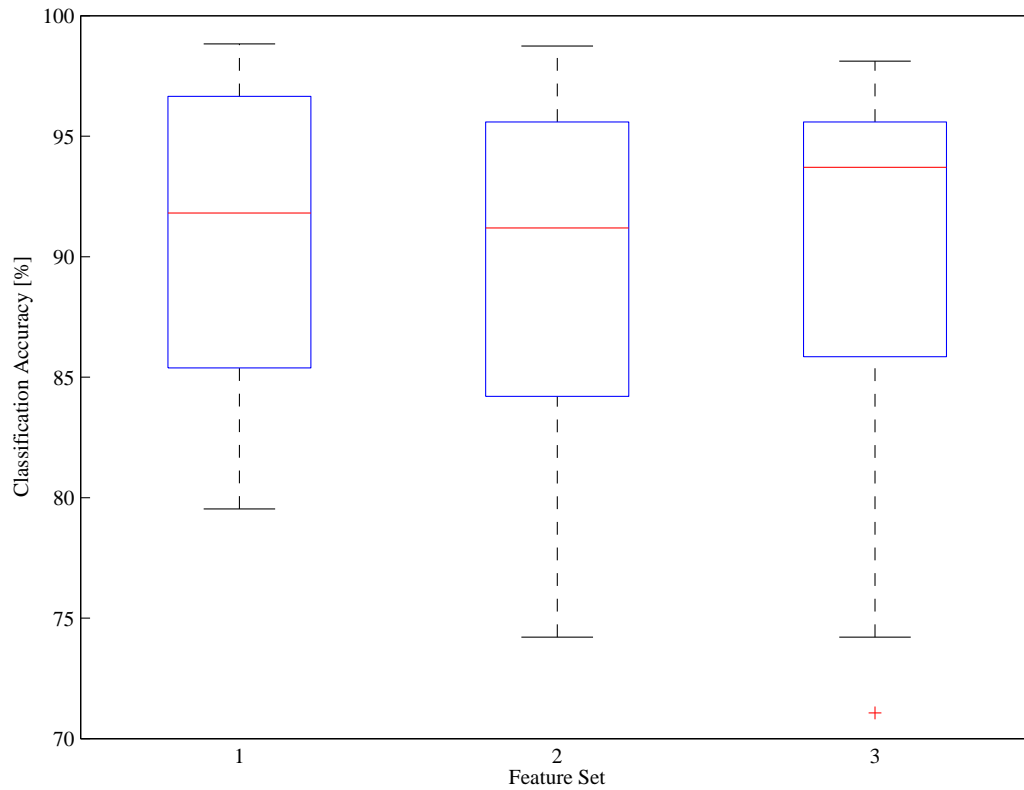


Figure 5.4: Comparison of Different Feature Sets - Phase I

The left of Figure 5.4 illustrates the distribution of the data. One-way ANOVA was used to test the probability of differences between the three groups and was calculated as 0.86. It was concluded that none of the groups had significantly different means. Feature set 3 had the highest median of 93.71 % while feature set 1 had the highest mean of 90.81 % with the smallest confidence interval of 2.88 % and standard deviation of 6.3 %.

The window size and shift sizes of the feature set with the highest mean classification rate was used to recalculate the live classification rate using the live EMG data recorded during each test. This calculation was done offline on MATLAB. A new SOM was trained using the best parameters of feature set 1 and the confusion matrix for feature set 1 is displayed in Figure 5.5.

5. PROTOTYPE TESTING

Confusion Matrix

Output Class	1	784 14.6%	8 0.1%	31 0.6%	0 0.0%	95.3% 4.7%
	2	268 5.0%	1032 19.2%	292 5.4%	226 4.2%	56.8% 43.2%
	3	148 2.7%	35 0.7%	846 15.7%	4 0.1%	81.9% 18.1%
	4	0 0.0%	0 0.0%	0 0.0%	1709 31.7%	100% 0.0%
		65.3% 34.7%	96.0% 4.0%	72.4% 27.6%	88.1% 11.9%	81.2% 18.8%
	1	2	3	4		
	Target Class					

Figure 5.5: Live Confusion Plot with Overall Best Parameters - Phase I

Feature set 1 had a live classification rate of 81.2 %. Feature set 2 and 3 both had a live classification rate of 76.9 %.

5.2.3 Phase I Discussion

The main purpose of Phase I was to determine the overall classification rate of the SOM using participants with non-amputated upper limbs. Figure 5.3 illustrated that the 'Tripod Grasp' and the 'Index Extend Gesture' had the highest misclassification among the four different grasps. This could be because these two grasps use similar muscles in the forearm to perform the grasps. A study regarding muscle activation for the four different grasps was done in Section 5.5

5. PROTOTYPE TESTING

Another purpose of this phase was to establish whether different features, window sizes and shift sizes had a significant impact on the classification rate. From these results it was clear that for the range of window sizes and shift sizes tested in this project no significant difference between the different parameters were calculated. As seen in Table 5.1 it was calculated that feature set 1 had the highest mean training classification rate. No significant difference was calculated between different feature sets, nevertheless the feature set with the best mean was used.

The live confusion matrix of the best parameters was calculated offline. Figure 5.5 displayed the same characteristics as Figure 5.3 where the ‘Tripod Grasp’ and the ‘Index Extension Gesture’ were misclassified with each other. This problem can be solved in future tests by training the subject to better distinguish between different muscles when performing these two grasps. As mentioned in Section 2.4.2 when the user has had more experience with a system the muscle movements will become more constant which leads to higher classification rates.

The best parameters were calculated for each subject and were different from the overall best parameters. The training calculation time of the training algorithm could be decreased if one particular set of parameters could be used for all subjects. The best parameters were used to make direct comparisons between the different features sets. It was found that using feature set 1, 30 window size and 1 shift size a live classification rate of 81.2 % could be achieved. These parameters also had the lowest p-value. As these were not the best parameters per subject it was expected that the overall live classification rate would be lower than Figure 5.3. Using the best parameters for each subject the mean training classification rate was calculated as 96.2 % with a live classification rate of 87.2 %.

The live classification rate can be compared to the live classification rate in Gehani *et al.* (2013) where a SOM was used to classify between opening and closing the hand. A classification rate of 97.22 % was achieved by classifying between an open and closed hand using 3 subjects. This was the only comparable study found at the time.

The window size also had an effect on the reaction time of the SOM. A bigger window size had a longer reaction time. Therefore when choosing a window size it should be as small as possible to decrease the reaction time of the prosthetic device. As feature set 1 had the smallest window size and the best classification rate it was concluded that a window size of 30 EMG samples was suitable for this application.

5. PROTOTYPE TESTING

5.3 Phase II - Grasp Force

5.3.1 Phase II Methodology

This phase consisted of two stages. In stage one the delay of the prosthetic device was compared to a human hand. A total number of 10 subjects were used for this test. The test setup is illustrated in Figure 5.6.

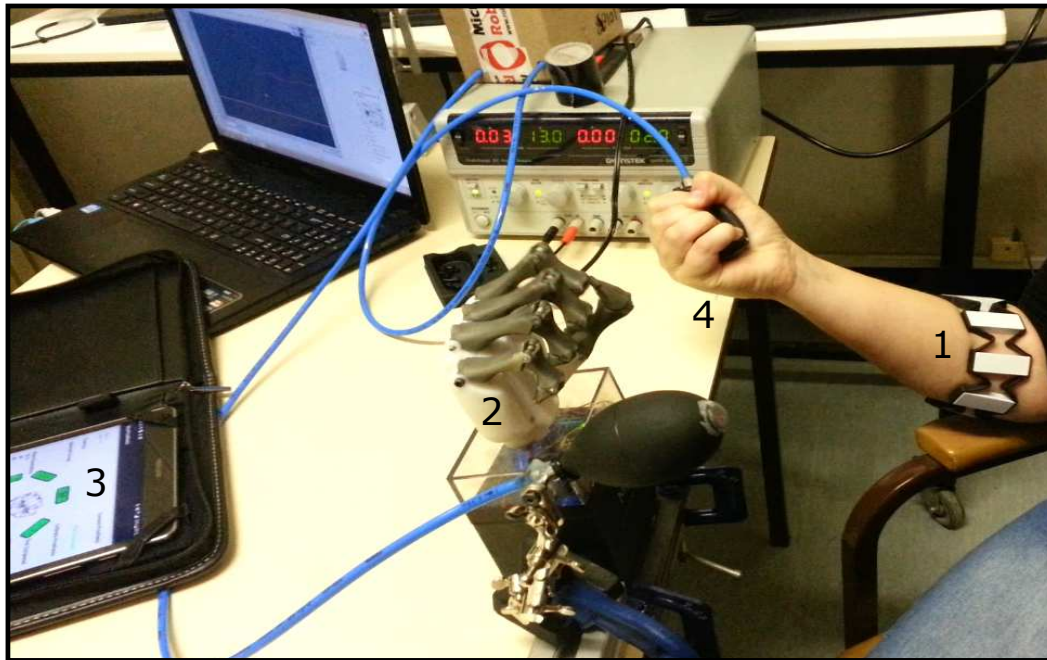


Figure 5.6: Test Setup for Phase II Stage 1 (Illustration: LC Theron)

The Myo Armband [1] was attached to the forearm of the subject's dominant hand. The prosthetic hand [2] was fixed next to the subject on a stand. The EMG signals were processed using the Android application [3] developed in this project. The same pressure sensing system [4] was held by the prosthetic device and the human hand attached to the Myo Armband.

The pressure sensing system consisted of a pneumatic balloon filled with air and attached to a digital pressure gauge (WIKA, 2016). The pressure gauges were connected to the same DAQ (NI, 2016) and the output was saved on a computer. Both of the pressure gauges were calibrated using a manometer and the calibration curves of these gauges can be seen in Figure C.2 in Appendix C.2.

During this stage each subject was asked to perform 5 power sphere grasps on the balloon. The subject was asked to gradually increase the force on the balloon until the prosthetic hand mimics the human hand. After each repetition the subject rested for 5 seconds.

5. PROTOTYPE TESTING

The pressure reading from the human hand was used to determine when the participant had initiated a power sphere grasp while the pressure reading from the prosthetic device determined when the prosthetic device reacted to the human hand. The EMG data was recorded and stored in the database. This database could be used to determine some relation between the grasp strength and EMG data.

When these tests were performed the motors were not set at maximum power and therefore these tests were only used to determine the reaction time of the prosthetic device. This reaction time was the time it took for the algorithm to classify a grasp, send the data to the prosthetic device and the time it took for the device to close until it reached the balloon. The time it took for the prosthetic hand to reach the balloon was much greater than the other two. Therefore it should be clear that this was not the classification time.

In stage 2 the aim was to validate the analytical model developed in Section 4.1. It was decided to calculate the normal forces exerted by the distal phalanx when the fingers were fully extended. The test setup can be seen in Figure 5.7.

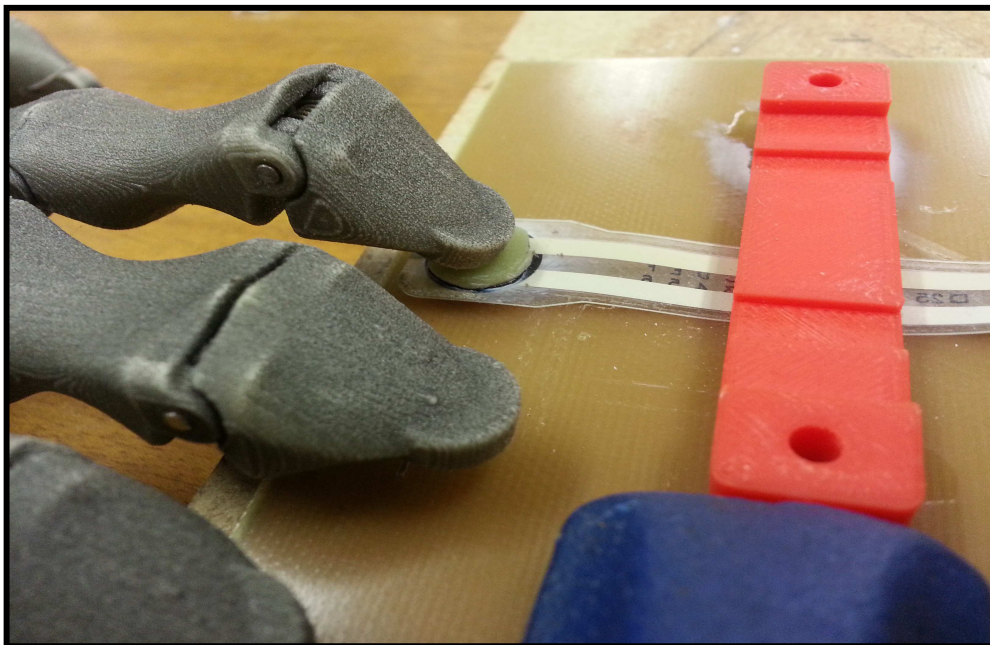


Figure 5.7: Test Setup for Phase II Stage 2 (Illustration: LC Theron)

A force sensitive resistor (FSR) from Tekscan (2016) was used to determine the force exerted by the distal phalanx when fully extended. The FSR was calibrated using weights in 1 kg increments. The FSR was calibrated up

5. PROTOTYPE TESTING

to 80 N. Figure C.3 in Appendix C.2 displays the calibration curve for the FSR used in this project.

The current of the motor used for the flexion of the finger was measured using the current sensor developed in this project. The output of the current sensor as well as the output of the FSR circuit was measured using the same DAQ. The current of the motor was converted to torque using the datasheet provided by the motor supplier. The current was increased to four different set points to increase the motor torque. The force measured by the FSR was compared to the analytical model developed in this project.

5.3.2 Phase II Results

Figure 5.8 illustrates an example of three repetitions from one of the participants in stage 1. The EMG data was recorded using the Myo Armband and could therefore not be plotted on the same time axis as the grasp strength.

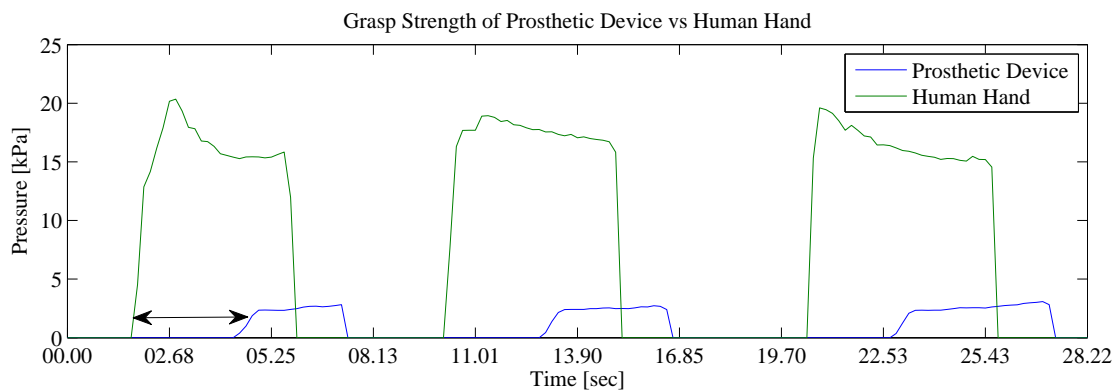


Figure 5.8: Example of Phase II, Stage 1 Results

The delay is indicated by the arrow in the graph. The delay was calculated as the difference in time between the first positive pressure measured by the prosthetic pressure sensing system and the first positive pressure measured by the human hand pressure sensing system.

The average of these delays were taken for each subject for five repetitions. The average for 10 subjects was 2.48 seconds with a standard deviation of 0.44 seconds.

An example of the data collected in stage 2 can be seen in Figure 5.9. It was decided to use the middle finger to validate the analytical model and to compare to commercial devices. The average of 10 repetitions were taken at four current set points. The average force and the standard deviation of the three set points are illustrated in Figure 5.10.

5. PROTOTYPE TESTING

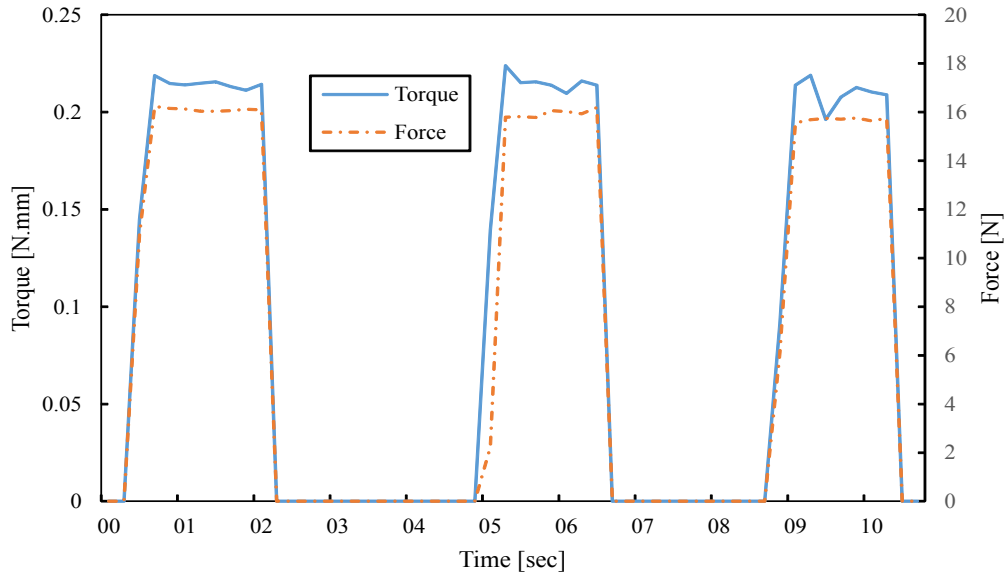


Figure 5.9: Example for Phase II Stage 2

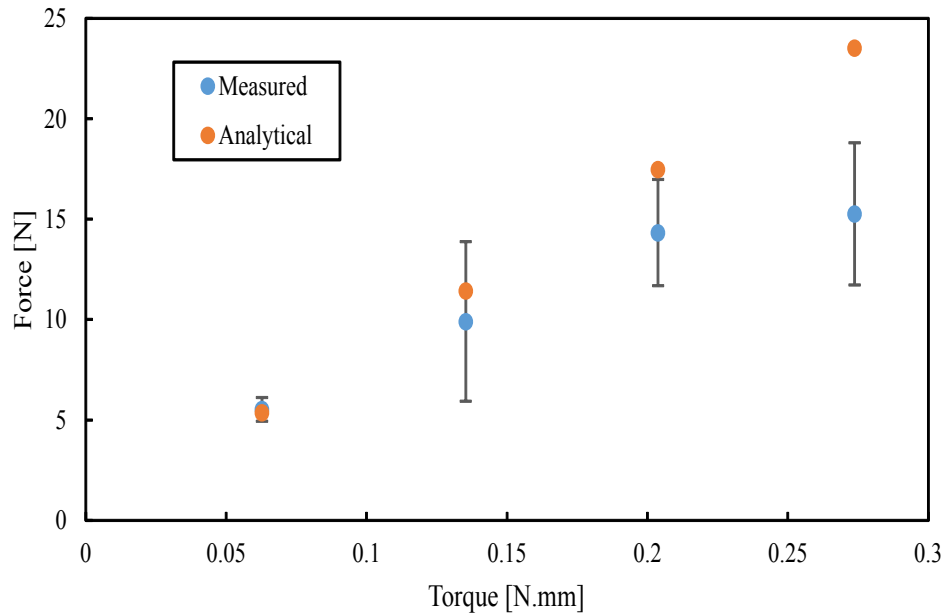


Figure 5.10: Results for Phase II, Stage 2

The force measured was compared to the analytical model developed in Section 4.1. It can be seen that as the torque increased the error between the analytical model and measured values increased from 2.5 % to 39.1 %.

5. PROTOTYPE TESTING

5.3.3 Phase II Discussion

The delay of 2.48 seconds calculated in this phase was the time it took for the prosthetic device to exert a force on the pressure sensing system described in this phase. It should be noted that at the time these tests were performed the motors were not set at maximum current setpoint. In a study done by Belter *et al.* (2013) the time it took for the bebionic™ hand to perform a power grasp was 1.9 seconds. This meant that the prosthetic device developed in this project performed 580 ms slower.

In the study done by Belter *et al.* (2013) the force at the finger tip for commercially available devices was calculated. The Bebionic hand had the highest middle finger distal phalanx force of 12.25 N. These tests were performed using a load cell while measuring the force at the tip of the finger when the finger was fully extended. The highest force measured in this project at 14 % of the maximum torque was 15.56 N. This was an indication that the prosthetic hand could exert the same grasp forces as commercially available devices.

The grip force of commercial devices is usually measured using a grip dynamometer. As it was too expensive to acquire one it was not possible to relate the grip force of this prosthesis to the commercial devices. The study done by Belter *et al.* (2013) was similar to this study and therefore the results were comparable.

It should be noted that the tests performed here was an indication that the prosthetic device could exert the forces described by the analytical model at the four set points tested. It was seen that when the torque increased above 0.273 N.m the force on the FSR did not increase linearly. This and the increase in error when the torque was increased can be explained by the elasticity of the material used to manufacture this prosthesis. The assumption of a rigid material made in the analytical model contributed to this error. These motors could not exert its maximum torque at 0 RPM when the distal phalanx was fixed. This also explains the error at the fourth set point tested. It was decided not to include higher current setpoints for the reasons mentioned above. It was concluded that these tests were satisfactory as a greater force was measured than the commercial device.

5.4 Phase III - Amputee Grasp Classification

5.4.1 Phase III Methodology

In this phase the grasp classification accuracy of the myoelectric prosthesis was tested with amputated subjects. This test determined the final grasp classification success rate.

The population for this study consisted of two amputated subjects. In this phase any participants willing to partake in the study were included in this study. Phase III was partially done at Mr Rossouw's practice in Melk-

5. PROTOTYPE TESTING

bosstrand, Eugene Rossouw Orthotics and Prosthetics. A minor amendment was approved by the HREC to perform some of the tests at the subject's home. This was required because one of the subjects were unable to travel to Melkbosstrand.

Phase III was conducted on the same principles as Phase I except that transradial amputees were used in this phase. Due to the cost of manufacturing a socket for each amputee it was decided to attach the Myo Armband to the remaining limb instead of manufacturing and fitting a socket for each amputee. The prosthetic device was therefore also situated on the stand next to the subject. The Myo Armband was orientated to the same orientation for each subject. The EMG signals were processed by the Android device. Phase III was also divided into two stages. The first stage was the training stage. This gave the subject the chance to become familiar with the experimental setup.

The EMG signals were processed by the Android application which classified the EMG pattern recorded based on the grasp associated with the pattern. Each subject was asked to perform a certain grasp with both his/her non-amputated arm and his/her remaining limb repeatedly to train the classifier. After a discussion with Rossouw (2015) it was decided not to use Mirror Visual Feedback (MVF) but to use the Android application as visual feedback. As described in Section 4.4.2 the user was able to see the grasp as well as real-time EMG graphs on the Android device. This aided in training as the user was able to see which muscles contract when doing certain movements. Prosthesis Guided Training (PGT) was used in this project to aid in the visual feedback for the amputee. PGT was discussed in Section 2.4.4. The test setup is illustrated in Figure 5.11.



Figure 5.11: Test Setup for Phase III (Illustration: LC Theron)

5. PROTOTYPE TESTING

In the second stage the same procedure was followed as in stage one except that a classification rate was calculated based on whether the software was able to classify a grasp correctly.

Each subject was asked to perform the same grasp three times. Each grasp was held for 2 seconds. In between each repetition the subject rested for 3 seconds and in between each grasp type the subject rested for 10 seconds. The Android application stored all the EMG data and classification results on the mobile device's memory. This data was processed using MATLAB.

Each amputee had to complete a Prosthetic Evaluation Questionnaire (PEQ) after completion of the test. This PEQ was developed by Legro *et al.* (1998) to fill the need for a comprehensive self-report instrument. This questionnaire is an industry accepted questionnaire for the evaluation of prosthetic devices. The PEQ was adapted from Legro *et al.* (1998) and is given in Appendix C.3.

5.4.2 Phase III Results

It was expected that the classification accuracy may be dependent on the nature of each amputee's remaining limb. Table 5.2 provides amputation related information for each amputee tested in this project. The results of each subject were summarised in Table C.4 in Appendix C.3. The first column gives the maximum training rate achieved for the best feature set, window size and shift size. The maximum average classification rate was 94.3 % with an average standard deviation between subjects of 2.6 %.

Table 5.2: Summary of Subject Information

	Limb	Laterality	Age	Remaining Forearm [%]	Years Passed since Amputation	Cause	Type of Device Used	Years Used
1	Left	Right	44	50	26	Accident	Mechanical/ Cosmetic	25
2	Right	Right	26	20	3.5	Accident	None	0

The live classification rate was based on the parameters which achieved the maximum training classification rate. The live classification rate was calculated online. The average live classification rate was 85.3 % with a standard deviation of 8.1 % in between subjects. Figure 5.3 displays the confusion matrix of the best parameters selected for each subject.

5. PROTOTYPE TESTING

Confusion Matrix

Output Class	1	66 13.9%	0 0.0%	0 0.0%	0 0.0%	100% 0.0%
	2	49 10.3%	84 17.6%	21 4.4%	0 0.0%	54.5% 45.5%
	3	0 0.0%	0 0.0%	76 16.0%	0 0.0%	100% 0.0%
	4	0 0.0%	0 0.0%	0 0.0%	180 37.8%	100% 0.0%
		57.4% 42.6%	100% 0.0%	78.4% 21.6%	100% 0.0%	85.3% 14.7%
	1	2	3	4		
	Target Class					

Figure 5.12: Live Confusion Matrix for the Best Parameters - Phase III

From Figure 5.12 it could be seen that class 1, 3 and 4 had the highest classification rate at 100 % while class 2 had the highest misclassification rate of 45.5 % with most of the samples being classified as class 1.

Figure C.4 in Appendix C.3 displays the mean training classification rate across subjects compared to the window size and shift size for each feature set. One-way ANOVA was used to determine whether this difference was statistically significant. The p-value for each group was calculated. Table C.6 in Appendix C.3 gives the probability calculated when the data was arranged in shift size groups. Table C.5 in Appendix C.3 gives the probability calculated when the data was arranged in window size groups. It can be seen that there existed no statistical significance between the different groups as all of the p-

5. PROTOTYPE TESTING

values were above 0.05. Feature set 3 with a window shift size of 0.75 had the lowest p-value of 0.127.

The maximum mean training classification rate for each feature set was used to determine the best window and shift sizes. A summary of the best parameters per feature set is given in Table 5.3.

Table 5.3: Summary of best Parameters - Phase III

Feature Set	Mean	STD	Window Size	Shift Size
1	93.7	1.8	80	0.50
2	92.9	3.3	60	0.75
3	93.5	2.5	60	1.00

Using the parameters in Table 5.3 the three feature sets were compared and are illustrated in Figure 5.13. One-way ANOVA was used to test the probability between the three groups and was calculated as 0.95. Using the mean classification rate it was calculated that feature set 1 had the highest classification accuracy with a mean training classification accuracy of 93.7 %.

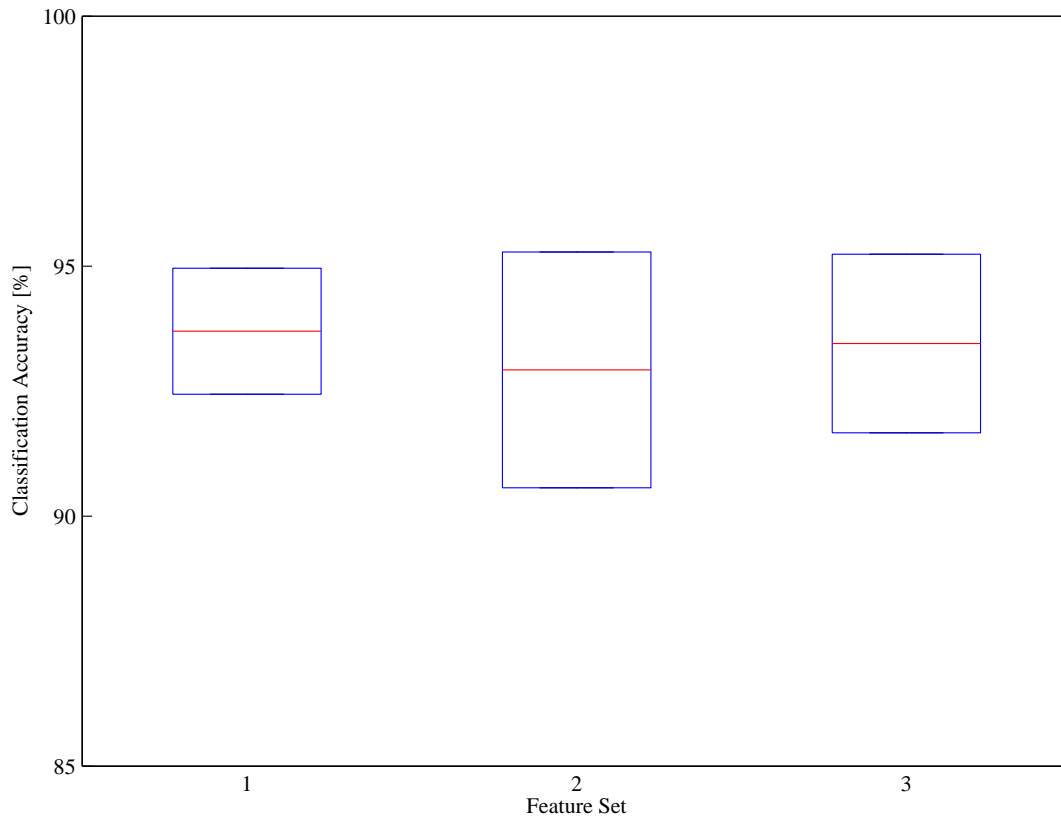


Figure 5.13: Comparison of Different Feature Sets - Phase III

5. PROTOTYPE TESTING

The best window size and shift size of feature set 1 were used to recalculate the live classification rate. These parameters were used to make direct comparisons between the different features sets. It was decided to recalculate all of the feature sets because the means were within 2 % of each other. This calculation was done offline on MATLAB. A new SOM was trained with the best parameters of feature set 1 and the confusion matrix for feature set 1 is displayed in Figure 5.14.

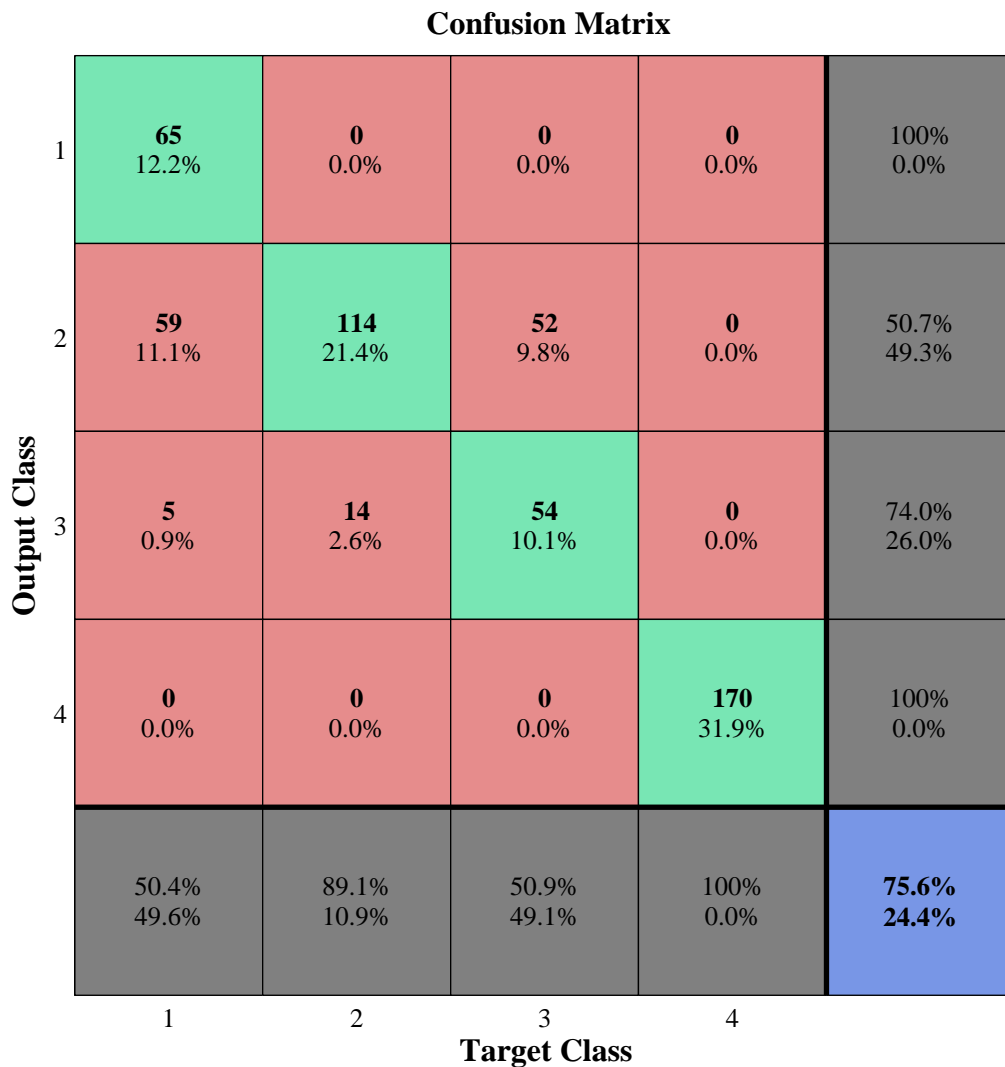


Figure 5.14: Live Confusion Plot with Overall Best Parameters - Phase III

Feature set 1 had a live classification rate of 75.6 %. Feature set 2 achieved a rate of 73.4 % and feature set 3 achieved a rate of 69.8 %.

5. PROTOTYPE TESTING

5.4.3 Phase III Discussion

The main purpose of Phase III was to determine the overall classification rate of the SOM using participants with transradial amputations. Figure 5.12 implied that the ‘Tripod Grasp’ had the highest misclassification among the four different grasps. The ‘Tripod Grasp’ were classified as a ‘Power Grasp’ the most times. This was different in comparison to Phase I where the ‘Tripod Grasp’ and the ‘Index Point Gesture’ had the highest misclassification rate.

Another purpose of this phase was to establish whether different features, window sizes and shift sizes had a significant impact on the classification rate of amputated subjects. For the range of window sizes and shift sizes tested in this project no significant difference between the different parameters were calculated. Feature set 1 had the highest mean training classification rate. There was no significant difference between different feature sets and therefore it was concluded that not one feature set achieved a higher classification rate than the other.

The live confusion matrix of the best parameters were calculated. Figure 5.14 displayed the same characteristics as Figure 5.12 where the ‘Tripod Grasp’ was misclassified as a ‘Power Grasp’ the most times. This problem can be solved in future tests by training the subject to better distinguish between different muscles when performing these two grasps.

Using feature set 1, 80 window size and 0.5 shift size a live classification rate of 93.7 % was achieved. As these were not the best parameters per subject it was expected that the overall live classification rate would be lower than that in Figure 5.12. Using the best parameters for each subject the mean training classification rate was 94.3 % with a live classification rate of 85.3 %. When using the best parameters per subject the live classification rate was 9.7 % higher than when using the overall best parameters. This was because the overall best parameters were based on the training classification rate.

The live classification results from the amputated subjects can be compared to the live classification results from the non-amputated subjects if more amputated subjects were included in this study. A t-test could determine whether there is a statistical difference in the data. This can indicate whether the results could be transferable to amputated subjects when the classifier is tested on non-amputated subjects. More amputees needs to be tested to confirm the possibility of transferring the results from non-amputated subjects to amputated subjects.

It was observed that when a higher EMG window size was chosen for the amputees they could operate the prosthetic hand with more confidence. The classifier took longer to classify the grasps and this suited the amputees as they had more time to manipulate their remaining muscles to the requirements of each grasp. The first amputee were amputated 26 years before this test was conducted. This amputee explained that the muscles in his limb took longer to feel relaxed after a grasp was initiated. The amputee took longer resting time

5. PROTOTYPE TESTING

between grasps as the grasps caused a numbing sensation in his limb. This could be because some of his forearm muscles were not as strong as it used to be and were exhausted from just a few contractions.

The results for the PEQ were summarised in Table C.7 in Appendix C.3. These results were collected subjectively from amputees and can be used for future research. It was concluded that the amputees were overall satisfied with the training and feedback of the prototype.

5.5 Offline Muscle Verification

5.5.1 Methodology

It was stated in Section 2.3.5 that the RMS is an accepted maximum likelihood estimator for EMG amplitude as it provides the average power of the muscle. Four different features were tested in this phase including RMS, MAV, WL and WAMP. The training sets of EMG data from both amputated subjects and non-amputated subjects were used to verify which muscles in the forearm were activated during the four different grasp types. The results from this verification can be used in future research to enhance feature extraction procedures and pattern classification techniques. These results can also be used to determine which sensors on the Myo Armband did not have a significant contribution towards the classification process.

The Myo Armband was set to the same orientation on each subject. These sensors were mapped to the specific forearm muscles in the human anatomy. Table 5.4 illustrates the muscle to sensor relationship. This was the relationship when the Myo Armband was placed close to the elbow as displayed in Figure 5.6. The anatomy discussed here can be seen in Figure 2.2 in Section 2.1.1.

Table 5.4: Muscle-Sensor Relationship

Sensor	Muscle
1	Palmaris longus/ Flexor carpi ulnaris
2	Flexor carpi ulnaris
3	Flexor carpi ulnaris
4	Extensor carpi ulnaris
5	Extensor digitorum
6	Extensor carpi radialis brevis/ Extensor carpi radialis longus
7	Brachioradialis / Flexor carpi radialis
8	Flexor carpi radialis

5. PROTOTYPE TESTING

5.5.2 Results

Figure 5.15 illustrates the average RMS values for 15 non-amputated subjects taken over a window of 40 EMG samples. The graph illustrates the mean RMS value and the 95 % confidence interval for each sensor on the arm. This method was followed for MAV, WL and WAMP and can be seen in Appendix C.4 in Figures C.5, C.6 and C.7. Using these graphs the dominant sensors were determined for each feature and grasp type as the three sensors with the highest amplitude. Three dominant sensors were determined for each feature and grasp and were summarised in Table 5.5.

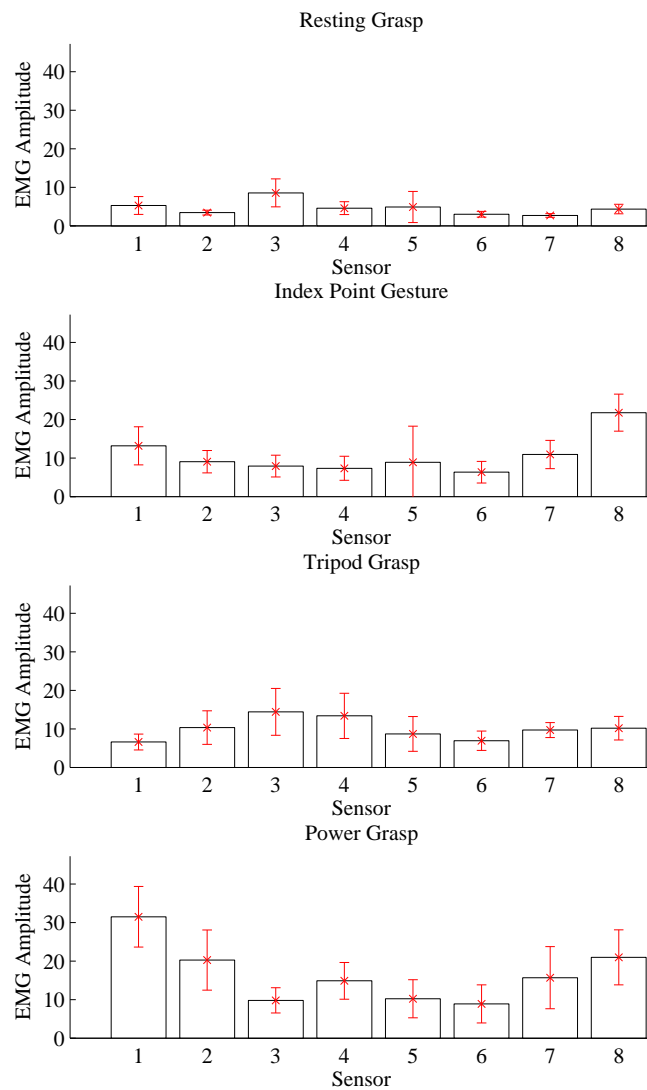


Figure 5.15: Average RMS values Non-Amputated Subjects for 8 sensors

5. PROTOTYPE TESTING

Table 5.5: Summary of Dominant Sensors for each Grasp Type and Feature

Grasp Type	Feature	Dominant Sensor		
		1st	2nd	3rd
Rest	RMS	3	1	5
	MAV	4	1	3
	WL	3	1	5
	WAMP	3	1	4
Index	RMS	8	1	7
	MAV	8	1	4
	WL	8	1	7
	WAMP	8	1	5
Tripod	RMS	3	4	2
	MAV	3	4	2
	WL	3	4	8
	WAMP	3	4	7
Power	RMS	1	8	2
	MAV	2	1	5
	WL	1	8	2
	WAMP	1	2	8

5.5.3 Discussion

The results of this test determined which sensors were dominant for each grasp type. The sensors were related to the anatomy of the non-amputated subjects tested in Phase I. Using Table 5.4 and Table 5.5 it was determined which muscles were dominant in each grasp type.

It was expected that the amplitude of the EMG signal should be small across all sensors for a resting grasp. The dominant sensor for this grasp was sensor 3 which was situated on the flexor carpi ulnaris. This sensor was not substantially more active than the other sensors therefore this dominance was subscribed to the flexion of the wrist as subjects relaxed their fingers.

The dominant sensor for an index point gesture was sensor 8 which was situated on the flexor carpi radialis. This muscle is responsible for flexion of the hand as in an index point gesture. Sensor 7 was situated on the brachoradialis which flexes when the forearm is pronated.

Sensor 3 and 4 were the dominant sensors for the tripod grasp. Sensor 3 was situated on the flexor carpi ulnaris which is responsible for the flexion of the fingers. Sensor 4 was situated on the extensor carpi ulnaris which is responsible for extending the fingers. In the tripod grasp configuration the first three digits was flexed and the fourth and fifth digit was extended. This explains the phenomenon of having both flexion and extension dominant

5. PROTOTYPE TESTING

sensors.

The dominant sensors for a power grasp was 1, 2 and 8. All of these sensors were situated on muscles responsible for flexion of the fingers. A power grasp therefore only had flexion dominant sensors.

Sensor 6 was the only sensor which did not contribute to dominant sensors. This sensor was located on muscles responsible for extension of the fingers and wrist. The fact that none of the grasps had full extension of the fingers explains that sensor 6 was never a dominant sensor.

Chapter 6

Conclusion

6.1 Outcomes

A literature study was done to investigate the required objectives of this project. Investigation was done on the anatomy of the human arm to provide an understanding of muscle activation in the forearm. Several biosignal acquisition and processing techniques were investigated. Existing prosthetic devices were summarised to understand the limitations and features of current prosthetic devices. From the literature study and interviews with Rossouw (2015) it was clear that there was a need for an affordable electronic prosthetic device for transradial amputees.

Several classification techniques and feature sets were tested on an existing database. The pattern classification verification tests were used to determine the most suited classification technique and feature sets. It was concluded that a SOM classifier should be used with three different feature sets each including three different features. These decisions were based on the classification rate, computational time and previous experience within the research group.

An electronic actuation system for the mechanical prototype developed by Tenim (2014) was developed. A working prosthetic device for transradial amputees was designed and tested. An analytical model was adapted from Tenim (2014) and the theoretical grasp strength of the prosthetic hand was calculated. The motors were specified using this model and the rest of the electronic components were selected. A custom PCB was designed and manufactured which was able to accurately measure the current of each motor used in this prosthetic device. The current of each motor was related to the torque of the motors and the torque was related to the grasp strength of this prosthesis. The EMG signals were measured using the Myo Armband. A compact microprocessor was specified and implemented the grasp control algorithm of this prosthetic device. The grasp strength of the prosthetic device was tested and compared to existing prosthetic devices. The force measured at the distal phalanx at 14 % of the maximum motor torque was 3.31 N higher than a

6. CONCLUSION

comparable commercial device.

An Android mobile application was developed to control the training and implementation phase of the SOM. This could help the user to train the classifier without the assistance of a prosthetist. The user can also enhance the training data should the user not be satisfied with the classification rate. The mobile application was written to easily add extra features, classification techniques or different grasp types. Feedback was provided via the vibrotactile feedback mechanism of the Myo Armband. The feedback mechanisms were not as rigorously tested as the classifier but was used as an amputee training aid in this project.

The last objective was to test the prototype on non-amputated subjects as well as amputated subjects. The dataset of this project contained the EMG data from four different grasps repeated eight times for 15 non-amputated subjects and two amputated subjects. This dataset also contained the grasp strength related to EMG data for 15 non-amputated subjects. Using the best features for each subject the average training classification rate among 15 non-amputated subjects was calculated at 96.2 % with a live classification rate of 87.2 %. The average training classification rate among two amputated subjects was calculated as 94.3 % with a live classification rate of 85.3 %. It was concluded that there was no significant difference between the feature sets tested in this project for both amputated and non-amputated subjects. More amputated subjects are required to determine whether there is a statistical difference between amputated subjects and non-amputated subjects. If more amputated subjects are tested it could be determined whether the results from non-amputated subjects are transferable to amputated subjects.

A testing protocol for evaluating a classification technique on transradial amputees were developed and tested in this project and appears to be promising. The testing protocol developed in this project could be implemented in future projects where the classification rate of non-amputated and amputated subjects needs to be calculated. The ethical approval protocol was submitted and approved by the HREC. The protocol established in this project could be used when ethical approval is required for a similar project.

The material cost for this prototype was R7 265.54. Compared to the available prosthetic devices on the market and the amount of money provided by the WCF and medical aids this could be regarded as an affordable device. The prototype cost was considered to be promising in a developing country such as South Africa. It was found that it is possible to develop an affordable electronic prosthetic device which could potentially provide more functionalities for transradial amputees.

6. CONCLUSION

6.2 Limitations

The mechanical design of the prosthetic hand had limitations regarding concepts for actuating the fingers. The only solution was to actuate the fingers using a cable and spool system. This solution had limitations on the grasping capabilities of the prosthetic hand. The phalanges closed separately with the DIP closing first and the PIP closing last.

By using other concepts such as linkage driven mechanisms inside the fingers the phalanges should be able to close more systematically. By using this technique better finger positional control can be achieved. The space inside the palm was also limited and only four motors could be fitted inside of the palm. If the palm design could be changed it should be possible to fit five motors inside the palm.

At the time of completion there existed no library to retrieve raw EMG data from the Myo armband using a microprocessor. As an Android library existed at the time this was solved by processing EMG data using an Android device. The EMG data could be accessed by writing a C-library for the Myo Bluetooth protocol but it was decided that this was not in the scope of this project. The training phase could be kept on the Android device but then the user should be given the option in transferring the trained classifier to the microprocessor.

The development of an affordable prosthetic device limited the quality of components used in this project. The structure of the hand was printed using ABS material on an extrusion 3D printer. The structure could have been printed using a more suitable but more expensive material like Nylon using a powder sintered 3D printer. Nylon would have been more suitable as it is stronger and with this technique no support structure needed to be printed.

The motors used in this project were selected based on dimensions, torque and cost. The motors were the cheapest motors found which satisfied all of the requirements. If more expensive motors were used the positional control could be improved. The noise emission from the motors could also be decreased by using more expensive motors.

The number of amputated subjects found for this project had limitations on the results. It could not be shown statistically whether there was a difference between amputated and non-amputated subjects. The number of amputated subjects found was two. Subject recruitment was the responsibility of Rossouw (2015) and the researcher. It was difficult to find amputees willing to partake in this study as there was no interest.

The grasp strength test of the prosthetic hand was limited by the available equipment to test the grasp strength. A dynamometer could not be acquired for this project because of the cost of a dynamometer. A pressure sensing system was developed to compensate for this limitation. This system had limitations as the grasp strength could not be compared to existing studies. This was solved by testing the force on the distal phalanx when the fingers

6. CONCLUSION

were fully extended. In this way the analytical model could be validated and give some indication if the hand could achieve the grasp forces calculated by the analytical model.

6.3 Future Recommendations

This section includes recommendations and suggestions based on the limitations and possible research opportunities.

The current mechanical design of the prosthetic device had limitations regarding the design of the actuation system of the fingers. The mechanical aspects of this device can be redesigned to increase the grasping capabilities of this device. It is suggested to substitute the cable and spool system with linkages inside of the fingers.

If the nodes of the SOM classifier is increased there is a possibility that the classification rate of the SOM classifier could increase. The performance of other classification techniques such as LDA and kNN could also be tested using the platform that was developed in this project other classification techniques can easily be implemented. The test protocol developed in this project can also be implemented when testing other techniques. Other feature sets and classification techniques can be tested on the existing EMG data that was collected from both non-amputated subjects and amputated subjects. When the offline tests are completed the test protocol and platform developed in this project could be used to test new techniques.

The database containing EMG data and grasp strength data for 15 non-amputated subjects could be used to calculate parameters to control the grasp strength of the prosthetic device. With this study the grasp strength of the prosthetic device can possibly be controlled proportionally to EMG data measured from the amputated subject. A greater population of amputated subjects needs to be tested when these tests are completed. The current classification technique was tested for four different grasps. More grasp types can be included for future tests, however it should not decrease the classification rate of the device.

The current EMG sensors contributed to one-third of the cost of this prosthetic device. EMG sensors can be designed using front-end IC's and can be manufactured using PCB's. This can greatly decrease the price of the current prosthetic device.

List of References

- Ajiboye, B. and Weir, R. (2005). A heuristic fuzzy logic approach to emg pattern recognition for multifunctional prosthesis control. *IEEE Transactions on neural systems and rehabilitation engineering*, vol. 13, no. 3, pp. 280–291.
- AndroidStudio[®] (2015). *version 1.4*. Google[®], Natick, Massachusetts.
- Arduino[®] (2016). *version 1.6.7*. Arduino.cc.
- Arms Within Reach Foundation (2015). *Prosthetic Options*. [Online] Available at: http://www.armswithinreach.org/amputee_information/prosthetic_options.html [Accessed 2 June 2015].
- Atzori, M., Muller, H. and Baechler, M. (2013). Recognition of hand movements in a trans-radial amputated subject by semg. In: *Rehabilitation Robotics (ICORR), 2013 IEEE International Conference*, pp. 1–5.
- Bach, F. (2009). *Myoelectric signal features for upper limb prostheses*. Master's thesis, Norwegian University of Science and Technology.
- Belter, J., Segil, J., Dollar, A. and Weir, R.F. (2013). The mechanical design and performance specifications of anthropomorphic prosthetic hands: A review. *Journal for Rehabilitation Research and Development (JRRD)*, vol. 50, no. 55, pp. 599–618.
- Bronzino, J. (2006). *Biomedical Engineering Fundamentals*. CRC Press.
- Cahan, D. (1993). *Hermann von Helmholtz and the foundations of nineteenth-century science*. University of California Press.
- Carrozza, M., Micera, S., Massa, B., Zecca, M., Lazzanant, R., Canelli, N. and Dario, P. (2001). The development of a novel biomechatronic hand - ongoing research and preliminary results. *Advanced Intelligent Mechatronics*, vol. 1, no. 1, pp. 249–254.
- Castellini, C., Artemiadis, P., Wininger, M. and Ajoudani, A. (2014). Going beyond traditional surface electromyography. In: *Proceedings of the first workshop on Peripheral Machine Interfaces*, vol. 8, pp. 1–17.
- Chicoine, C., Simon, A. and Hargrove, L. (2012). Prosthesis-guided training of pattern recognition-controlled myoelectric prosthesis. In: *2012 Annual International Conference of the IEEE Engineering in Medicine and Biology Society*, pp. 1876–1879.

6. LIST OF REFERENCES

- Christiansen, R., Contreras-Vidal, J.L., Gillespie, R.B., Shewokis, P.A. and O'Malley, M.K. (2013). Vibrotactile feedback of pose error enhances myoelectric control of a prosthetic hand. In: *World Haptics Conference (WHC), 2013*, pp. 531–536.
- Cutkosky, M.R. (1989). On grasp choice, grasp models, and the design of hands for manufacturing tasks. *IEEE Transactions on Robotics and Automation*, vol. 5, no. 3, pp. 269–279.
- Daley, T., Scott, R., Parker, P. and Lovely, D. (1990). Operator performance in myoelectric control of a multifunction prosthesis stimulator. *Journal of Rehabilitation Research and Development*, vol. 27, no. 1, pp. 9–18.
- Day, S. (2002). *Important factors in surface EMG measurement*. [Online] (Reviewed 2002) Available at: <http://www.bortec.ca/Images/pdf/EMG%20measurement%20and%20recording.pdf> [Accessed 2 July 2015].
- Eorthopod (2015). *Finger Fusion Surgery*. [Online] Available at: http://www.eorthopod.com/sites/default/files/images/finger_fusion_anat02.jpg [Accessed 7 July 2015].
- Feix, T., Pawlik, R., Schmiedmayer, H.-B., Romero, J. and Kragic, D. (2009). A comprehensive grasp taxonomy. In: *Robotics, science and systems conference: workshop on understanding the human hand for advancing robotic manipulation*, pp. 4169–4175.
- Ferguson, S. and Dunlop, C. (2002). Grasp recognition from myoelectric signals. *Australasian Conference on Robotics and Automation*, pp. 83–87.
- Fisher, R.A. (1936). The use of multiple measurements in taxonomic problems. *Annals of Eugenics*, vol. 7, pp. 179–188.
- Fukuda, O., Tsuji, T., Kaneko, M. and Otsuka, A. (2003). A human-assisting manipulator teleoperated by emg signals and arm motions. *IEEE Transactions on Robotics and Automation*, vol. 19, no. 2, pp. 210–220.
- Gazzoni, M., Celadon, N., Mastrapasqua, D., Paleari, M., Margaria, V. and Ariano, P. (2014). Quantifying forearm muscle activity during wrist and finger movements by means of multi-channel electromyography. *PLOS ONE*, vol. 9, no. 10, pp. 1–11.
- Gehani, A., Mohamed, S., Busedra, H. and Gawedar, A. (2013). Emg pattern recognition system based on self-organizing map for myo-electric prosthesis. In: *International Conference on Electrical and Computer Engineering (ICECE)*, pp. 1–5.
- Hermens, H.J., Freriks, B., Disselhorst-Klug, C. and Rau, G. (2000). Development of recommendations for {SEMG} sensors and sensor placement procedures. *Journal of Electromyography and Kinesiology*, vol. 10, no. 5, pp. 361 – 374.
- Kulley, M. (2003). *Hand Prosthetics*. [Online] Available at: http://biomed.brown.edu/Courses/BI108/BI108_2003_Groups/Hand_Prosthetics/stats.html [Accessed 1 June 2015].

6. LIST OF REFERENCES

- Kutafina, E., Laukamp, D. and Jonas, S. (2015). Wearable sensors in medical education: Supporting hand hygiene training with a forearm emg. *Stud Health Technology Informations*, pp. 286–91.
- Legro, M., Reiber, G., Smith, D. and Aguila, M. (1998). Prosthesis evaluation questionnaire for persons with lower limb amputations: assessing prosthesis-related quality of life. *Archives of Physical Medicine and Rehabilitation*, pp. 931–938.
- Li, G., Schultz, A. and Kuiken, T. (2010). Quantifying pattern recognition-based myoelectric control of multifunctional transradial prostheses. *IEEE Transactions on neural systems and rehabilitation engineering*, vol. 18, no. 2, pp. 185–192.
- MacKenzie, C. and Iberall, T. (1994). *The Grasping Hand*, vol. 104. Elsevier Science B.V.
- MATLAB[®] (2014). *version 8.3.0 (R2014a)*. The MathWorks Inc., Natick, Massachusetts.
- Micera, S., Rossini, P., Rigosa, J., Citi, L. and Carpaneto, J. (2011). Decoding of grasping information from neural signals recorded using peripheral intrafascicular interfaces. *Journal of NeuroEngineering and Rehabilitation*, vol. 8, no. 53, pp. 1–17.
- Millstein, S.G., Heger, H. and Hunter, G. (1986). Prosthetic use in adult upper limb amputees: a comparison of the body powered and electrically powered prostheses. *Prosthetics and Orthotics International*, vol. 10, no. 1, pp. 27–34.
- Napier, J.R. (1956 nov). The prehensile movements of the hand. *J Bone Joint Surg Br*, vol. 38-B, no. 4, pp. 902–913.
- Ngeo, J.G., Tamei, T. and Shibata, T. (2014). Continuous and simultaneous estimation of finger kinematics using inputs from an emg-to-muscle activation model. *Journal of neuroengineering and rehabilitation*, vol. 11, no. 1, pp. 1–14.
- NI (2016). *National Instruments NI USB-6218*. [Online] (Reviewed September 2016) Available at: <http://sine.ni.com/nips/cds/view/p/lang/en/nid/203484> [Accessed 3 July 2016].
- NinaPro (2014). *The Ninapro Database*. [Online] (Reviewed June 2006) Available at: <http://ninapro.hevs.ch/> [Accessed 2 June 2015].
- NoExcuseHealth (2013). *Forearm-muscles*. [Online], Available at: <https://noexcuseshealth.files.wordpress.com/2013/03/forearm-muscles.jpg> [Accessed 20 May 2015].
- Pololu (2016). *Pololu*. [Online] (Reviewed 2016) Available at: <https://www.pololu.com/product/2218> [Accessed 6 June 2016].
- Rodriguez-Cheu, L. and Casals, A. (2006). Sensing and control of a prosthetic hand with myoelectric feedback. *The First IEEE/RAS-EMBS International Conference on Biomedical Robotics and Biomechatronics, 2006.*, pp. 607–612.

6. LIST OF REFERENCES

- Rossouw, E. (2015). *Prosthetic hand Considerations*. [Interview][23 July 2015].
- Sebelius, F., Rosen, B. and Lundborg, G. (2005). Refined myoelectric control in below-elbow amputees using artificial neural networks and a data glove. *The Journal of Hand Surgery*, vol. 30A, no. 4, pp. 780–788.
- Steeper (2015). *bebionic*. [Online] (Reviewed 2015) Available at: <http://bebionic.com/> [Accessed 23 June 2015].
- Taylor, T. (1999). *Muscles of the Arm and Hand*. [Online] (Reviewed 1999) Available at: <http://http://www.innerbody.com/anatomy/muscular/arm-hand> [Accessed 7 March 2015].
- Tekscan (2016). *Tekscan FlexiForce A201*. [Online] (Reviewed September 2016) Available at: <https://www.tekscan.com/products-solutions/force-sensors/a201> [Accessed 20 July 2016].
- Tenim, S. (2014). *Design of an Affordable Anthropomorphic Mechanical Prosthetic Hand*. Master's thesis, University of Cape Town.
- Touchbionics (2015). *i-limb Ultra*. [Online] (Reviewed 2015) Available at: www.touchbionics.com/products/active-prostheses/i-limb-ultra [Accessed 23 June 2015].
- UCSF Medical Centre (2006). *Myoelectric Prostheses Offer Advantages*. [Online] (Reviewed June 2006) Available at: <http://orthoinfo.aaos.org> [Accessed 24 June 2015].
- WIKA (2016). *WIKA Instruments A-10*. [Online] (Reviewed September 2016) Available at: http://www.wika.co.za/a_10_en_co.WIKA [Accessed 2 July 2016].
- Zecca, M., Micera, S., Carrozza, M. and Dario, P. (2002). Control of multifunctional prosthetic hands by processing the electromyographic signal. *Critical Reviews in Biomedical Engineering*, vol. 30, pp. 459–485.
- Zheng, J., De La Rosa, S. and Dollar, A. (2011). An investigation of grasp type and frequency in daily household and machine shop tasks. In: *Proceedings of the 2011 IEEE International Conference on Robotics and Automation (ICRA)*, pp. 9–13.
- Zortrax (2016). *Z-ABS*. [Online] (Reviewed 2016) Available at: https://zortrax.com/materials/#cases//case_z-abs [Accessed 4 January 2016].

Appendices

Appendix A

Classification Verification

A.1 Classification Techniques

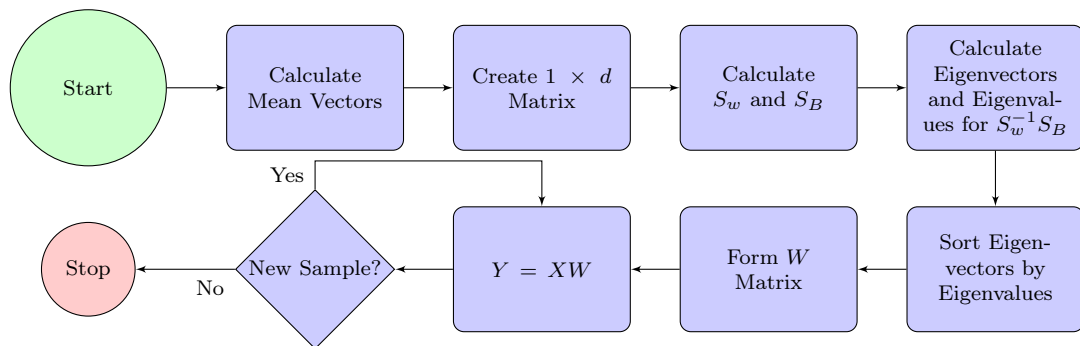


Figure A.1: Flow Diagram for LDA(Illustration: LC Theron)

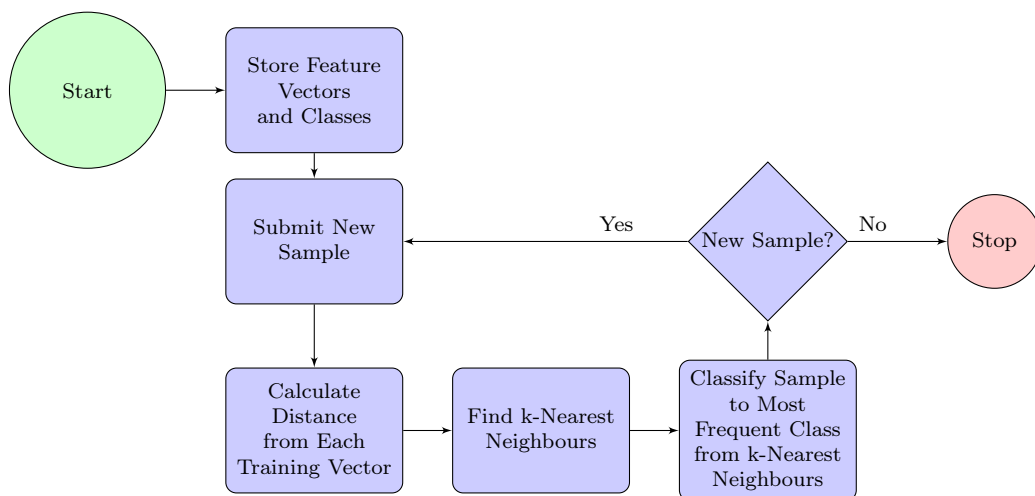


Figure A.2: Flow Diagram for kNN(Illustration: LC Theron)

A. CLASSIFICATION VERIFICATION

A.2 Preliminary Results

Table A.1: Description of Feature Set Numbers

Set	Features	Set	Features	Set	Features
1	RMS,MAV,VAR	29	MAV,VAR,WAMP	57	VAR,MYOP,WL
2	RMS,MAV,WAMP	30	MAV,VAR,MYOP	58	VAR,MYOP,AR
3	RMS,MAV,MYOP	31	MAV,VAR,SSC	59	VAR,SSC,EWC
4	RMS,MAV,SSC	32	MAV,VAR,EWC	60	VAR,SSC,WL
5	RMS,MAV,EWC	33	MAV,VAR,WL	61	VAR,SSC,AR
6	RMS,MAV,WL	34	MAV,VAR,AR	62	VAR,EWC,WL
7	RMS,MAV,AR	35	MAV,WAMP,MYOP	63	VAR,EWC,AR
8	RMS,VAR,WAMP	36	MAV,WAMP,SSC	64	VAR,WL,AR
9	RMS,VAR,MYOP	37	MAV,WAMP,EWC	65	WAMP,WL,AR
10	RMS,VAR,SSC	38	MAV,WAMP,WL	66	WAMP,EWC,AR
11	RMS,VAR,EWC	39	MAV,WAMP,AR	67	WAMP,EWC,WL
12	RMS,VAR,WL	40	MAV,MYOP,SSC	68	WAMP,SSC,AR
13	RMS,VAR,AR	41	MAV,MYOP,EWC	69	WAMP,SSC,WL
14	RMS,WAMP,MYOP	42	MAV,MYOP,WL	70	WAMP,SSC,EWC
15	RMS,WAMP,SSC	43	MAV,MYOP,AR	71	WAMP,MYOP,AR
16	RMS,WAMP,EWC	44	MAV,SSC,EWC	72	WAMP,MYOP,WL
17	RMS,WAMP,WL	45	MAV,SSC,WL	73	WAMP,MYOP,EWC
18	RMS,WAMP,AR	46	MAV,SSC,AR	74	WAMP,MYOP,SSC
19	RMS,MYOP,SSC	47	MAV,EWC,WL	75	MYOP,WL,AR
20	RMS,MYOP,EWC	48	MAV,EWC,AR	76	MYOP,EWC,AR
21	RMS,MYOP,WL	49	MAV,WL,AR	77	MYOP,EWC,WL
22	RMS,MYOP,AR	50	VAR,WAMP,MYOP	78	MYOP,SSC,AR
23	RMS,SSC,EWC	51	VAR,WAMP,SSC	79	MYOP,SSC,WL
24	RMS,SSC,WL	52	VAR,WAMP,EWC	80	MYOP,SSC,EWC
25	RMS,SSC,AR	53	VAR,WAMP,WL	81	SSC,EWC,WL
26	RMS,EWC,WL	54	VAR,WAMP,AR	82	SSC,EWC,AR
27	RMS,EWC,AR	55	VAR,MYOP,SSC	83	SSC,WL,AR
28	RMS,WL,AR	56	VAR,MYOP,EWC	84	EWC,WL,AR

A. CLASSIFICATION VERIFICATION

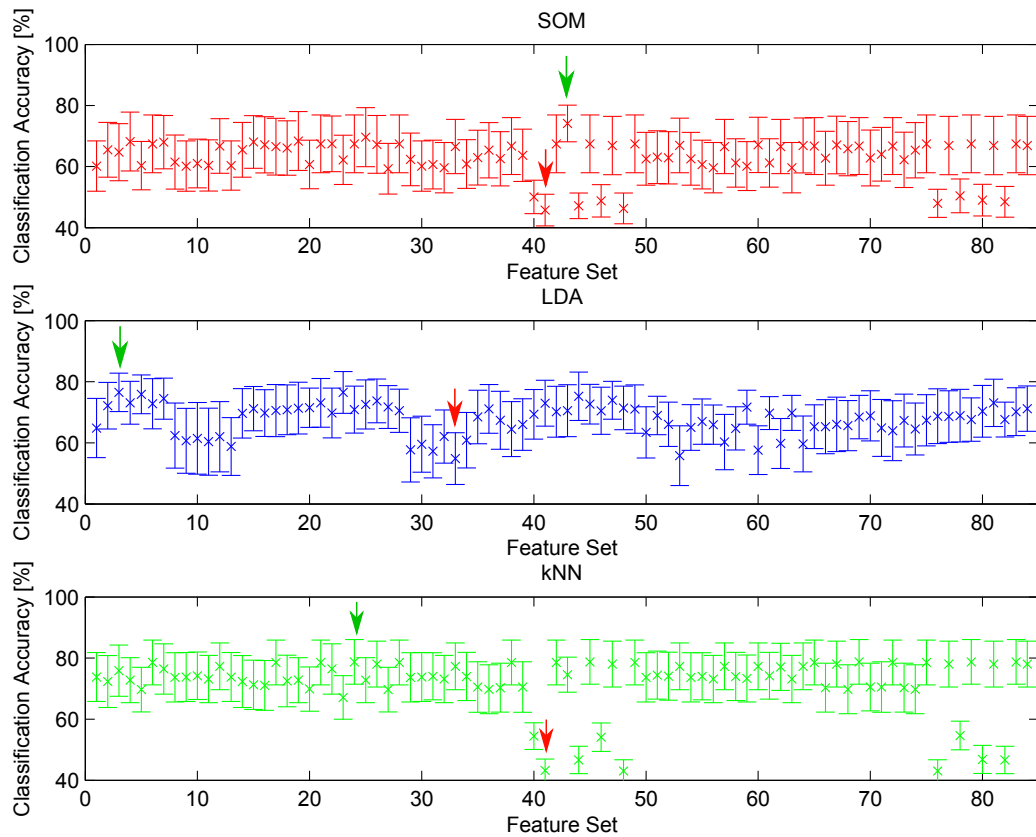


Figure A.3: Comparison of Different Classification Techniques and Feature Sets for Non-Amputated Subjects

A. CLASSIFICATION VERIFICATION

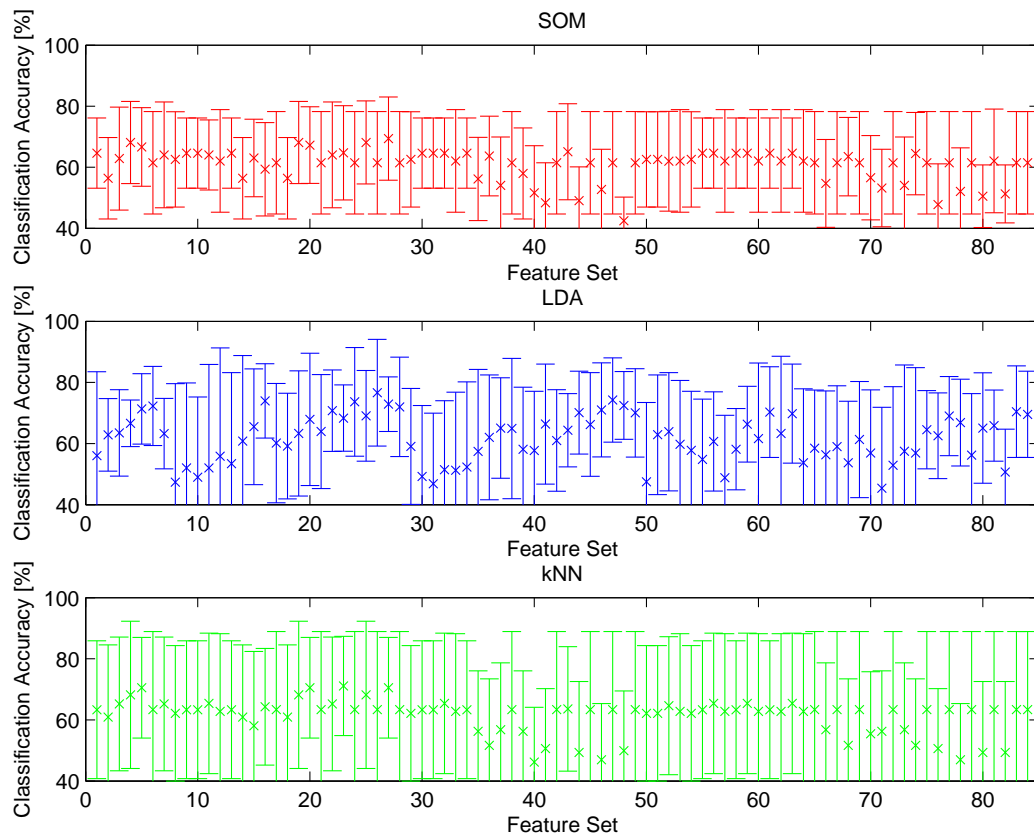


Figure A.4: Comparison of Different Classification Techniques and Feature Sets for Amputated Subjects

Appendix B

Design

B.1 Analytical Model

The analytical model of the mechanical hand was developed by Tenim (2014) and an overview of the model is described in this appendix. The free body diagram is illustrated in Figure B.1.

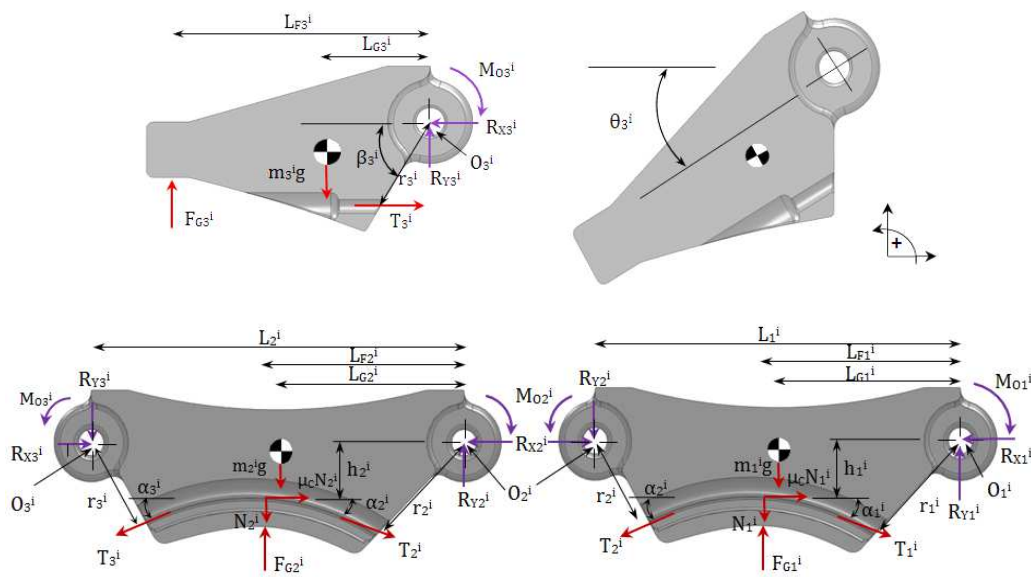


Figure B.1: Free Body Diagram (Adapted from: (Tenim, 2014))

Tenim (2014) developed a model for all three phalanges combined and derived equations for the moments. Equations B.1 - B.10 were derived by Tenim (2014) and describe the counter-clockwise moments around O_1^i .

B. DESIGN

$$\begin{aligned} \sum M_{Mass1}^i &= m_1^i g(L_{G1}^i \cos(\theta_1^i)) + m_2^i g(L_{G1}^i \cos(\theta_1^i) + L_{G2}^i \cos(\theta_1^i + \theta_2^i)) \\ &\quad + m_3^i g(L_{G1}^i \cos(\theta_1^i) + L_{G2}^i \cos(\theta_1^i + \theta_2^i) + L_{G3}^i \cos(\theta_1^i + \theta_2^i + \theta_3^i)) \end{aligned} \quad (B.1)$$

$$\sum M_{Spring1}^i = -\frac{\theta_1^i d^4 E}{64 D N a} \quad (B.2)$$

$$\sum M_{Tension1}^i = T_3^i (r_3^i \sin(\beta_3^i + \theta_3^i)) + N_2^i ((L_1^i + L_{F2}^i) + \mu_C h_2^i) + N_1^i (L_{F1}^i + \mu_C h_1^i) \quad (B.3)$$

$$\begin{aligned} \sum M_{Hinge1}^i &= -\mu_r r_P^i \left(((m_1^i + m_2^i + m_3^i)g - (F_{G1}^i + F_{G2}^i + F_{G3}^i) + N_1^i + N_2^i)^2 \right. \\ &\quad \left. + (T_3^i + \mu_C N_1^i + \mu_C N_2^i)^2 \right)^{0.5} \end{aligned} \quad (B.4)$$

$$\begin{aligned} \sum M_{Grasp1}^i &= -F_{G1}^i L_{F1}^i - F_{G1}^i (L_{F1}^i + L_{F2}^i \cos(\theta_2^i)) \\ &\quad - F_{G1}^i (L_{F1}^i + L_{F2}^i + L_{F3}^i \cos(\theta_3^i)) \end{aligned} \quad (B.5)$$

$$N_1^i = T_1^i \sin(\alpha_1^i) + T_2^i \sin(\alpha_2^i) \quad (B.6)$$

$$N_2^i = T_2^i \sin(\alpha_2^i) + T_3^i \sin(\alpha_3^i) \quad (B.7)$$

$$T_1^i = F_i \quad (B.8)$$

$$T_2^i = \frac{1 - \mu_C \sin(\alpha_1^i)}{1 + \mu_C \sin(\alpha_2^i)} F_i \quad (B.9)$$

$$T_3^i = (1 - \mu_C \sin(\alpha_1^i)) \left(1 - \frac{\mu_C 2 \sin(\alpha_2^i)}{1 + \mu_C \sin(\alpha_2^i)} \right) / (1 + \mu_C \sin(\alpha_3^i)) F_i \quad (B.10)$$

$$\sum M_{Grasp}^i = \sum M_{Tension}^i - \sum M_{Mass}^i - \sum M_{Spring}^i - \sum M_{Hinge}^i \quad (B.11)$$

Where:

B. DESIGN

- L_G - distance from pivot to centre of gravity
- T - cable (tendon) tension
- M_O - hinge reaction moment
- g - gravitational acceleration
- β - angle of interphalangeal phalanx face
- L_F - distance from pivot to applied grip force and/or normal force
- d - spring wire diameter
- D - radial mean coil diameter
 - μ_r - estimated coefficient of hinge friction (static)
- L - length of phalanx
- h - distance of tendon friction force from hinge/pivot
- α - angle of deviation of actuating wire
- M_{Grasp} - Grasp moment
- $M_{Tension}$ - Tension moment
- M_{Spring} - Spring moment
- F_G - applied grasp force
- R_X/Y - hinge reaction forces in x and y directions
- m - distance mass of phalanx
- r - radial channel distance from pivot
- i - identifier for fingers/digits
- θ - flexion angle of each phalange
- E - Young's Modulus of spring material
- Na - number of active turns of spring
- r_p - hinge pin radius
- N - normal reaction force of cable/tendon on the phalanx
- μ_c - coefficient of channel friction (static)
- F_i - Input force
- M_{Mass} - Mass moment
- M_{Hinge} - Hinge moment

Equations B.6 - B.7 were solved by substituting Equations B.8 - B.10 for different input forces F_i . Equations B.6 - B.7 were substituted into Equations B.3 - B.4. Equations B.1 - B.5 were substituted into Equation B.11 and the grasp forces were calculated for different angles of θ .

B.2 PCB Design

The schematic of the PCB designed for the current sensor is illustrated in Figure B.2.

The Integrated Circuit (IC) used on this board was an INA169 IC from Texas Instruments. The INA169 is a high-side current monitor. The INA169 outputs a current based on the voltage drop measured across a shunt resistor, R_S in Figure B.2. A load resistor R_L was placed to ground at the output of the INA169 and a voltage was measured from the output to ground. The INA169 can measure a maximum of 500 mV across the shunt resistor. For this application the maximum difference was calculated as 312 mV with a maximum stall current of 1600 mA and a shunt resistor R_S of 0.195 Ω . The INA169 can not accurately measure a voltage drop below 35 mV. Including the voltage drop across the internal transistor of the INA169 the maximum output voltage that could be measured was 2.288 V.

A load resistor of 7.32 k Ω was used. A bypass capacitor C of 100 nF was used to remove any unwanted noise from the signal. Using Equation B.12 the current can be calculated by substituting the voltage measured at the output.

$$I_s = \frac{(V_o \times 1k\Omega)}{(R_s \times R_L)} \quad (\text{B.12})$$

Here I_s was the current flowing through the shunt resistor, V_o the voltage measured at the output and the 1 k Ω the internal resistance of the INA169.

B. DESIGN

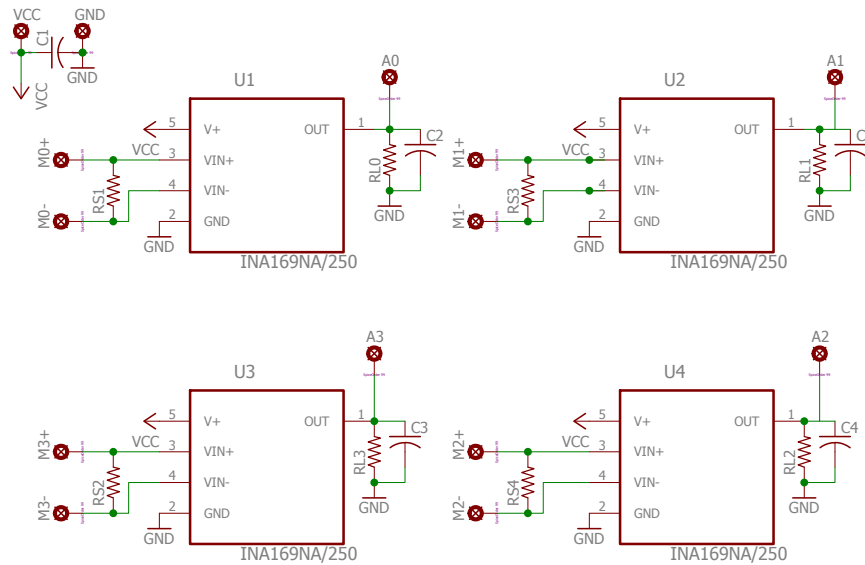


Figure B.2: Current Sensor Schematic (Illustration: LC Theron)

Using Equation B.12 with a maximum output voltage of 2.288 V a maximum current of 1602 mA can be measured with this configuration. The current sensor was calibrated and the calibration curve is illustrated in Figure B.3. The test was repeated five times to account for repeatability.

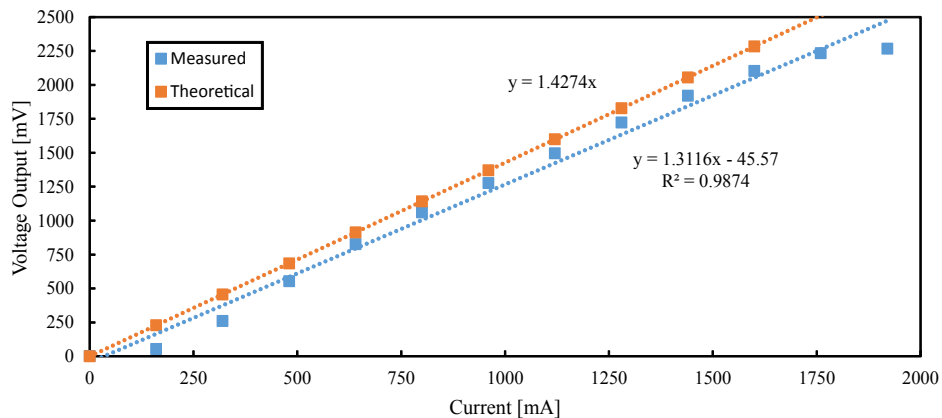


Figure B.3: Current Sensor Calibration Curve

A linear equation for the sensor was derived and can be seen in Figure B.3. The squared-residual value was calculated as 0.987 for this linear regression curve which was a relative good fit. It was calculated theoretical that the current sensor can only measure between 0.179 mA and 1602 mA and this can be seen in the graph.

B. DESIGN

The power supply schematic is illustrated in Figure B.4.

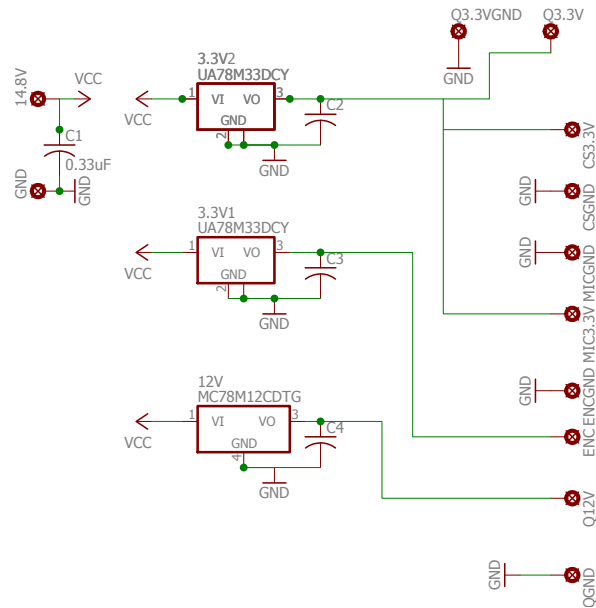


Figure B.4: Power Supply Schematic (Illustration: LC Theron)

Bypass capacitors were placed on the power supply to this PCB as well as the outputs of the voltage regulators to provide a steady voltage. All components required 3.3 V except for the motor drivers which were powered at 12 V.

B. DESIGN

B.3 Android Development

Table B.1: Functions Written in Java

Class	Function	Description
GetFeatures.java	training (features, featnum) liveInput (livefeatures) computeInput (vectorArray, vectorNumber) updateWeights (features, vectorNumber, BMU) minimum (nodeArray) printResults (features, graspVector, featnum) getMaxPos (array, size) printRepeating (array, size) GetRMS (data, windowSec) GetFeats (data, windowSec, whatFeat)	Responsible for the training of the SOM Calculated the class based on live EMG data Computed the input for all nodes Updated the weights of the SOM using the BMU Finds the minimum of the nodes Calculated a comparison matrix Finds the maximum inside an array Determined if a class had been misclassified Calculated the RMS value for the live display of EMG data Extracted several features sets
Calculations.java	calculate (EMGData, GraspData, dataCounter, whatFeats) double liveCalculate (EMGDATA, GraspData, dataCounter, whatFeats)	Did several iterations to determine the best feature set, window size and window shift size Used for live classification with the best feature set, window size and window shift size
Files.java	clear (path) append (path, text) write (path, text)	Cleared a text file Appended data to a text file Cleared a text file and then wrote the data to a text file
MyoInfoView.java	onFinishInflate () onAttachedToWindow () onNewEmgData (emgData) onNewImuData (imuData)	After the view was inflated this function set up the Bluetooth and the user interface All the buttons were set up and the Myo Armband was set to EMG mode When new EMG data was available this function recorded EMG data and controlled the window size and shift size Calculates the yaw, roll and pith of the Myo

B.4 Assembly

This appendix describes the assembly of the mechanical and electronic parts situated inside of the palm. A complete assembly of the fingers was stipulated by (Tenim, 2014). Figure B.5 illustrates the components necessary for assembly. The components were assembled according to the numbering system on Figure B.5.

B. DESIGN

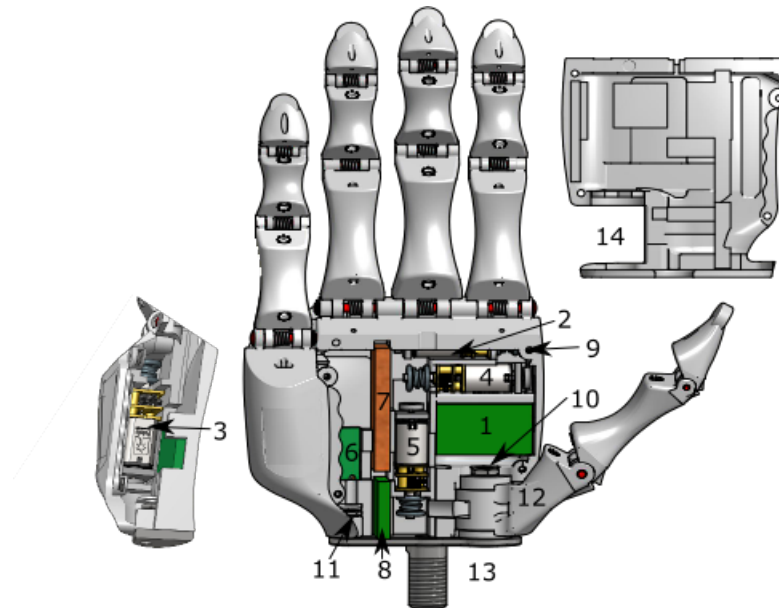


Figure B.5: Assembly of Prosthesis (Illustration: LC Theron)

The motor drivers [1] were assembled on top of each other in order to save space and create a daisy chain of the serial line. Before the drivers were placed into the rectangular slot, all the wires were soldered onto the pins.

The encoders of all the DC motors were soldered into place before the motors were placed into their respective slots. The cable for the 2nd digit was threaded through the channels in the phalanges and through the hole above the spool. The cable was threaded through the hole in the spool and a grub screw was set in the other hole in the spool. The DC motor for the 2nd digit [2] were slotted into to spool after the spool was situated in its slot. The grub screw was tightened to keep the cable and spool in place.

The DC motor for the 4th and 5th digits [3] was pre-assembled with its encoder and spool. The same procedure for fixing the spool and cable was followed. This motor was slotted in to its rectangular slot underneath the left side of the palm. The same procedure was followed for the DC motor of the 3rd [4] and 1st [5] digit. After all of the grub screws were tightened the cables were fed through the channels in the phalanges.

The wires of the power supply PCB [6] were soldered onto the board and the board was fixed to the palm with glue. The same procedure was followed for the microprocessor [7] and current sensor [8].

The four nuts on top of the palm [9] were set in place for the palm cover. After the nut for the bolt on the thumb side [10] was set in place and then a nut for the bolt on the other side [11] was set in place. The torsional spring for the thumb [12] was set in place and the 1st digit was slotted into place. The wrist fitting [13] was set in place and the positive and ground wires leading to the battery were fed through the center hole of the wrist fitting. The palm

B. DESIGN

cover [14] was set in place on top of the palm and was fixed to the palm using 6 screws. Two of these bolts at the wrist side and 4 of these bolts on the palm side. A bolt was inserted through the palm cover, wrist stem fitting and proximal phalanx of the thumb from position 13 to 10. Another bolt was inserted to fix to the nut at position 11.

B.5 Affordability

Table B.2: Cost Breakdown A

Component	Description	Manufacturer	Quantity	Unit Cost	Total Cost
Fasteners					
E-Clip	1.5 mm	BMG	20	R0.08	R1.60
E-Clip	1.9 mm	BMG	11	R0.10	R1.10
Nut	M2	Topfast	4	R1.04	R4.16
Screw	M2 x 8 Self-Tapping	Topfast	4	R1.10	R4.40
Screw	M1.6 x 5 Countersunk	Topfast	8	R1.50	R12.00
Screw	M2 x 3 Grub Screw	Topfast	4	R3.50	R14.00
Screw	M6 x 35	Topfast	1	R1.90	R1.90
Nut	M6	Topfast	1	R1.10	R1.10
Screw	M4 x 16	Topfast	1	R1.20	R1.20
Nut	M4	Topfast	1	R1.04	R1.04
					R42.50
Assembly					
			(min)	R/min	
Current Sensor	Solder components	N/A	30	R1.00	R30.00
Power Supply	Solder components	N/A	20	R1.00	R20.00
Motors + Encoders	Attach Encoders	N/A	20	R1.00	R20.00
Phalanges + Springs + Pins + Mandrels	Assemble each phalange	N/A	30	R1.00	R30.00
Motor Drivers	Attach motor drivers to each other	N/A	20	R1.00	R20.00
Spools + Cables	Attach motor assembly to spools and cables	N/A	20	R1.00	R20.00
Palm	Attach above assemblies to palm	N/A	40	R1.00	R40.00
Wiring	Complete all wiring	N/A	30	R1.00	R30.00
Battery + Power Supply	Solder battery to power supply PCB	N/A	3	R1.00	R3.00
Palm Cover + Wrist Stem	Assemble palm cover and wrist stem	N/A	3	R1.00	R3.00
					R216.00

B. DESIGN

Table B.3: Cost Breakdown B

Component	Description	Manufacturer	Quantity	Unit Cost	Total Cost
Electronic Components					
Motor	Micro Mmetal Gearmotor 298:1 + external shaft	Pololu	4	R220.00	R880.00
Encoder	Magnetic	Pololu	4	R130.00	R520.00
Motor Driver	Qik 2s9v1	Pololu	2	R300.00	R600.00
Microprocessor	BlendMicro	Redbearlab	1	R318.00	R318.00
EMG Sensor	Myo Armband	Thalmic	1	R2 724.65	R2 724.65
Battery	Ansmann 14.8 V, 2600 mAh	Ansmann	1	R750.69	R750.69
Battery Charger	Ansmann 4 Cell, 33.6 W	Ansmann		R622.96	R622.96
					R6 416.30
Current Sensor					
PCB	Custom PCB	TraX	1	R33.62	R33.62
Resistor	390 m ERJ6B Series Thick Film 0805	Panasonic	8	R2.76	R22.08
Resistor	7.32 k ERA Series Thin Film 0603	Panasonic	4	R2.68	R10.72
Capacitor	100 nF Ceramic Capacitor	Murata	4	R1.05	R4.20
Capacitor	330 nF Ceramic Capacitor	TDK	1	R1.65	R1.65
Current IC	INA169	TI			R0.00
					R72.27
Power Supply					
PCB	Custom PCB	TraX	1	R33.62	R33.62
Voltage Regulator	MC7812CDTG 12 V	ON	1	R5.20	R5.20
Voltage Regulator	UA78M33CDCY 3.3V	TI	2	R6.51	R13.02
Capacitor	100 nF Ceramic Capacitor	Murata	3	R1.05	R3.15
Capacitor	330 nF Ceramic Capacitor	TDK	1	R1.65	R1.65
					R56.64
Manufactured Components					
			[g]	R/g	
Palm	Zortrax ABS Material	BERG	64	R0.65	R41.60
Palm Cover	Zortrax ABS Material	BERG	20.8	R0.65	R13.58
Wrist Stem	Zortrax ABS Material	BERG	5.8	R0.65	R3.82
1st Digit	Zortrax ABS Material	BERG	21.6	R0.65	R14.05
2nd Digit	Zortrax ABS Material	BERG	13.3	R0.65	R8.66
3rd Digit	Zortrax ABS Material	BERG	15.7	R0.65	R10.25
4th Digit	Zortrax ABS Material	BERG	13.3	R0.65	R8.66
5th Digit	Zortrax ABS Material	BERG	9.4	R0.65	R6.12
4 Spools	Zortrax ABS Material	BERG	1.2	R0.65	R0.78
					R107.51
Mechanical Components					
Spring	Helical torsion springs (3<N <6)	Gellini	14	R4.65	R65.10
Spring	∅6mm Helical torsion springs N = 5	Springman	1	R103.00	R103.00
Mandrel	∅5mm Spring Mandrel	UCT	14	R2.94	R41.16
Pin	Several Pins for Phalanges	UCT	12	N/A	R143.11
Cable	Nylon Coated Stainless Steel	FishMate	50 cm	R0.04	R1.95
					R354.32

Appendix C

Results

C. RESULTS



UNIVERSITEIT • STELLENBOSCH • UNIVERSITY
jou kennisvennoot • your knowledge partner

Approval Notice Response to Modifications- (New Application)

25-Jan-2016
Theron, Landolf LC

Ethics Reference #: M15/09/031

Title: Grasp classification accuracy of a myoelectric prosthetic device

Dear Mr. Landolf Theron,

The **Response to Modifications - (New Application)** received on **12-Jan-2016**, was reviewed by members of **Health Research Ethics Committee 2** via Expedited review procedures on **21-Jan-2016** and was approved.
Please note the following information about your approved research protocol:

Protocol Approval Period: **21-Jan-2016 -20-Jan-2017**

Please remember to use your **protocol number (M15/09/031)** on any documents or correspondence with the HREC concerning your research protocol.

Please note that the HREC has the prerogative and authority to ask further questions, seek additional information, require further modifications, or monitor the conduct of your research and the consent process.

After Ethical Review:

Please note a template of the progress report is obtainable on www.sun.ac.za/rds and should be submitted to the Committee before the year has expired. The Committee will then consider the continuation of the project for a further year (if necessary). Annually a number of projects may be selected randomly for an external audit.

Translation of the consent document to the language applicable to the study participants should be submitted.

Federal Wide Assurance Number: 00001372

Institutional Review Board (IRB) Number: IRB0005239

The Health Research Ethics Committee complies with the SA National Health Act No.61 2003 as it pertains to health research and the United States Code of Federal Regulations Title 45 Part 46. This committee abides by the ethical norms and principles for research, established by the Declaration of Helsinki, the South African Medical Research Council Guidelines as well as the Guidelines for Ethical Research: Principles Structures and Processes 2004 (Department of Health).

Provincial and City of Cape Town Approval

Please note that for research at a primary or secondary healthcare facility permission must still be obtained from the relevant authorities (Western Cape Department of Health and/or City Health) to conduct the research as stated in the protocol. Contact persons are Ms Claudette Abrahams at Western Cape Department of Health (healthres@pgwc.gov.za Tel: +27 21 483 9907) and Dr Helene Visser at City Health (Helene.Visser@capetown.gov.za Tel: +27 21 400 3981). Research that will be conducted at any tertiary academic institution requires approval from the relevant hospital manager. Ethics

C. RESULTS

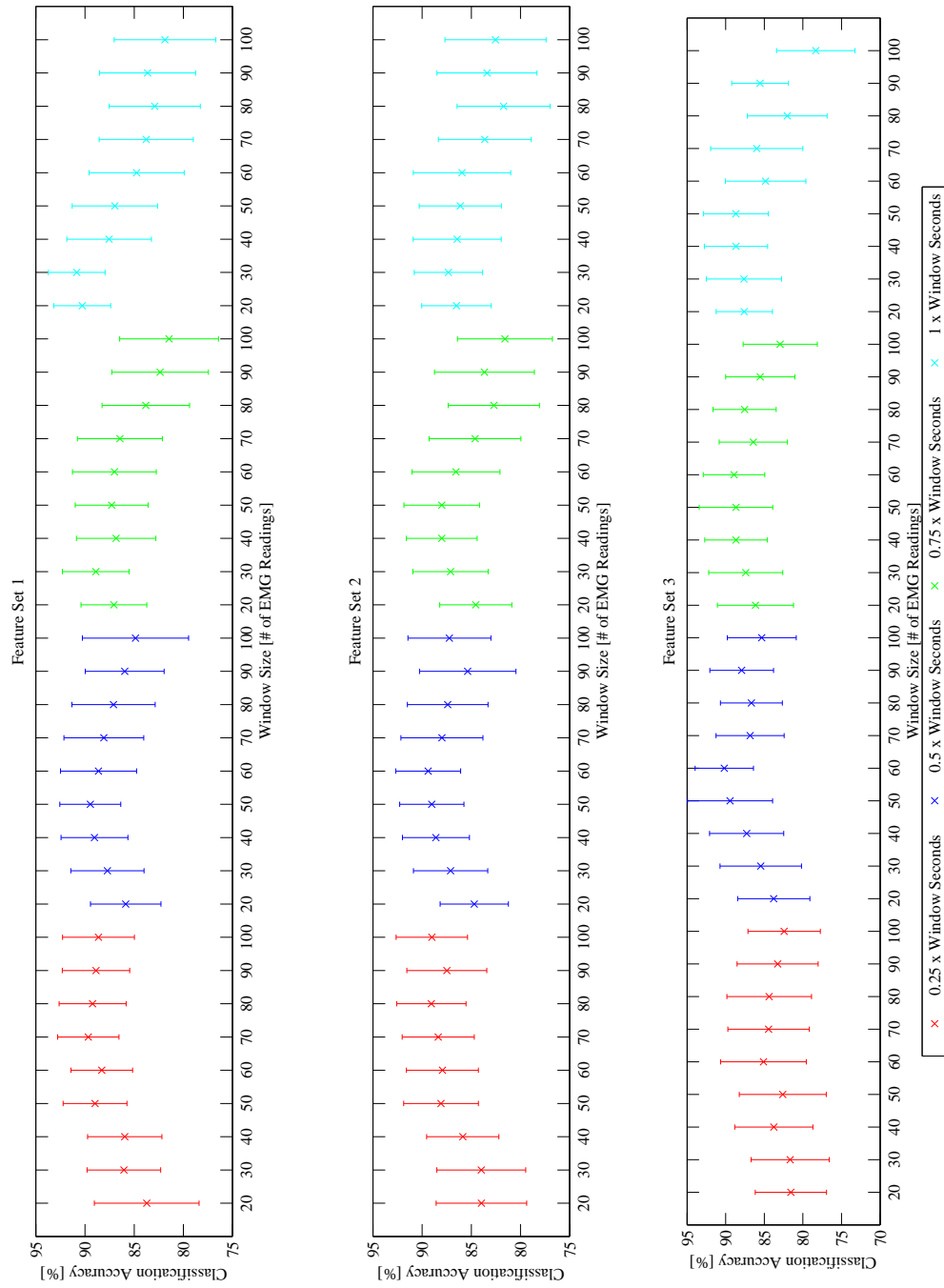


Figure C.1: Classification Results for all Non-Amputated Subjects per Feature

C. RESULTS

C.1 Phase I

Table C.1: Classification Results per Non-Amputated Subject

Subject	Training %	Feature	Window Size	Shift Size	Test %
1	95.3	3	70	0.25	79.2
2	96.4	3	90	1.00	89.6
3	98.8	2	60	1.00	91.9
4	96.7	1	70	0.75	90.9
5	93.5	1	70	0.25	87.3
6	86.8	3	50	0.75	95.7
7	100.0	2	80	0.50	76.2
8	92.8	1	80	0.25	76.4
9	97.6	2	60	1.00	86.3
10	93.0	1	90	0.75	88.5
11	100.0	2	60	1.00	94.8
12	95.8	1	80	0.50	86.6
13	98.6	3	70	1.00	87.8
14	98.3	3	20	0.75	93.0
15	99.6	1	20	1.00	94.5
	96.2				87.2

Table C.2: ANOVA Probability with Window Size as Groups for Non-Amputated Subjects

Feature Set	Shift Size			
	0.25	0.5	0.75	1
1	0.514	0.862	0.355	0.106
2	0.600	0.846	0.514	0.755
3	0.992	0.776	0.805	0.124

C. RESULTS

Table C.3: ANOVA Probability with Shift Size as Groups for Non-Amputated Subjects

Feature Set	Window Size								
	20	30	40	50	60	70	80	90	100
1	0.216	0.374	0.791	0.784	0.632	0.334	0.223	0.270	0.239
2	0.859	0.672	0.787	0.811	0.736	0.427	0.104	0.699	0.126
3	0.364	0.422	0.494	0.310	0.388	0.941	0.471	0.634	0.335

C.2 Phase II

Two A-10 pressure transducers manufactured by WIKA (2016) was used to measure the pressure for Phase II. These pressure transducers were able to measure between 0-100 kPa. The current drawn by the pressure transducers were linear dependent on the pressure applied to the membrane. This current was measured by measuring the voltage drop over a 250 Ω resistor. The voltage was measured using a 10-bit ADC. Measurements were taken in increments of 10 kPa and was repeated five times.

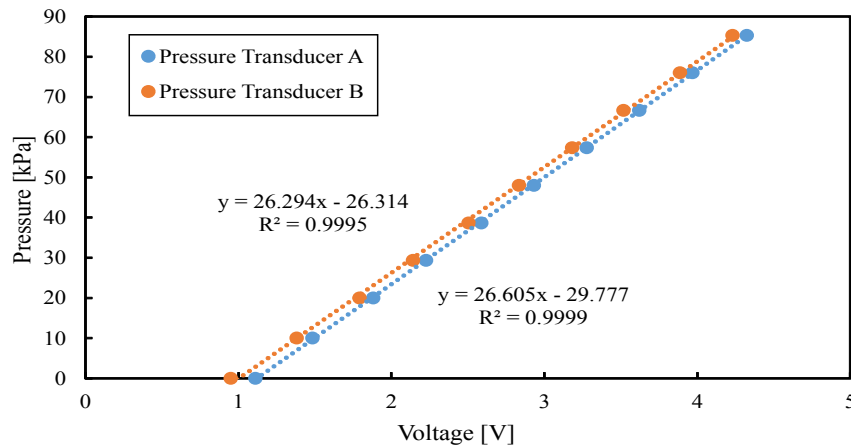


Figure C.2: Calibration Curve for Pressure Gauges

The best linear line of fit was calculated for each pressure transducer and can be seen in Figure C.2. These equations were used to determine the pressure for Phase II.

A FlexiForce FSR manufactured by Tekscan (2016) was used to measure the distal phalanx force in Phase II. The FSR was calibrated using weights in increments of 1 kg with a maximum of 8 kg and was repeated five times.

C. RESULTS

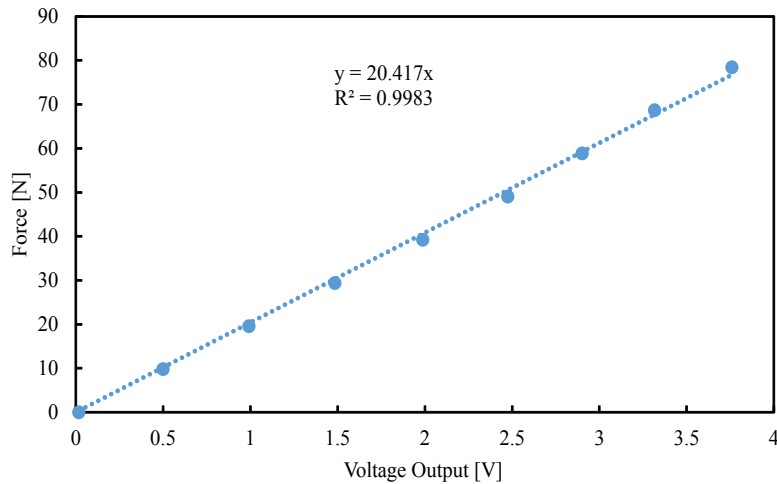


Figure C.3: Calibration Curve for FSR

The best linear line of fit was calculated for for the FSR and the equation displayed in Figure C.3 was used to determine the force in Phase II.

C.3 Phase III

Table C.4: Classification Results per Amputated Subject

Subject	Training %	Feature	Window Size	Shift Size	Test %
1	92.4	1	80	0.50	91.1
2	96.1	1	50	0.75	79.7
	94.3				85.3

Table C.5: ANOVA Probability with Window Size as Groups for Two Amputated Subjects

Feature Set	Shift Size			
	0.25	0.5	0.75	1
1	1.000	0.984	0.967	0.938
2	0.440	0.443	0.787	0.608
3	0.159	0.194	0.127	0.191

C. RESULTS

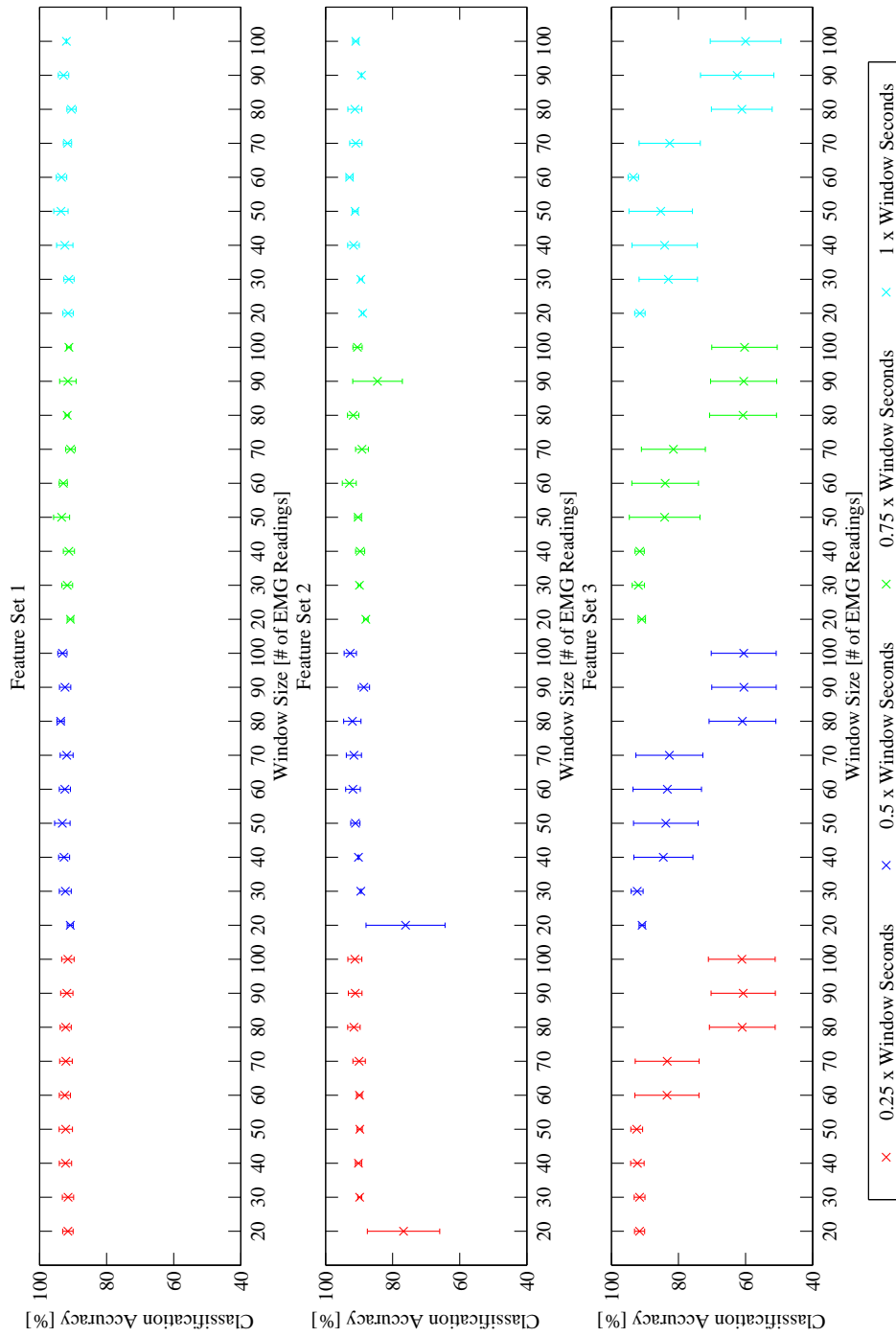


Figure C.4: Classification Results for Two Amputated Subjects per Feature

C. RESULTS

Table C.6: ANOVA Probability with Shift Size as Groups for Two Amputated Subjects

Feature Set	Window Size								
	20	30	40	50	60	70	80	90	100
1	0.967	0.978	0.966	0.976	0.970	0.954	0.527	0.973	0.782
2	0.659	0.890	0.765	0.816	0.670	0.874	0.996	0.767	0.859
3	0.973	0.589	0.804	0.910	0.855	0.999	1.000	0.999	1.000

Table C.7: PEQ Results from Amputated Subjects

Question	Subject	
	1	2
A	8	9
B	1	1
C	5	10
D	9	10
E	7	10
F	7	10
G	None	None
H	9	10
I	9	10

C. RESULTS



UNIVERSITEIT • STELLENBOSCH • UNIVERSITY
jou kennisvennoot • your knowledge partner

STELLENBOSCH UNIVERSITY

Prosthetic Evaluation Questionnaire

Introduction

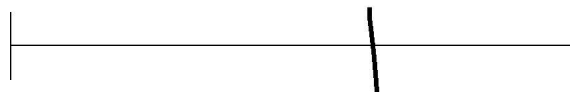
The myoelectric prosthetic device has been developed and tested and is ready to be tested on amputees. Thank you for volunteering to participate in this study. The questionnaire which follows should be completed at the end of this evaluation. The data collected in this questionnaire will be held confidential at all times. Please follow the instructions and take your time to complete the questionnaire.

Instructions

As you read each question, remember there is no right or wrong answer. Just think of your own opinion on the topic and make a mark through the line anywhere along the line from one end to the other to show us your opinion.

Example

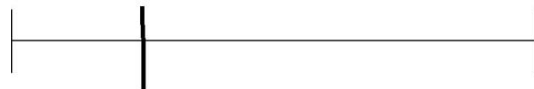
How important is it to you to have coffee in the morning?



NOT AT ALL

EXTREMELY IMPORTANT

Over the past three weeks, rate your morning coffee.



TERRIBLE

EXCELLENT

OR check ___I haven't drunk coffee in the morning in the past three weeks.

This example shows that the person who answered these questions feels that having coffee in the morning is important to him. He also thinks the coffee he has had lately has not been very good. If he hadn't drunk any coffee in the last three weeks, he would have put a check by that statement instead of putting a mark on the line between TERRIBLE and EXCELLENT. As in this example, make a mark across the line rather than using an X or an O.

Please answer all the questions.

C. RESULTS

A. How satisfied are you with the training you have received on using this prosthesis?



B. Would you rather use a prosthetic device which can naturally detect your intentions or would you use a device which you need to activate grasps by command?

(Circle answer)

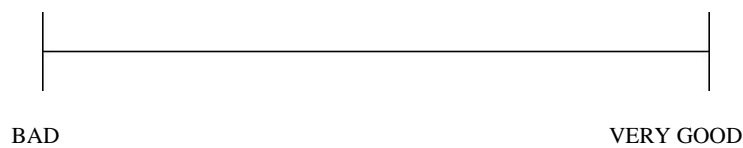
1) Naturally detect

2) Command

C. How difficult was it to activate different grasps?



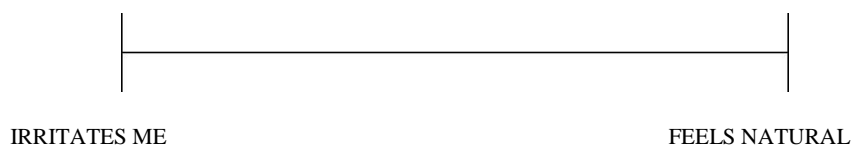
D. The grasping capabilities is...



E. The feedback this prosthesis gives me...



F. The feedback of my prosthesis...



G. What other grasps would you like to be able to do with this prosthesis?

- a. _____
- b. _____
- c. _____
- d. _____

C. RESULTS

H. How would you rate the mobile application?



NOT HELPFUL VERY HELPFUL

I. How comfortable is the Myo Armband?



NOT AT ALL FEELS NATURAL

Final Notes

- A. Please share with us anything else about you or your prosthesis that you think would be helpful for us to know (continue on the back of this page if you need more space).

THANK YOU VERY MUCH!

C. RESULTS

C.4 Offline Muscle Verification

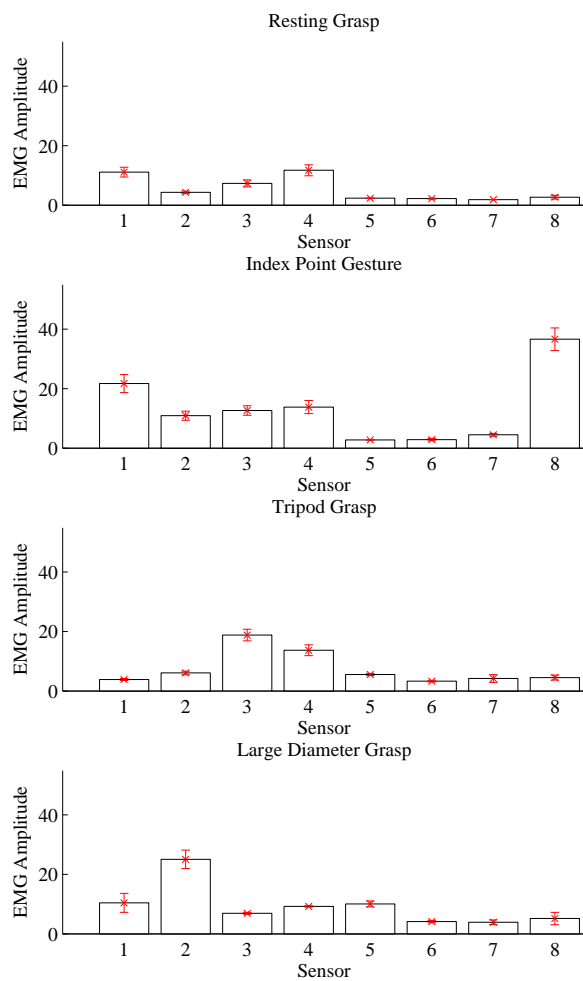


Figure C.5: Average MAV values Non-Amputated Subjects for 8 Sensors

C. RESULTS

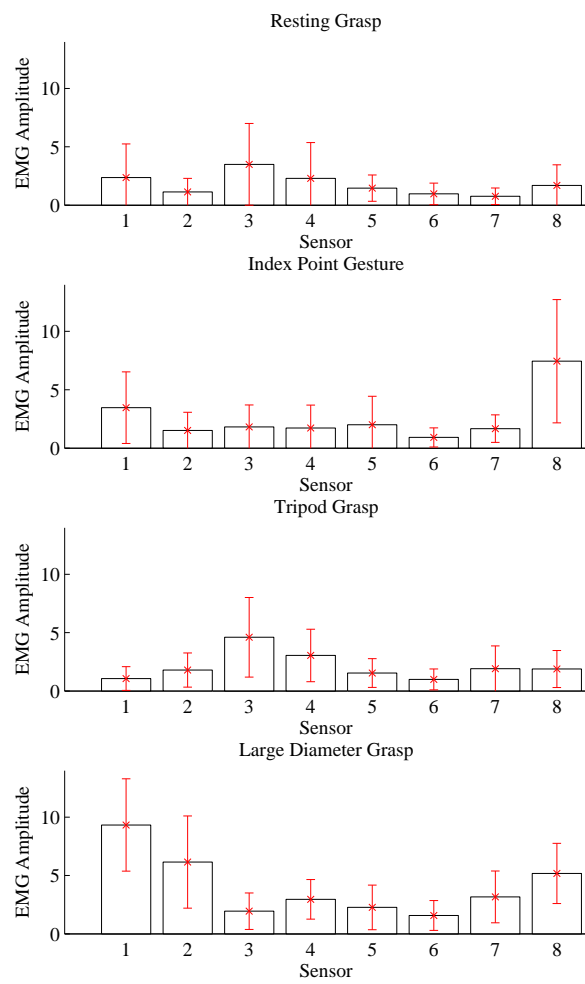


Figure C.6: Average WL values Non-Amputated Subjects for 8 Sensors

C. RESULTS

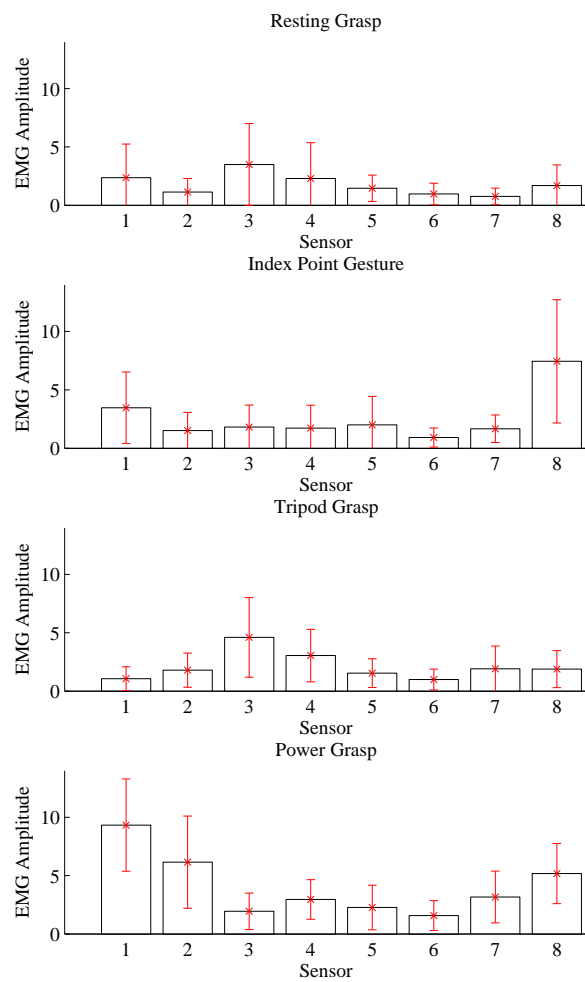


Figure C.7: Average WAMP values Non-Amputated Subjects for 8 Sensors